Diploma Thesis

Investigation of non-standard period-doubling in a piecewise continuous dynamical system

written by
Dipl.-Ing.(FH) Florian Großmann

TU Clausthal - Zellerfeld, July 19, 2004

Referee	Dr. Prellberg
Coreferee	Prof. Dr. Mayer

Before their eyes in sudden view appear
The secrets of the hoary deep, a dark
Illimitable ocean, without bound,
Without dimension, where length, breadth and height,
And time, and place, are lost, where eldest Night
And Chaos, ancestors of Nature, hold
eternal anarchy, amidst the noise
of endless wars, and by confusion stand.

Excerpted from *Paradise Lost* by John Milton 1667 A.D.

Contents

Chapter 1

Introduction

Today's computing is of fundamental importance to mankind in science, economics, domestic use and thereby to the gross national product of industry nations. In a few years Moore's law faces the trial of physical boundaries reached in semiconductor physics. Therefore efforts to elaborate tomorrow's computing take versatile directions and range from quantum computing [20] via optical computing [12] to 3-dimensional nano-mechanical computing [21].

Recent research in nonlinear science treats today's computers as dynamical systems characterized as being operational close at the edge of chaos [14]. Studies related to the human brain reveal its mode of operation close at the edge of chaos, too. Inspired by these powerful natural computers being viewed as complex adaptive systems [13], there are efforts to leave the domain of sequential *CPUs* to obtain self-learning and independently acting computers or robots respectively via neural networks.

To start engineering in this field, devices which exhibit nonlinear behavior and transitions to chaos, are of fundamental need. Some concepts of computers make use of periodic or aperiodic function generators [12], that are stable and reliable in their operation. This directly hints to the dynamical system studied in this thesis, as it is almost always superstable, despite high sensitivity to control parameters in some regions. An engineering interest may be signal shaping by parameterizing a dynamical system. This may even be discerned as an approch to non-dual memories similar to the approach discussed in [19].

The dynamical system studied in this thesis exhibits very simple as well as very complicated behavior. One of these phenomena is period-doubling unlike the well known period-doubling of unimodal maps. To discover the mechanism of period-doubling is the main subject of this thesis and is studied in Chapter 3. Common investigations often focus merely on the transient behavior of dynamical systems and iterated maps respectively in contrary to this work. The dynamical system's behaviour is primarily studied deterministically as a function of its control parameter after the transient behavior is already accomplished. The transient behavior is studied in Chapter 4.

The dynamical system studied in this thesis is based on a a physical model of a particle in a horizontally shaken box, discussed in the end of Chapter 2 and is based on a publication of my supervisor Mr. Prellberg and Mrs. Drossel [1].
The origin of the iterated map under study hints to applications in nano-mechanical computing, but the mathematical interest is there as well, because this system reveals new aspects of period-doubling in unimodal maps, due to an interesting relationship discovered in Section 3.4 of this thesis. Especially the newly introduced **T**-transformations and the wide absorption interval relate results of this thesis to unimodal period-doubling.

Knowledge of discrete dynamical systems is quite important in general, even without any application, because Poincaré sections in nonlinear dynamics often resemble the dynamics of continuous systems e.g. the movement of planets.

Due to the high level of abstraction, the nature of this work is of rather mathematical origin, but many fields of applications are of relevance today, such as tomorrows computers [12].

Chapter 2

Basics

This chapter is intended to introduce the reader to the well-known standard period-doubling of unimodal maps. Of great importance are the unimodal *logistic map* and the *Feigenbaum scenario* resulting in the definition of the *Feigenbaum constants*. There are some methods to be mentioned like the benefit of the *kneading theory* or the *word lifting technique* in order to apply them in the later chapters of this thesis to further treatment of the *cup map*, that features a shape similar to the cross section of a tea-cup and will be studied in chapter 3.

2.1 Deterministic dynamical systems

Discrete dynamical systems showing some sort of deterministic behavior can be modeled in iterated maps, which are also called *Lamerey diagrams*, if the iteration is visualized graphically [9]. Classical examples of these dynamical systems are evolution processes in which time has an intrinsic discrete nature. This can be found in models of time dependent growth of any kind of populations like biological species or even concentrations of chemicals. It also is a common technique to reduce continuous dynamical systems like nonlinear differential equations i.e. the *Volterra-Lotka model* to Lamerey diagrams by applying Poincaré sections in their phase space. This modeling allows the investigation of the long term behavior of the system without solving the nonlinear equations explicitly. Finally, discrete dynamical systems are known to have a wide field of applications, which makes their study rather necessary than merely interesting.

2.1.1 Unimodal maps

The most prominent discrete dynamical system is the discrete logistic map. Unlike the continuous logistic map, which possesses an analytical solution [2], the discrete version shows some new phenomena like the period-doubling route to chaos and chaos itself. It is a proven fact, that these properties are shared by any unimodal map for which the Schwarzian derivative

$$Sf(x) = \frac{\frac{d^3 f(x)}{dx^3}}{\frac{df(x)}{dx}} - \frac{3}{2}\left(\frac{\frac{d^2 f(x)}{dx^2}}{\frac{df(x)}{dx}}\right)^2 \tag{2.1}$$

is negative. These maps are often referred to as *S-unimodal maps* for clarity. Unimodality of the smooth function $f(x)$ is defined by

$$\begin{aligned} f : [a,b] \longrightarrow \mathbb{R} \quad \text{with} \quad & a < c < b, \\ & \left.\frac{df(x)}{dx}\right|_{x\in[a,c[} > 0, \\ & \left.\frac{df(x)}{dx}\right|_{x\in]c,b]} < 0. \end{aligned} \tag{2.2}$$

By some definitions found in literature [8], condition

$$f(0) = f(1) = 0 \tag{2.3}$$

is also demanded for unimodality for $a = 0$ and $b = 1$.

In this work Definition (2.2) following Metzler [10] is used for convenience when showing up the relationship between the *cup map* and unimodal maps in Section 3.4.

The discrete logistic map

$$f_r(x) = rx(1-x) \tag{2.4}$$

is the most prominent unimodal map with a critical point at $c = \frac{1}{2}$ with $f(c) = \frac{r}{4}$, where the monotonicity ends. Under iteration $x_n = f^{(n)}(x_0)$ of an arbitrary $x_0 \in [0,1]$, function f_r shows a period-doubling route to chaos shown in the lower part of Figure 2.1 when the control parameter r increases from zero to r_∞. The orbit diagram in Figure 2.1 displays the points of iteration versus the control parameter r after a sufficiently long iteration. The single point $x_0^* = 0$ appears to be a fixed point in all cases, possessing another preimage $x = 1$.

As long as $r \leq r_\infty$, all points of the interval $]0,1[$ are attracted toward an attractive periodic orbit undergoing drastic changes as a function of the control parameter r. These drastic changes in behavior are called bifurcations. With $0 < r < 1$ there exists just the fixed point $x_0^* = 0$ attracting the whole phase space $[0,1]$. In case of $1 < r < 3$ the primary fixed point x_0^* becomes unstable as another fixed point x_1^* emerges and becomes the attractive periodic orbit of the map attracting the interval $]0,1[$.
For $r > 3$ the fixed point x_1^* becomes unstable too. To allow another attractive periodic orbit to exist as stated above, another fixed point has to appear. It is obvious that no more fixed points can be found in the discrete logistic map itself, but in the higher iterates new fixed points $x_n^* = f_r^{(n)}(x_n^*)$ are allowed to emerge. An important property of these fixed points is their period n nature when inserted in the logistic map. If r reaches even higher values, the fixed point x_n^* will become unstable and give rise to another fixed point $x_{2n}^* = f_r^{(2n)}(x_{2n}^*)$ beginning with $n = 2$ until r_∞ is reached associated with a fixed point of period $p_\infty = \infty$. These successive bifurcations in dependence of the control parameter are called the *Feigenbaum scenario.*

With $r > r_\infty$ almost all orbits show aperiodic behavior and sensitivity to the initial condition, which is associated to chaotic behavior. Consequently the orbit diagram shows so called bands of chaotic orbits in dependence of the control parameter r undergoing a reverse *Feigenbaum scenario.* The reverse bifurcations of chaotic bands are called *band merging.* But the logistic map does not exhibit aperiodicity for all $r \in [r_\infty, 4]$. There exist special $r_p > r_\infty$ embedded in the chaotic bands showing attractive periodic orbits of period p too. These orbits show another Feigenbaum scenario as r increases. For further details on the location and properties of these periodic windows refer to [6].

2.1.2 The Feigenbaum constant δ

A special property of the *Feigenbaum scenario* in S-unimodal maps is the scaling behavior of the bifurcations in the orbit diagram 2.1 revealing the first Feigenbaum constant δ

$$\delta_n = \frac{r_n - r_{n-1}}{r_{n+1} - r_n} \qquad \delta = \lim_{n\to\infty} \delta_n = 4.6692\ldots \tag{2.5}$$

with $n \to \infty$. The control parameter r_n is associated with the bifurcation from period $\frac{p}{2} = 2^{n-1}$ to period $p = 2^n$ with $n \in \mathbb{N}$ and $r_1 = 1$ in accordance with the orbit diagram in Figure 2.1.

2.1.3 Skeleton of the logistic map

To introduce an important method concerning the precise calculation of control parameter values to a given orbit i.e. finding all r_3 associated with a period $p = 3$. The generation of the *skeleton* of the logistic map is explained here. The skeleton of the map consists of polynomials in the control parameter generated by successive iteration of the critical value of the unimodal map defined by

$$P_n(r) = f_r^{(n)}(c) \qquad \Longleftrightarrow \qquad P_{n+1}(r) = f_r(P_n(r)) \qquad \forall n \in \mathbb{N}_0\,. \tag{2.6}$$

The plot of these polynomials in the interval $[0, 4]$ is called the skeleton of the map and reproduces many properties, like superstability and chaotic band merging points. The following equations show the first polynomials of the logistic map with x the critical point $c = \frac{1}{2}$. Other S-unimodal maps can be treated the same way by redefining $f_r(x)$ and c.

$$P_0(r) = \frac{1}{2}$$

$$P_1(r) = \frac{1}{4}r$$

$$P_2(r) = -\frac{1}{16}r^3 + \frac{1}{4}r^2$$

$$P_3(r) = -\frac{1}{256}r^7 + \frac{1}{32}r^6 - \frac{1}{16}r^5 - \frac{1}{16}r^4 + \frac{1}{4}r^3$$

Figure 2.1 shows the skeleton of the unimodal map consisting of the polynomials up to $P_{10}(r)$.
Comparing the skeleton and the orbit diagram it is easily verified that the polynomials reproduce the orbit diagram at the superstable orbits as a consequence of their definition as iteration of the critical point.

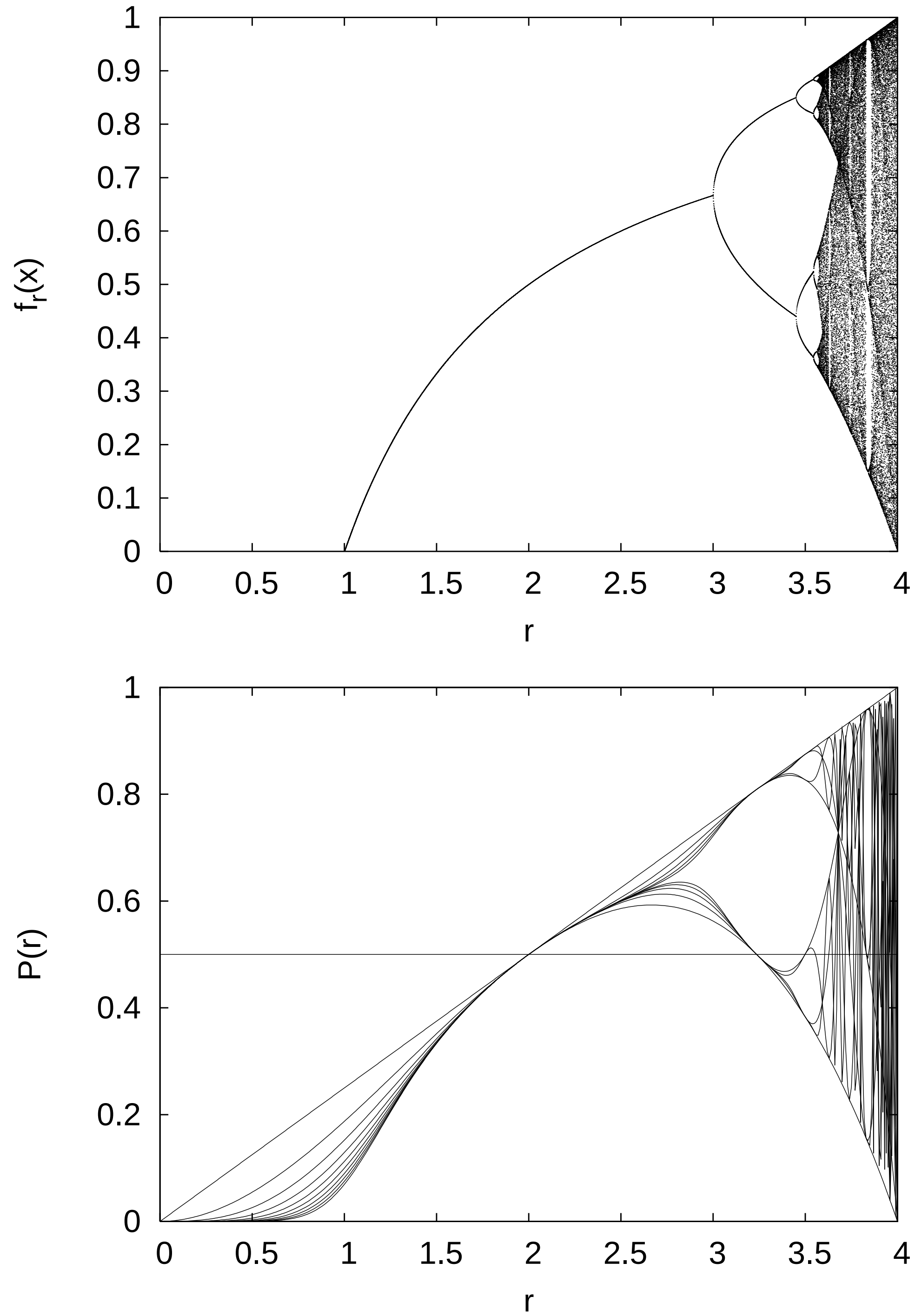

Figure 2.1: The orbit diagram of the logistic map above shows the iterated points x_ν of an arbitrary seedvalue $x_0 \in]0,1[$ versus the control parameter r after sufficient iteration. In the left attractive periodic orbits exist and in the right chaotic bands prevail. The skeleton reproduces the orbit diagram at superstable points.

2.1.4 Superstability and the Lyapunov exponent

Another important property of unimodal maps is the existence of superstable orbits. Superstable orbits in unimodal maps show a quadratic instead of a linear convergence rate toward the attractive periodic orbits [6]. As already shown in the last section the iteration of a seed-value $x_0 \in]0,1[$ with a given r_p to its associated period p results in the existence of a fixed point $x_p^* = f^{(p)}(x_p^*)$ in the p'th iterate. By investigating the stability of this fixed point, the derivative of the iterate has to fulfill the stability criterion

$$\left| \frac{df^{(n)}(x_n^*)}{dx} \right| < 1 \tag{2.7}$$

for one-dimensional maps. In case of an orbit e.g. the attractive periodic orbit $O_p = \{x_\nu\}$, $0 \leq \nu \leq p-1$ of period p the function $f(x)$ transforms the seed value $x_0 \in O_p$ successively in the following way $x_0 \to x_1 \to \ldots \to x_{p-1} \to x_0 \ldots$. When calculating derivative

$$\frac{df^{(p)}(x_0)}{dx} = \prod_{\nu=0}^{p-1} \left(\frac{df}{dx} \right)(x_\nu) \tag{2.8}$$

the chain rule has to be applied, which leads to a product of the function's derivative evaluated at all points x_ν of the orbit. Superstability of an orbit is defined by

$$\frac{df^{(n)}(x)}{dx} = 0 \tag{2.9}$$

compelling the product in equation 2.8 to vanish. The ultimate consequence is $c \in O_p$ for unimodal maps.

Another approach to superstability makes use of the *Lyapunov exponent* Λ

$$|f^{(n)}(x_{0,1}) - f^{(n)}(x_{0,2})| \sim |x_{0,1} - x_{0,2}| e^{\Lambda n} \qquad n \gg 1. \tag{2.10}$$

It is a direct measure to sensitivity to the initial condition and is a useful indicator for chaos, if $\Lambda > 0$. The Lyapunov exponent measures the average development of distances between initially closely located seed values $x_{0,1}$ and $x_{0,2}$ satisfying $|x_{0,1} - x_{0,2}| \leq \epsilon << 1$ after n iterations. As it is easily seen $\Lambda < 0$ indicates the distance between adjacent points to shrink opposed to $\Lambda > 0$ implying the distance to grow under iteration[1].

[1] Usually equation (2.10) is valid until growing distances reach the diameter of the phase space or an attractor [2].

The Lyapunov exponent can be expressed in another representation by resolving equation (2.10) for Λ and introducing a small $\epsilon = |x_{0,1} - x_{0,2}|$

$$\Lambda = \lim_{n\to\infty} \frac{1}{n} \lim_{\epsilon\to 0} \ \ln \left| \frac{f^{(n)}(x_{0,1}) - f^{(n)}(x_{0,2})}{\epsilon} \right|. \tag{2.11}$$

By performing the limiting process consisting of $\epsilon \to 0$ and $n \to \infty$

$$\Lambda = \lim_{n\to\infty} \frac{1}{n} \lim_{\epsilon\to 0} \ \ln \left| \frac{f^{(n)}(x_{0,1}) - f^{(n)}(x_{0,2})}{\epsilon} \right| \tag{2.12}$$

is derived, allowing the Lyapunov exponent to be calculated by the iterated functions derivative. Applying the chain rule to the derivative of the iterated function expresses

$$\Lambda = \lim_{n\to\infty} \frac{1}{n} \ln \left| \left(\frac{df^{(n)}}{dx} \right) (x_0) \right| \tag{2.13}$$

as product of the functions derivative evaluated at the points x_ν of the orbit.

$$\Lambda = \lim_{n\to\infty} \frac{1}{n} \ln \left| \prod_{\nu=0}^{n-1} \left(\frac{df}{dx} \right) (x_\nu) \right| \tag{2.14}$$

Rewriting the logarithm, shows the useful representation of the Lyapunov exponent

$$\Lambda = \lim_{n\to\infty} \frac{1}{n} \sum_{\nu=0}^{n-1} \ln \left| \left(\frac{df}{dx} \right) (x_\nu) \right|. \tag{2.15}$$

A periodic orbit of period p allows to set $n = kp$, $k \in \mathbb{N}$ and to replace $\lim_{n\to\infty}$ by $\lim_{k\to\infty}$ yielding a finite sum

$$\Lambda = \lim_{k\to\infty} \frac{1}{kp} k \sum_{\nu=0}^{p-1} \ln \left| \left(\frac{df}{dx} \right) (x_\nu) \right|. \tag{2.16}$$

Equation 2.16 implies the Lyapunov exponent to diverge to $-\infty$ in a limiting process as one derivative in the sum vanishes, so superstability of the periodic orbit is associated with a Lyapunov exponent of $\Lambda_{superstable} = -\infty$.

2.2 Symbolic dynamics

The previous section dealt with some basic properties of unimodal maps and the discrete logistic equation. In this section a powerful method will be introduced allowing further treatment of an even wider class of maps. But the

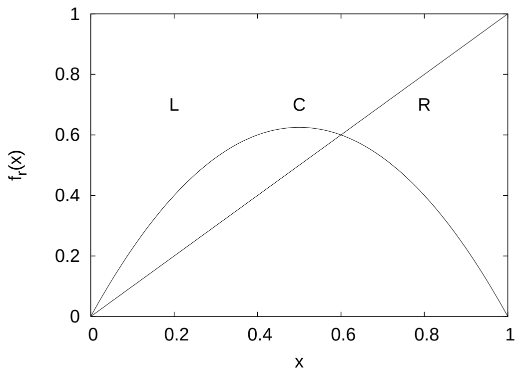

Figure 2.2: Illustration of an order introduced on numbers $x \in [0, 1]$.

emphasis will be kept on the logistic equation, whose orbits can be examined quantitatively by using symbolic dynamics and the word lifting technique.

To characterize a number x located in the interval $[0, 1]$ a symbol sequence may be introduced to assign its location under iteration in partitions by use of symbols. A useful notation of partitions for symbolics dynamics is by means of the symbols L and R, related to the left and the right monotonous part of the function as illustrated in Figure 2.2. The symbol C denotes the point to be the critical point c at the maximum of $f(x)$. For example the point x represented by symbol sequence $s_x = L$ simply states the point to be located in the interval $[0, c[$. The order

$$L < C < R \tag{2.17}$$

is obviously valid. To specify the point x less coarsely the symbolic sequence $s_x = s_{x,1}s_{x,2}s_{x,3}\ldots$ representing x has to consist of more digits. The digits $s_{x,\nu}$ tell, in which interval the number $f^{(\nu)}(x)$ is found after ν iterations of x. The simple Order (2.17) has to be slightly modified to be correct for any *parity* of the words. Extending the order represented by

$$\begin{array}{ll} L < C < R & \text{if } s_\iota \text{ is even} \\ R < C < L & \text{if } s_\iota \text{ is odd} \end{array} \tag{2.18}$$

to words of arbitrary length, the parity of words has to be introduced. To compare two numbers $x \neq y$ represented by their symbol sequences s_x and s_y, the finite symbol sequence s_ι is defined by

$$s_\iota = s_{x,1}s_{x,2}\dots s_{x,\iota} = \prod_{\nu=1}^{\iota} s_{x,\nu} \qquad\qquad s_{x,\nu} = s_{y,\nu} \quad \forall\nu \le \iota, s_{x,\iota+1} \ne s_{y,\iota+1}. \tag{2.19}$$

The words s_x and s_y are obviously identical to the ι'th symbol and differ in their $\iota + 1$'th digit.
A finite symbol sequence $s_\iota = s_{x,1}s_{x,2},\dots,s_{x,\iota}$ is of even parity, if the number of R's contained in s_ι is even, otherwise it is called odd. If s_ι is empty, it is even. Easily the primary Order (2.17) is verified to toggle each time a negative slope of the map is hit during iteration that is indicated by symbol R.
To compare the numbers x and y in their symbolic representation, Order (2.18) has to be applied to $s_{x,\iota+1}, s_{y,\iota+1}$ with the unique ι in equation (2.19).

2.2.1 Period-doubling

The period-doubling phenomenon of unimodal maps is well understood and shows quite a regular behavior when treated in symbolic dynamics. As the orbit of period p bifurcates into an orbit of period $2p$, the symbolic sequence s_p defined by

$$s_p = \overline{\sigma_p s_{p,p}} \qquad\qquad \sigma_p = \prod_{\nu=1}^{p-1} \sigma_{p,\nu} \tag{2.20}$$

represents the orbit p and allows to obtain the orbit s_{2p} by using the recurrence relation

$$\sigma_{2p} = \sigma_p \omega \sigma_p \qquad\qquad \omega = \begin{cases} R & \text{if } \sigma_p \text{ is even} \\ L & \text{if } \sigma_p \text{ is odd} \end{cases} . \tag{2.21}$$

The periodic orbit[2] s_p consists of a basic sequence σ_p of length $p-1$, which is constant for a special period p and its associated control parameter $r \in]r_p, r_{p+1}[$. The final digit $s_{p,p} \in \{L, C, R\}$ runs through all symbols as the control parameter r increases from r_p to r_{p+1}. This behavior can be verified in the orbit diagram of the logistic map in Figure 2.1, where one of the stable points always crosses the superstability condition $f(x) = c = \frac{1}{2}$, indicating a change from L to R via C and vice versa at the next bifurcation always increasing the value of the symbolic sequence with respect to Order (2.18).

[2]Periodicity is explicitly indicated by the line over the sequence of digits known to repeat.

Period p	Sequence s_p	$*$-composition
1	$s_{1,1}$	$s_1 = s_{1,1}$
2	$Rs_{2,2}$	$s_2 = Rs_{2,2}$
4	$RLRs_{4,4}$	$s_4 = (R * R)s_{4,4}$
8	$RLRRRLRs_{8,8}$	$s_8 = (R * R * R)s_{8,8}$
$\vdots$	$\vdots$	$\vdots$

Table 2.1: Sequences of standard period-doubling occurring in unimodal maps with $s_{p,p} \in \{L, C, R\}$.

It is common use to write the recurrence relation in a shorter more abstract term found in

$$\sigma_{2p} = \sigma_p * R = \mathop{*}_{\nu=1}^{n+1} R \qquad\qquad p = 2^n,\ n \in \mathbb{N}, \tag{2.22}$$

introducing a new operation on finite symbolic sequences called $*$-composition defined in

$$s_x * s_y = s_x s_{y,1} s_x s_{y,2} s_x \dots s_{y,\mu} s_x. \tag{2.23}$$

The $*$-composition uses symbolic sequences $s_x = s_{x,1} s_{x,2} \dots s_{x,\nu}$ and $s_y = s_{y,1} s_{y,2} \dots s_{y,\mu}$ of length ν and μ. Sometimes it is useful to treat special sequences resulting from $*$-compositions called the *Harmonic* $H(s)$ and the *Antiharmonic* $A(s)$ of sequence s defined by

$$\begin{array}{ll} H(s) = s * R & \qquad\text{Harmonic} \\ A(s) = s * L & \qquad\text{Antiharmonic.} \end{array} \tag{2.24}$$

The period doubling can generally be considered as recurrent harmonic generation leading to the sequences presented in Table 2.1.

2.2.2 Word lifting technique

The word lifting technique allows control parameters to be calculated explicitly, when given a symbolic representation $s_x = \overline{s_{x,0} \dots s_{x,p-1}}$ of a periodic orbit. To make this technique work properly, another equivalent representation of the logistic map

$$g_\mu(y) = 1 - \mu y^2 \qquad\qquad y \in [-1, 1] \tag{2.25}$$

is introduced. Both representations of the logistic map may be transferred into each other via a linear homeomorphism, that makes them topologically conjugate. The previous logistic map

$$f_r(x) = rx(1-x) \qquad\qquad x \in [0,1]$$

is more intuitive in modeling evolution problems, but produces inconvenient terms when using the word lifting technique. So the topologically conjugate representation $g_\mu(y)$ of $f_r(x)$ is used instead, allowing the ambiguous solving of complicated equations to be replaced by a simple converging iteration yielding the unique solution of interest.

By definition unimodal maps always posses two monotonic branches of the function, providing each point $y \in g_\mu([-1,1])$ with 2 different preimages, either left or right of the critical point, that can be calculated explicitly to the forms in

$$R(y) = \frac{1}{\mu}\sqrt{\mu - \mu y} \qquad\qquad L(y) = -\frac{1}{\mu}\sqrt{\mu - \mu y}. \tag{2.26}$$

As already known, superstable periodic orbits of period p satisfy $y_0 = y_c = g_\mu^{(p)}(y_c = 0)$. The orbit is equivalent to the symbolic representation $s_y = \overline{s_{y,0} \ldots s_{y,p-1}}$ of the point $y_1 = 1$ satisfying $y_0 = y_c = 0 = g_\mu^{(p-1)}(y_1)$. By knowing s_y the iteration can be inverted formally by successive application of the inverted function to the critical point $y_c = 0$ yielding the formally inverted function

$$y_1 = 1 = \left(g_\mu^{(p-1)}\right)^{-1}(g_\mu^{(p-1)}(y_1)) = \sigma_{y,1} \circ \ldots \circ \sigma_{y,p-1}(y_c = 0). \tag{2.27}$$

$$\sigma_{y,i} = \begin{cases} R(y) & s_{y,i} = R \\ L(y) & s_{y,i} = L \end{cases}$$

It is easy to confirm the form of the inverted Functions (2.26) is most convenient for iteration, obtaining the simplest expressions.

Example 2.2.1. *Suppose the superstable orbit of interest is $s_y = \overline{RLC}$ with period $p = 3$ resulting in the evaluation of the functions R and L with boundary conditions as indicated by*

$$s_y = \overline{RLC} = \ldots RLC \underbrace{\quad}_{=1} RL \underbrace{\quad}_{=0} CRLC \ldots.$$

Evaluating equation (2.27) yields

$$1 = R \circ L(0) = \frac{1}{\mu}\sqrt{\mu + \sqrt{\mu}}. \tag{2.28}$$

Multiplying equation (2.28) with μ and rewriting it to an iteration in μ yields

$$\mu_{n+1} = \sqrt{\mu_n + \sqrt{\mu_n}}, \tag{2.29}$$

which converges toward the control parameter μ related to the orbit $s_y = \overline{RLC}$ in a wide range of initial values $\{\mu_0\} \subset [0, 2]$.

The word lifting technique works well for any periodical orbit s_x and well chosen initial parameter μ_0 in the logistic map [6].

2.2.3 Kneading sequence

In this section the kneading sequence will be introduced, asserting whether the corresponding orbit to a given symbol sequence s_x with $x \in [0, 1]$ is admissible or not. Section 2.2 introduced order (2.18)

$$\begin{array}{ll} L < C < R & \text{if } s_\iota \text{ is even} \\ R < C < L & \text{if } s_\iota \text{ is odd} \end{array}$$

on points and their symbolic sequences respectively. Iteration of the critical point $c = \frac{1}{2}$ of the tent map or the discrete logistic map results in a unique symbolic string $C\kappa = CR\ldots$ defining the kneading sequence $\kappa = R\ldots$. Admissibility of orbits in maps can be refered to in [5] and is defined by

$$\kappa \geq \sup_k \sigma^k s_x \qquad k \in \mathbb{Z}_+ \tag{2.30}$$

with σ the *Bernoulli shift operator* that is equivalent to iteration in the symbolic representation of the orbit via

$$\sigma^k s_x = \sigma^k \prod_{i=0}^{n} s_{x,i} = \prod_{i=k}^{n} s_{x,i}. \tag{2.31}$$

Admissibility condition (2.30) simply takes into account, that a non-surjective map like the logistic or the tent map can not map a point $x \in [0, f\left(\frac{1}{2}\right)]$ into the interval $]f\left(\frac{1}{2}\right), 1]$.

Figure 2.3 shows an example to the tent map and the logistic map with the same kneading sequence. The logistic map may be viewed at as a deformed tent map under maintenance of continuity and strict monotonicity. Because of their identical kneading sequence both maps possess the same orbits [5] in their symbolic description according to the admissibility condition (2.30). Important to note is, that these maps are not topologically conjugate in general. An orbit s_x with

$$\sup_k \sigma^k s_x > \kappa$$

is not admissible due to violation of the non-surjectivity of the map.

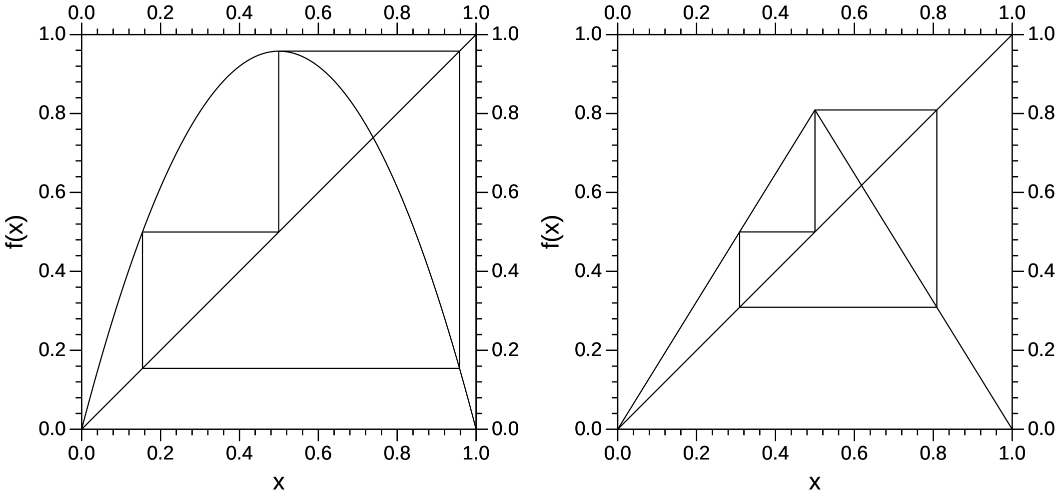

Figure 2.3: The discrete logistic map with $r = 3.83\ldots$ and the tent map with $r \approx 0.80$ kneading sequence $\kappa = \overline{RLC}$.

Example 2.2.2. *Orbit $s_x = \overline{RLLC}$ does not fulfill admissibility condition (2.30) because of*

$$\kappa = \underbrace{RL}_{w} C\overline{RLC} < \underbrace{RL}_{w} LC\overline{RLLC} = s_x.$$

Word w is odd, due to a single appearance of digit R in w and therefore order $R < C < L$ applies to digit 3 assigning $RLC < RLL$. Hence an orbit s_x directly violates the admissibility condition and demands the iterated function to map a point of its domain beyond its codomain. To make orbit s_x admissible the control parameter r has to be increased to increase the kneading sequence.

In conclusion the kneading sequence allows all possible words of letters R, L and even C[3] to exist, if the map is surjective. The kneading sequence of the surjective logistic map is $\kappa = R\overline{L}$ and represents the highest possible value with respect to order (2.18). The kneading sequence is a topological invariant that increases monotonically with the control parameter r [5].

[3]An orbit containing letter C has to be periodic, because the partition associated to C is a single point.

2.3 Stochastic dynamical systems

In case of complicated evolution processes of dynamical systems it may be more convenient to deal with probability distributions instead of tracing orbits of single seed values. This is most applicable in case of strongly developed sensitivity to the initial condition, because deterministically investigated orbits of closely located seed values separate at an exponential rate. A stochastic approach covers all contingencies of a deterministic approach and allows the most likely development of the system to be asserted.

To handle the discrete evolution of probability distributions concerning an iterated map $f(x)$ the *Perron-Frobenius operator* is a valuable tool defined by

$$\rho_{n+1}(x) = \mathbf{L}\rho_n(x). \tag{2.32}$$

The Perron-Frobenius operator acts on the probability distribution $\rho_n(x)$. For equation (2.32) to be correct, the operator has to satisfy conservation of probability

$$\int_A \rho_{n+1}(x)dx = \int_{A'} \rho_n(x)dx \tag{2.33}$$

with A' being the preimage of space A under the transformation with f. The operator can be expressed in form of equation

$$\mathbf{L}\rho_n(x) = \sum_\sigma \frac{\rho_n({f_\sigma}^{-1}(x))}{|f'({f_\sigma}^{-1}(x))|} \tag{2.34}$$

with σ numbering all preimages ${f_\sigma}^{-1}(x)$ of function $f(x)$. A derivation can be found in [3].

Treating a map $f(x)$, the Perron-Frobenius operator may possess eigenfunctions $\rho_i(x)$ to the eigenvalues λ_i fulfilling

$$\mathbf{L}\rho_i(x) = \lambda_i \rho_i(x). \tag{2.35}$$

The eigenfunction to the leading eigenvalue is called *invariant density* or *invariant distribution* with the eigenvalue describing the development of the probability. It is one if the map is endomorph. If the map is not endomorph, parts of the phase space leave the domain of the map under iteration e.g.

the logistic map $f_r(x)$ with $r > 4$ causes almost all orbits[4] to diverge. The leading eigenvalue $\lambda < 1$ quantifies the amount of probability, that leaves the invariant density under each iteration.

If the Perron-Frobenius operator possesses an invariant density $\rho(x)$ with an eigenvalue $\lambda < 1$ an *escape rate* can be defined. The invariant density loses the same share of probability each iteration expressed by

$$\mathbf{L}^n \rho(x) = \lambda^n \rho(x). \tag{2.36}$$

Therefore λ can be identified with

$$\lambda^n = e^{-\kappa n} \qquad \Longleftrightarrow \qquad \kappa = -\ln \lambda \tag{2.37}$$

introducing the escape rate κ.

2.4 A particle in a horizontally shaken box

This section deals with the physical model of a classical, pointlike particle trapped in an oscillating potential well according to [1]. To characterize the motion of the particle an iterated map is introduced.

Figure 2.4 shows the one-dimensional potential well of length L performing a harmonic oscillation with frequency ω and amplitude A. The particle is allowed to move almost freely within the well. The locations of the walls of the potential are given by equation

$$x_{lw}(t) = A \sin \omega t \tag{2.38}$$

and

$$x_{rw}(t) = A \sin \omega t + L. \tag{2.39}$$

By transforming the coordinate $x(t)$ of the particle according to

$$l(t) = x(t) - A \sin(\omega t) \tag{2.40}$$

the relative position of the particle with respect to the left wall is obtained. Obviously $l(t)$ is valid for $l(t) \in [0, L]$. The relative velocity of the particle with respect to the wall of the potential well is

$$u(t) = \frac{dl}{dt} = v(t) - A\omega \cos(\omega t). \tag{2.41}$$

[4]The remaining set of non-diverging orbits is called *cantor dust* and provides measure zero.

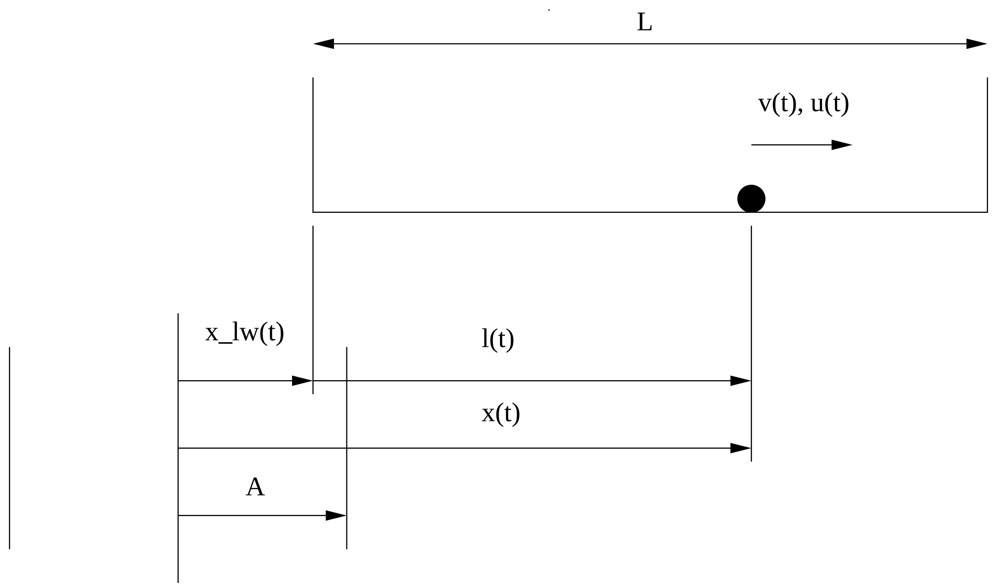

Figure 2.4: A particle in a horizontally shaken box.

Finally the acceleration $\frac{du}{dt}$ with respect to the potential well is of interest representing the equation of motion

$$\frac{du}{dt} = -\gamma u(t) + A\omega^2 \sin(\omega t) \qquad (2.42)$$

of the particle. Additionally the possibility of friction is taken into account by parameter γ and is modeled proportional to the relative velocity $u(t)$, which is done in similarity to the harmonic oscillator.
To simplify the previous equations the substitutions $\phi_0 = \omega t_0 \mod 2\pi$, $\alpha = \frac{L}{A}$ and $\tilde{\gamma} = \frac{\gamma}{\omega}$ will be applied. Solving the differential equation (2.42) by neglecting friction with $\gamma = 0$, using the initial velocity u_0 and demanding $l(\phi_0) = 0$ solution

$$l(\phi, \phi_0) = \sin(\phi_0) - \sin\phi + (\phi - \phi_0)(u_0 + \cos(\phi_0)) \qquad (2.43)$$

is easily obtained.

The initial velocity u_0 results from a previous collision at phase ϕ_0 of the particle at $l(\phi_0) = 0$, where the equation of motion starts to be valid. The velocity $\tilde{u}_0$ prior to the collision at phase ϕ_0 is transferred to the new initial velocity by the collision parameter η yielding

$$u_0 = -\eta \tilde{u}_0. \qquad (2.44)$$

To study the dynamics of the particle in the well of length L equation (2.43) has to be solved for $l(\phi_1, \phi_0) = \alpha$ and $l(\phi_1, \phi_0) = 0$ with all phases $\phi_0 \in [0, 2\pi]$. In some cases many solutions exist. The smallest $\phi_1 > \phi_0$ turns out to be the physically relevant solution indicating the next collision to be at the same or the opposite wall depending on the equation used to obtain ϕ_1. Figure 2.5 gives an idea of the motion of the particle with the characteristic period 4 control parameter $\alpha = 5.74$ and a complete inelastic collision with $\eta = 0$.

In practice the simplification of the problem by assuming $\eta = \tilde{\gamma} = 0$ does not change the problem all too much. As long as the map possesses monotony and continuity in f_1 the qualitative behavior is maintained. Control parameters α of interest are indicated by Figure 2.8 and are applicable as long as energy dissipation is sufficiently high. Therefore the results of the simplified problem still apply to the real problem.

- The most interesting behavior is found with $\phi_0 \in [0, \frac{\pi}{2}[$, leading to a collision at the opposite wall.
- Phases $\phi_0 \in [\frac{\pi}{2}, \phi_c = 1.79\ldots[$ lead to another collision at the same wall granting $\phi_1 \in [0, \frac{\pi}{2}]$.

$$0 = l(2\pi, \phi_c) = \sin(\phi_c) + (2\pi - \phi_c)\cos(\phi_c)$$

- For initial phases $\phi_0 \in [\phi_c, 0]$ the particle gets trapped at the wall until it is released with maximum velocity at $\phi_0 = 0$. This trapping simply occurs because of the positively accelerating wall.

The particles phase of impact at the opposite wall is of high interest characterizing the systems behavior i.e. the crossing of the potential well. Solving equation (2.43) under this premise yields an iterated map[5] displayed in Figure 2.7 representing the systems complete behavior.

To investigate the map's behavior under iteration it is useful to iterate the seed value $x_0 = 0$ and to count the iterations[6] until an absorption occurs associated with $x_p = 0$ and the period p.

[5] The phase $\phi = \frac{\pi}{2}$ has been rescaled to 1.

[6] Counting iterations means counting the particle's number of transits of the potential well.

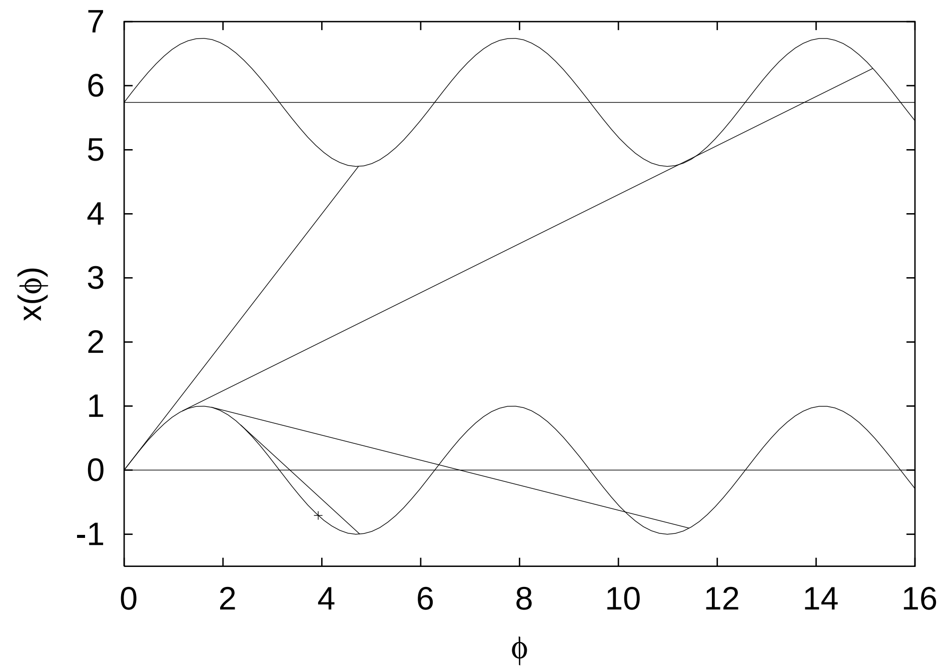

Figure 2.5: Different kinds of motion of the particle with $\alpha = 5.74$ starting at initial phases ϕ_0 in the left to the next collision at another wall in the right. Some motions are shown to posses ambiguous solutions. The motion starting at $\frac{5}{4}\pi$ indicated by the cross immediately collides as it starts and is considered to be *absorbed*.

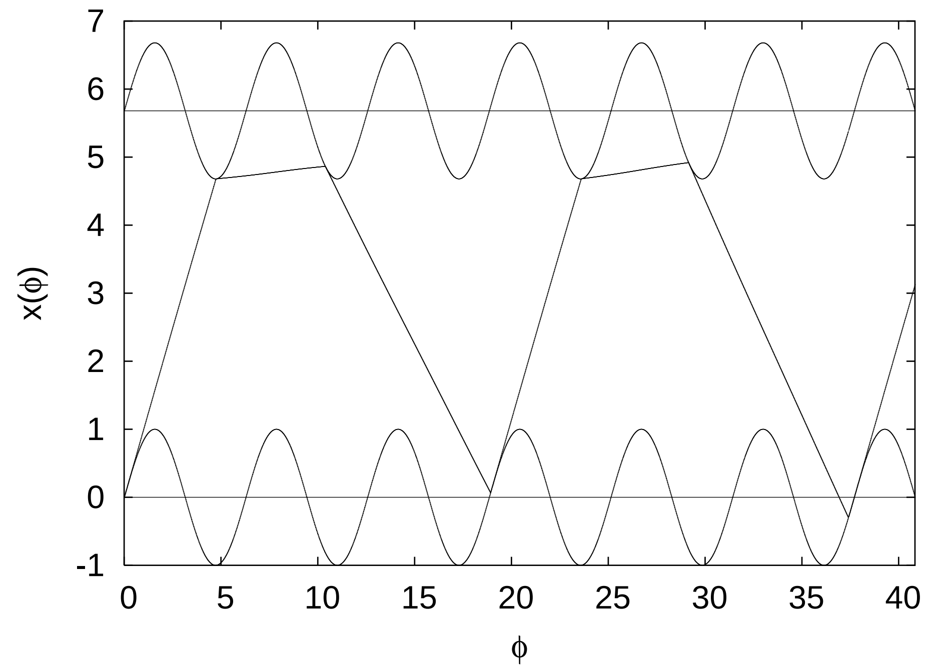

Figure 2.6: The position $x(\phi)$ plotted versus ϕ for $\alpha = 5.74$ for the iterated seed value $x_0 = 0$. The sine functions represent the oscillating walls.

The systems dependence on $\alpha = \frac{L}{A}$ is shown in Figure 2.8. It is easily verified the period of the system to be extremely dependent on α and therewith sensitive to the geometry L of the box and the amplitude A of its oscillation. As α decreases from $\alpha = 6$ to $\alpha \approx 5.7$, the period $p = 2$ undergoes a doubling phenomenon as is clearly visible in Figure 2.8. As shown in Chapter 3 this doubling is a special Feigenbaum scenario up to p_∞.

Decreasing α causes the convex branch of the iterated map of Figure 2.7 to increase. This behavior can be verified in Figure 2.6. Supposed that the upper wall comes closer to the lower one, the first hit at the opposite wall will lead to a flatter second line, causing $\phi_1(\phi_0 = 0)$ to increase[7].

On the other hand supposed that ϕ_0 increases, the slope of the leftmost line in Figure 2.6 will flatten, causing the slope of the second line to increase and to result in a smaller ϕ_1 explaining the map's convex branch.

The structure in the right side of the iterated map in Figure 2.7 will be titled *the maze* because of its complexity and the long time it may take the particle to leave it. The maze arises from $\phi_0 \to \frac{\pi}{2}$, yielding very flat lines, representing the particle to move very slowly with respect to the walls hitting the opposite wall at $\phi_1 \to \frac{\pi}{2}$, too.

A thorough investigation of the maps behavior under change of the control parameter α associated with the increase of the convex branch is found in Chapter 3. Chapter 4 explains the the behaviour via another approximation and the iteration function depicted in Figure 2.7 and will be pointed out to be continuous in the whole phase space.

[7]Remember, that the iterated map ignores collisions at the same wall.

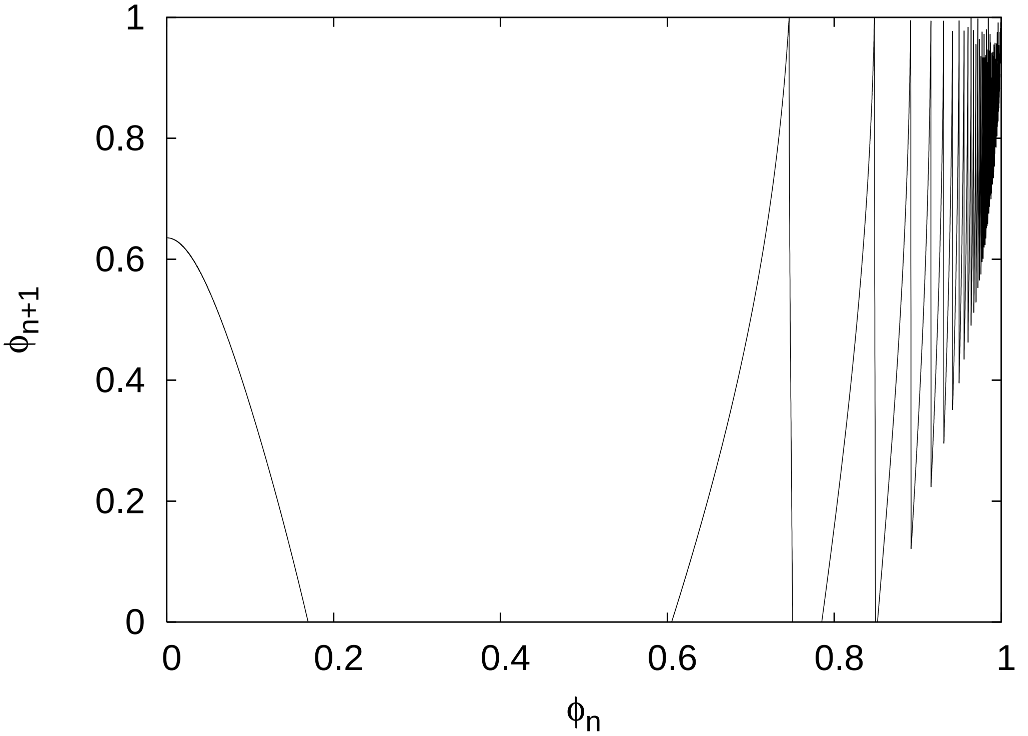

Figure 2.7: The iteration function for $\alpha = 5.74$ with a resulting period of $p = 4$.

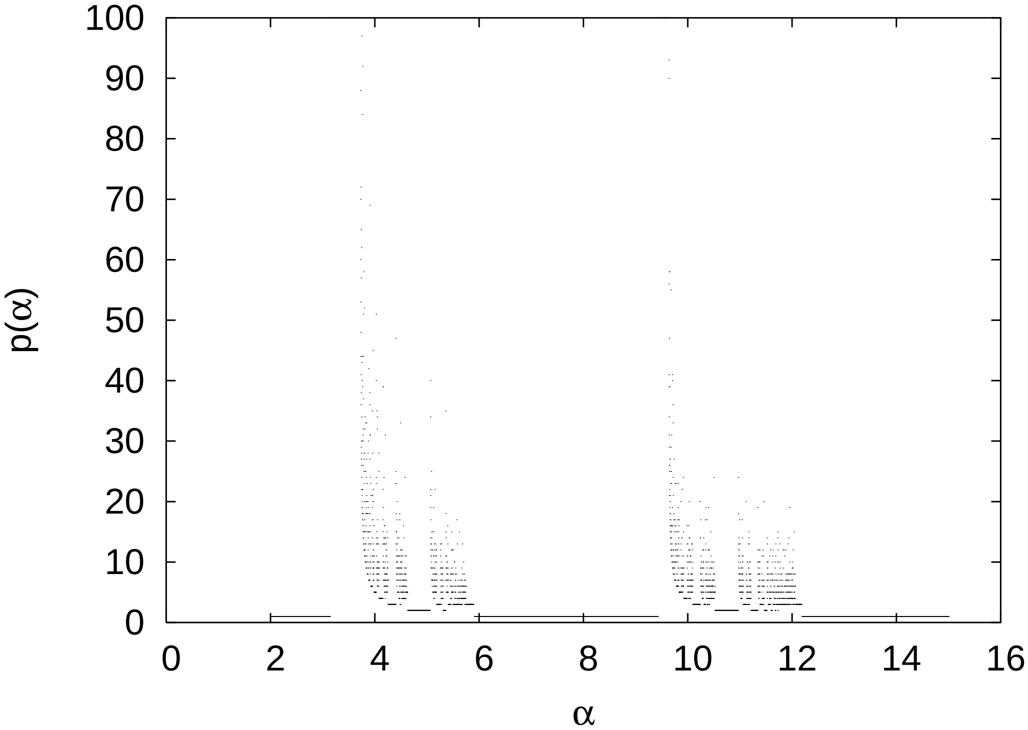

Figure 2.8: The period p to absorption over the control parameter α.

Chapter 3

The cup map

In Section 2.4 a strange iteration function occurred depicted in Figure 2.7 on page 26, showing a period-doubling phenomenon under variation of a parameter representing the relation between geometry and oscillation amplitude of the box. The most obvious effect was the increase of the convex left branch of the map. Due to this increase a reflection to small values of $x \neq 0$ sets in during iteration at the first branch of the *maze* like structure of the iteration function in Figure 2.7 causing the period to double in length. Figure 3.1 gives a clearly visible survey on the mechanism of period doubling in the *cup* like map.

3.1 The generic map

To understand the period doubling mechanism of the iteration function visualized in Figure 2.7, a generic model is represented by

$$f(x) = a\left(1 - \left(\frac{x}{b}\right)^{\rho}\right)\Theta(b-x) + \frac{x-c}{1-c}\Theta(x-c). \tag{3.1}$$

Figure 3.1 shows a plot of this function for the special value $\rho = 1$ and visualizes the influence of the control parameters a, b and c on the shape of the iteration function. As control parameter a increases period-doubling sets in. The major concern of this chapter is to characterize the period-doubling due to increasing a with $b = const$ and $c = const$.

In equation (3.1) Θ represents the Heaviside function and ρ the control of the functions convexity in the first partition as shown in Figure 3.2. The parameter b and c are always restricted by

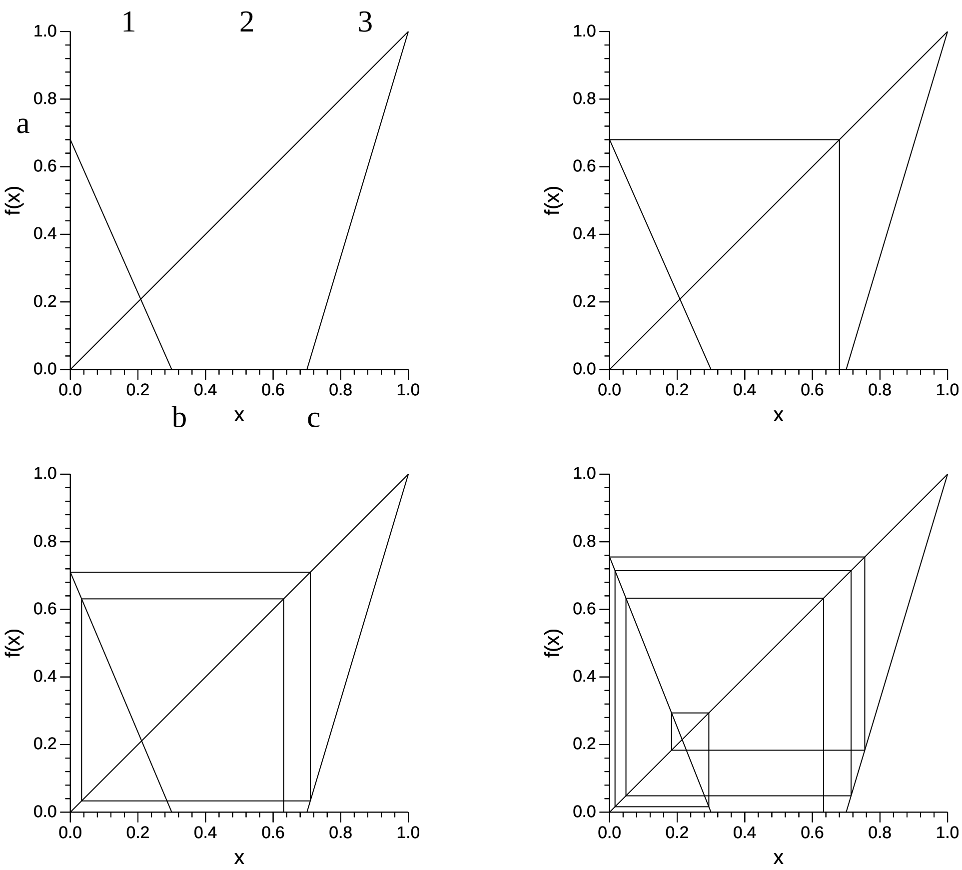

Figure 3.1: The cup map, its parameter a,b and c and the useful partitions 1, 2 and 3 plotted with $\rho = 1$. The onset of period-doubling is visualized in Lamerey diagrams with $a^{(2)} = 0.68$, $a^{(4)} = 0.71$ and $a^{(8)} = 7.55$ showing the periods $p = 2$, 4 and 8 respectively.

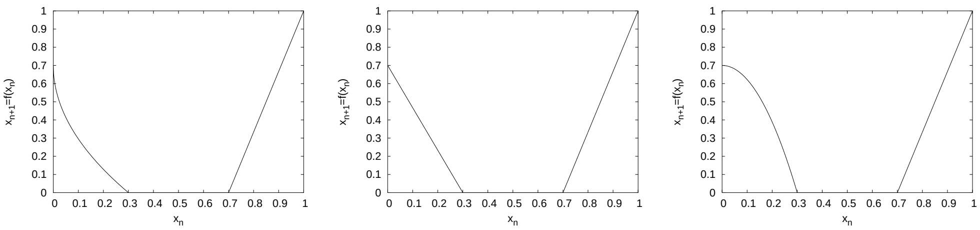

Figure 3.2: The shape of function 3.1 with $\rho = \frac{1}{2}$, $\rho = 1$ and $\rho = 2$ respectively.

$$0 < b < c < 1 \tag{3.2}$$

and $a \in [0, 1]$. Restriction (3.2) causes the iteration function to maintain its characteristic shape[1], which is of interest.

Symbolic treatment.

Function (3.1) can be be expressed in the form of

$$f(x) = \begin{cases} \mathbf{f}_1 x = a\left(1 - \left(\frac{x}{b}\right)^{\rho}\right) = -\frac{a}{b^{\rho}}x^{\rho} + a & x \in [0, b] \\ \mathbf{f}_2 x = 0 & x \in]b, c[\\ \mathbf{f}_3 x = \frac{x-c}{1-c} = \frac{1}{1-c}x + \frac{c}{1-c} & x \in [c, 1] \end{cases} \tag{3.3}$$

emphasizing the view on partitions i.e. intervals. The iteration of function $f(x)$ therefore can be expressed as successive application of the operators $\mathbf{f}_1$, $\mathbf{f}_2$ and $\mathbf{f}_3$ with respect to their domain. The operator representation is used to allow the formal and convenient inversion of the operator sequences corresponding to iterations associated to specific symbolic sequences. The operator associated to iteration according to arbitrary symbolic sequences is not certain to posses a non-empty domain. Because of this property operators are used instead of functions.
The operator representation of function $f(x)$ directly links operator $\mathbf{f}_i$ to partition i. Figure 3.1 illustrates which operator sequences are connected to the periods 2 to 8, summarized in Table 3.1.

In case of an attractive fixed point of f_1, period $p = 1$ is associated with a symbol sequence $s_1 = \overline{1}$ in a limiting process to $x_0 = 0$. Table 3.1 shows the orbits of successive periods in their symbolic representation. The operator representation is equivalent to the symbolic representation via

$$s_{\nu} = \overline{s_{\nu,0} \dots s_{\nu,\nu-1}} \qquad \Longleftrightarrow \qquad x_0 = \lim_{n\to\infty} \left(\mathbf{f}_{s_{\nu,\nu-1}} \dots \mathbf{f}_{s_{\nu,0}}\right)^n x_0. \tag{3.4}$$

Tracing the orbit of a seed value $x_0 = 0$ under increasing control parameter a shows the general period-doubling sequence (2.22) to be satisfied as indicated by Table 3.1. Therefore some identities can be realized in order to apply the recurrence relation (2.21) and the $*$-composition (2.22) introduced on page 16.

[1] There exist iterated function systems possessing overlapping branches featuring stochastic dynamics [11].

number n	period $p = 2^n$	symbol sequence s_p
0	1	$s_1 = \overline{1}$
1	2	$s_2 = \overline{12}$
2	4	$s_3 = \overline{1312}$
3	8	$s_4 = \overline{13111312}$
$\vdots$	$\vdots$	$\vdots$

Table 3.1: The period-doubling of the linear cup map and associated symbolic sequences.

$$1 \equiv R$$
$$2 \equiv C$$
$$3 \equiv L$$
$$\sigma_2 = 1 \qquad\qquad s_{2,2} = 2$$

Using the identities, the $*$-composition on symbolic sequences of period-doubling is rewritten to

$$\sigma_p = \mathop{*}_{\nu=1}^{n} 1 \qquad\qquad p = 2^n,\, n \in \mathbb{N} \tag{3.5}$$

providing the construction of period-doubled symbolic sequences

$$s_p = \overline{\sigma_p s_{p,p}} \qquad\qquad s_{p,p} \in \{1, 2, 3\}. \tag{3.6}$$

Equation (3.5) results in the following sequences matching the results of high precision numerical simulations.

$$\sigma_{2^2} = 1 * 1 = 131$$

$$\sigma_{2^3} = 1 * 1 * 1 = 131 * 1 = 1311131$$

The last digit of sequence $s_{p,p}$ passes through the symbols 1,2 and 3 or vice versa as the control parameter a is increased. It should be noted that $s_{p,p}$ runs through the symbols from higher to lower value with respect to order

$$\begin{array}{ll} 1 < 2 < 3 & \text{if } \sigma_p \text{ is even} \\ 3 < 2 < 1 & \text{if } \sigma_p \text{ is odd} \end{array} \tag{3.7}$$

in the contrary to unimodal maps.

Superstable orbits

Of great importance is the definition of the period p associated with $x_0 = f^{(p)}(x_0)$. In Section 2.4 the period has just been associated with the number of iterations to be performed between consecutive absorptions. This definition has to be restricted to superstable orbits only now as shown in Theorem 3.1.1.
In the previous discussion of symbolic sequences of period-doubling orbits, the last digit of the sequence is asserted to run through all available symbols, implying non-absorbing periodic orbits to exist. Concerning the linear case, these symbolic sequences are related to a single point $a_{s_p} \in [0,1]$ with $s_{p,p} \in \{1,3\}$ that satisfies in fact $x_{p-1} = f^{(p)}(x_0 = 0)$ with $x_{p-1} \in \{b,c\}$.
In contrast, in Section 3.3 periodic orbits of period $p = 2^n$ will appear in the convex case without undergoing an absorption[2] revealing an attractive periodic orbit of period p featured by a dense interval $\mathcal{A}_{s_p} \subset [0,1]$ instead of the degenerate point a_{s_p}.

Lemma 3.1.1. *Orbits of period p hitting partition 2 are superstable.*

Proof. The derivative

$$\frac{df}{dx} = -a\rho\frac{x^{\rho-1}}{b^\rho}\Theta(b-x)+\frac{1}{1-c}\Theta(x-c)-a\left(1-\left(\frac{x}{b}\right)^\rho\right)\delta(b-x)+\frac{x-c}{1-c}\delta(x-c) \tag{3.8}$$

of Function (3.1) yields

$$\left(\frac{df}{dx}\right)(x)\bigg|_{x\in]b,c[} = 0$$

and causes the Lyapunov exponent defined by equation (2.16) on page 13 to diverge and hence implies superstability. ☐

3.2 Linear case

Demanding continuity and monotonicity of the function in the first partition, 3 cases of convexity arise in the map, visualized in Figure 3.2. The symbolic representation of admissible orbits are the same for these maps as indicated by Section 2.2.3. A more detailed description of this fact will be worked out in Section 3.2.7 and further Section 3.3. Therefore the map can be studied in the simplest linear case associated with $\rho = 1$. After a detailed analysis of

[2]Absorption is always associated with hitting the 2'nd partition: $x_{p-1} \in]b,c[$.

the system's behavior in the linear case, the results can be transfered to the nonlinear cases by using the admissibility of the same orbits in these maps according to the kneading theory.

The linearization of function (3.1) by $\rho = 1$ makes the operator representation of the iteration function simpler due to the linear dependence of the operator result on x. Nonlinear operators of kind $\mathbf{f}_i = \alpha_i \cdot + \beta_i$ with $\alpha_i \neq 0$ are easily seen to form a group and represent affine transformations.

3.2.1 Trivial orbits

In the following *trivial orbits* of kind $s_{t_1} = 13(1)^n 2$, $s_{t_2} = 1(3)^n 2$ and $s_{t_3} = 1(3)^n(1)^k 2$ with $n, k \in \mathbb{N}$ are studied. The most useful seed value for starting an investigation appears to be $x_0 = 0$, because of the whole partition 2 being its preimage next to the points $x_{p-1} = b$ and $x_{p-1} = c$. In order to trace the orbits of any seed value $x_0 \in [0, 1]$ under forward iteration in a more systematic way, the preimages to any admissible sequence[3] s of the interval $[b, c]$ can be studied instead by using the inverse operators

$$\begin{aligned} \mathbf{f}_1^{-1} &= b\left(1 - \tfrac{\cdot}{a}\right) & \mathcal{D}(\mathbf{f}_1^{-1}) &= [0, a] \\ \mathbf{f}_3^{-1} &= (1 - c) \cdot + c & \mathcal{D}(\mathbf{f}_3^{-1}) &= [0, 1]. \end{aligned} \tag{3.9}$$

Each backward iteration of the absorbing interval directly reveals the future of points located within the preimage under forward iteration. Figure 3.4 shows a selection of preimages and the information gained by reverse iteration. In the following condition

$$a > b \tag{3.10}$$

will always be assumed valid unless otherwise mentioned.

Theorem 3.2.1. *Under condition $a < b$, the fixed point*

$$x_1^* = \frac{ab}{a + b} \tag{3.11}$$

is globally attractive.

Proof. The value of the slope of the function is $\left|\frac{df_1}{dx}\right| = \frac{a}{b} < 1$ by assumption. Therefore $f_1(x)$ fixed point (3.11) is stable and attractive in $[0, c[$. Condition (3.2) is always valid, implying $\frac{df_3}{dx} = \frac{1}{1-c} > 1$ and hence the fixed point $x_3^* = 1$

[3] The admissibility of sequences is discussed in Section 3.2.7

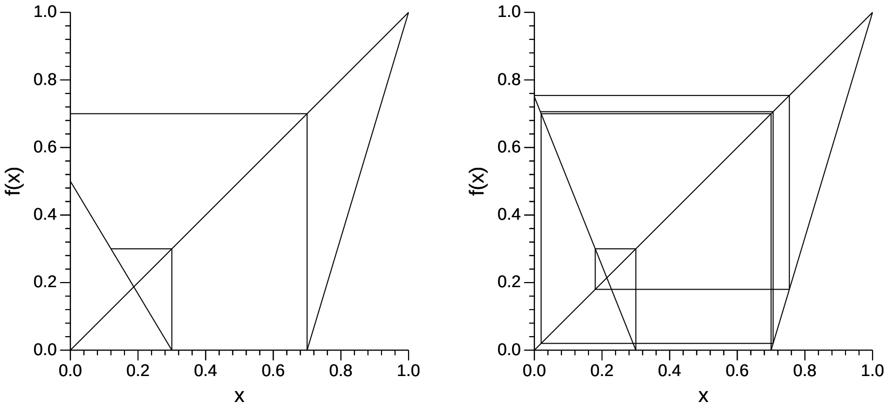

Figure 3.3: The point $x_0 = 0$ is located in the $\sigma_2 = 1$ preimage of $[b, c]$ implying period $p = 2$ under iteration of $x_0 = 0$ and $\sigma_4 = 131$ with $p = 4$ respectively .

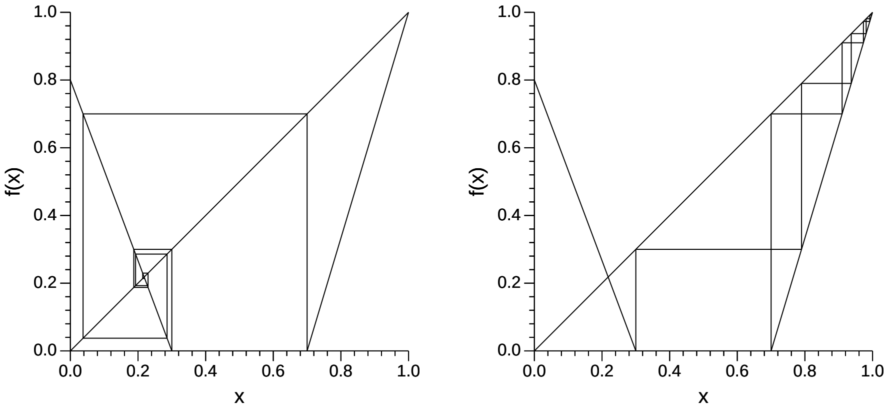

Figure 3.4: Illustration of $\mathbf{f}_1$ and $\mathbf{f}_3$ preimages with $a = 0.8$ and the absorption region $[0.3, 0.7]$. The preimages converge toward fixed points in the magnifying map.

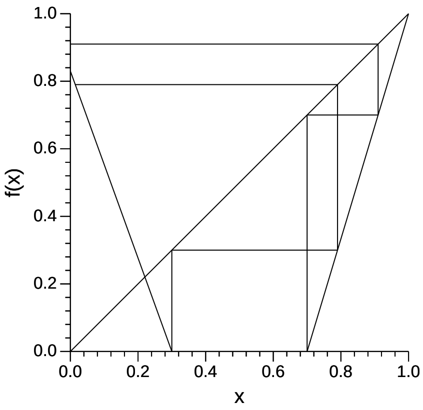

Figure 3.5: Even period $p = 3$ exists, implying orbits of arbitrary periods to exist by the *Šarkovskii* theorem [10, 8].

is unstable. Due to the surjective function $f_3(x)$ and the unstability of x_3^* every point $x \in [c, 1[$ possesses an image $f^{(n)}(x) \in [0, c[, \quad 0 < n < \infty$ and is attracted to fixed point x_1^*. $\square$

Arbitrary preimages of the single operators (3.9) can be calculated explicitly to

$$\mathbf{f}_1^{-1(n)} = \left(-\frac{b}{a}\right)^n \cdot -a \sum_{\nu=1}^{n} \left(-\frac{b}{a}\right) \qquad \mathcal{D}(\mathbf{f}_1^{-1(n)}) = [0, a] \tag{3.12}$$

and

$$\mathbf{f}_3^{-1(n)} = (1-c)^n \cdot +c \sum_{\nu=0}^{n-1} (1-c)^\nu \qquad \mathcal{D}(\mathbf{f}_3^{-1(n)}) = [0, 1] \tag{3.13}$$

by using successive application of the inverse operator. Their preimages converge toward fixed points, due to the expanding map illustrated in Figure 3.4. A first understanding of the complicated structures in Figure 3.8 can be achieved by iterating $x_0 = 0$ twice, watching it hit $\mathbf{f}_1$ preimages defined by

$$f^{(2)}(x_0) \in \left] \left(\mathbf{f}_1^{-1}\right)^{(n)} y_1, \left(\mathbf{f}_1^{-1}\right)^{(n)} y_2 \right[_{y_1 \cup y_2 = \{b, c\}} \qquad \Longleftrightarrow \qquad s_{t_1} = 13(1)^n 2 \tag{3.14}$$

$$n \in \mathbb{N}.$$

This effort is visualized in Figure 3.6 giving rise to the trivial orbits s_{t_1} of period $p_{s_{t_1}} = n + 3$.

Another trivial kind of orbit has to be taken into account defined by $s_{t_2} = 1(3)^n 2$ with period $p_{s_{t_1}} = n + 2$. These orbits are relevant for sufficiently large a. In Figure 3.9, orbits s_{t_1} and s_{t_2} are shown to explain the well ordered structures in Figure 3.8. In the left trivial orbits s_{t_1} and in the right trivial orbits s_{t_2} are visualized to reproduce the numerically obtained data about the period $p(a)$ versus control parameter a. Between the trivial orbits intervals of more complex origin are to be seen in Figure 3.9.
It is important to note the s_{t_1} orbits to be running through all preimages of f_1 with odd n, reaching infinity associated with hitting the unstable fixed point x_1^* as a increases. Starting with a higher $a \approx 0.85$ in Figure 3.9 and decreasing it, n will increase from $n = 2$ through all even values reaching the

instable fixed point, too.

Finally there exits a third kind of trivial orbit of period $p_{s_{t_3}} = n + k + 2$ associated with $s_{t_3} = 1(3)^n(1)^k 2$ with $n, k \in \mathbb{N}$ that are found in the neighborhood of s_{t_2} orbits. Due to their lower significance Figure 3.9 does not show them.

3.2.2 Non-trivial orbits

Non-trivial orbits are defined by $x_2 = (\mathbf{f}_3\mathbf{f}_1 x_0) \in]\mathbf{f}_1^{(n)} y, \mathbf{f}_1^{(\nu)} z[$ with $\nu = n + 2$ and $y = b$ and $z = c$ if n is odd and $\nu = n - 2$ with $y = c$ and $z = b$ if n is even. The arise of non-trivial orbits is demonstrated in Figure 3.7 giving a hint to the complicated nature of structures found in Figure 3.8 between the trivial orbits. As it is easily seen the f_1 preimages of $[b, c]$ barely move as a increases, while $x_2 = \mathbf{f}_3(a)\mathbf{f}_1(a)x_0$ slides through all these preimages and the not yet investigated spaces between them resulting in interesting periods $p(a)$ with $x_0 = 0$ to be seen in Figure 3.8.
In Figure 3.7 interval $[0, \mathbf{f}_1^{-1} c]$ is easily seen to be iterated via $s_1 = 131$. Part of the s_1-image yet completely covers its preimage due to the rapid expansion of the map. Another part lies in the first f_1 preimage $\mathbf{f}_1^{-1}[b, c]$ resulting in an absorption. The most interesting third part is partially projected on its preimage via $s_3 = 1311$. The essence of the iteration of interval $[0, \mathbf{f}_1^{-1} c]$ under this condition is stretching, and back folding quite similar to *Smale's horse shoe* as illustrated in Figure 3.10.

3.2.3 T-transformations

To handle the magnifying map, converging[4] inverse dynamics is stressed once more by introducing useful transformations $\mathbf{T}_i$ in order to obtain all possible orbits of points $x \in [0, \mathbf{f}_1^{-1} c]$ under forward iteration. The following investigation is strictly limited to $a \in [\mathbf{f}_3^{-1}\mathbf{f}_1^{-1} b, \mathbf{f}_3^{-1}\left(\mathbf{f}_1^{-1}\right)^3 c]$, which implies that $\mathbf{f}_3\mathbf{f}_1 x_0 = \mathbf{f}_3 a$ is located between the first and third f_1 preimage of b and c as pictured in Figure 3.7.

[4]Inverse dynamics cause the magnifying map to be endomorph under backward iteration that leads to converging preimages of e.g. $\mathbf{f}_1^{(n)}$ preimages of $[b, c]$.

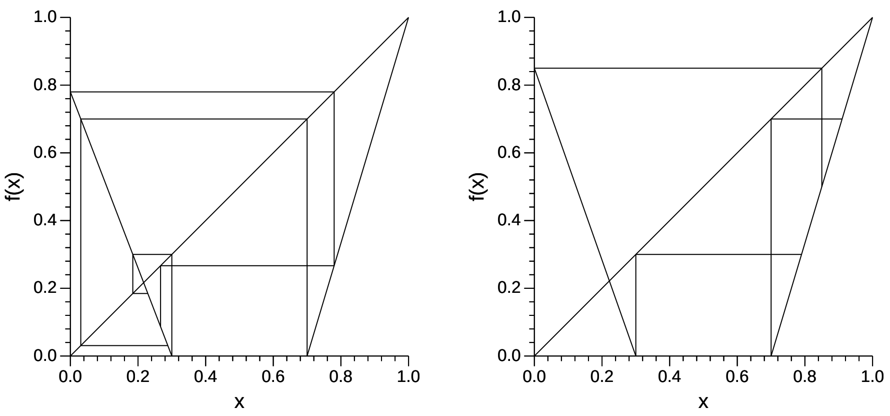

Figure 3.6: After two iterations a $\mathbf{f}_1^{-1}[b,c]$ and after one iteration a $\mathbf{f}_3^{-1}[b,c]$ image is hit respectively.

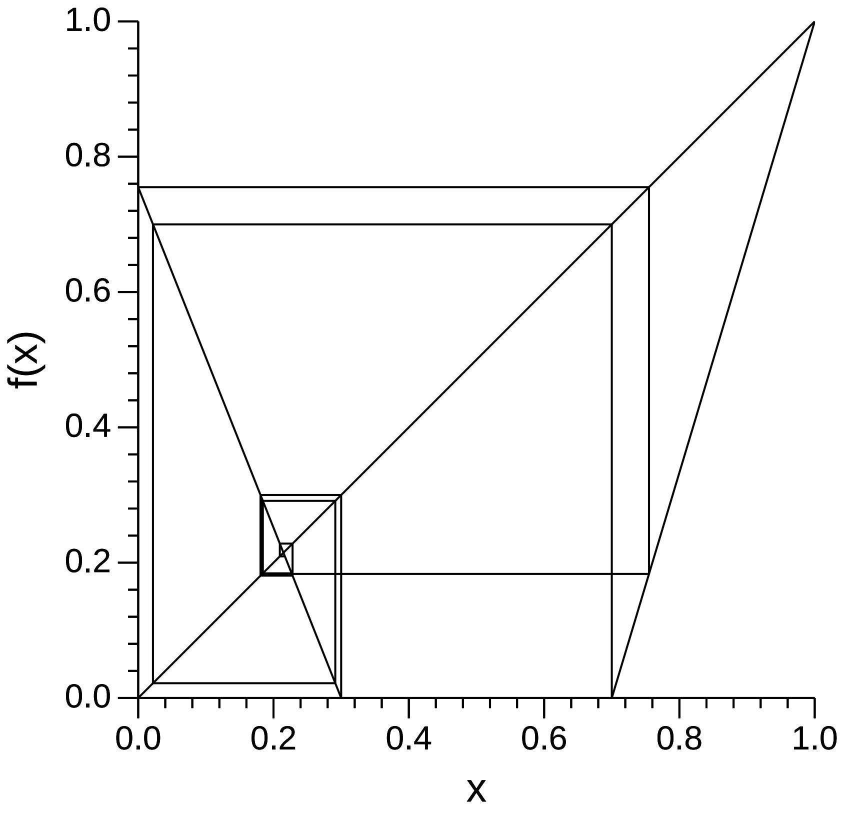

Figure 3.7: The arise of non-trivial orbits due to the partial projection of $[0, \mathbf{f}_1^{-1}c]$ on itself via $s = 1311$.

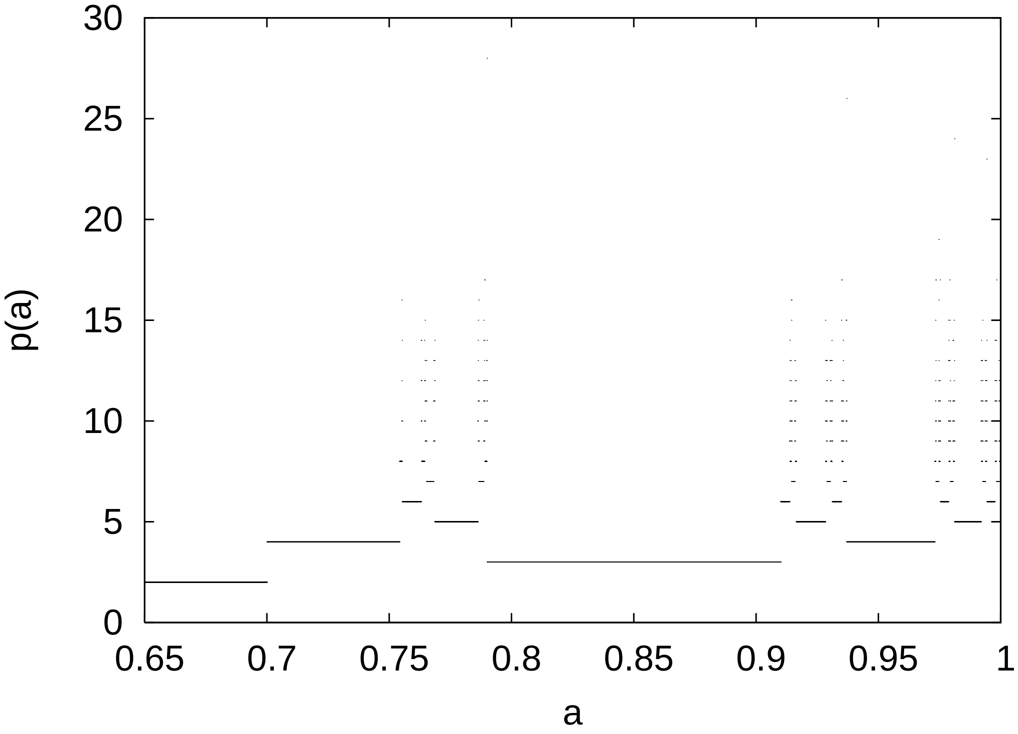

Figure 3.8: The period to absorption $p(a)$ of the seed value $x_0 = 0$ under iteration with $\rho = 1$.

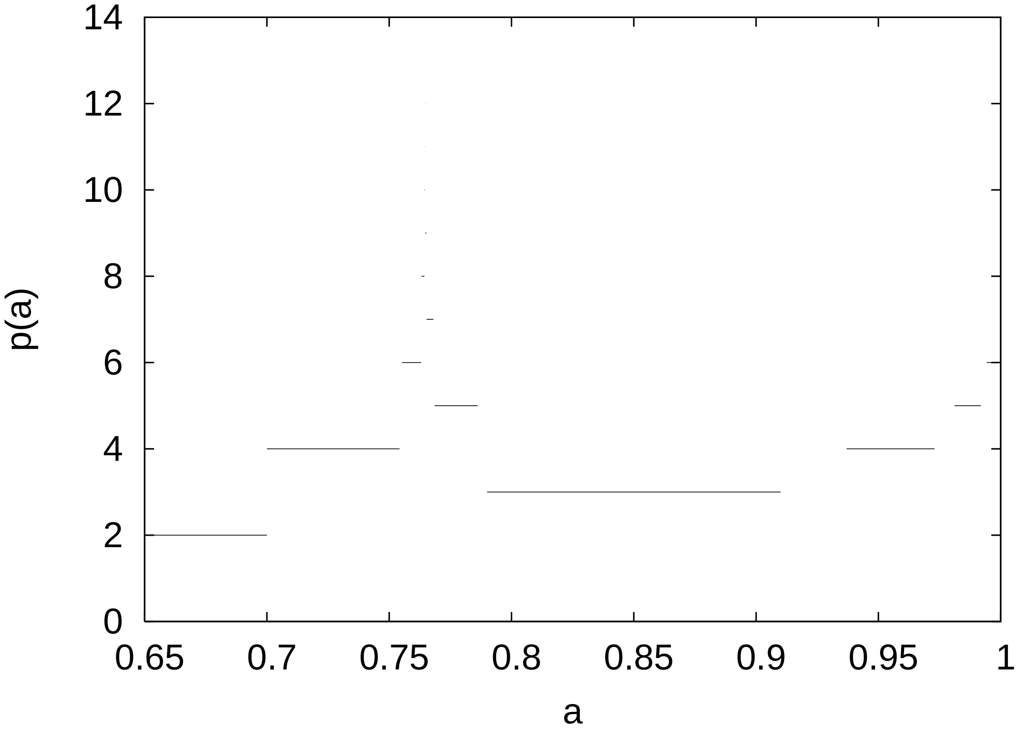

Figure 3.9: Trivial orbits explain most of the structures. Between 0.7 and ≈ 0.9 $s_{t_1} = 13(1)^n 2$ orbits are found and from ≈ 0.95 to 1 $s_{t_2} = 1(3)^n 2$ orbits are shown.

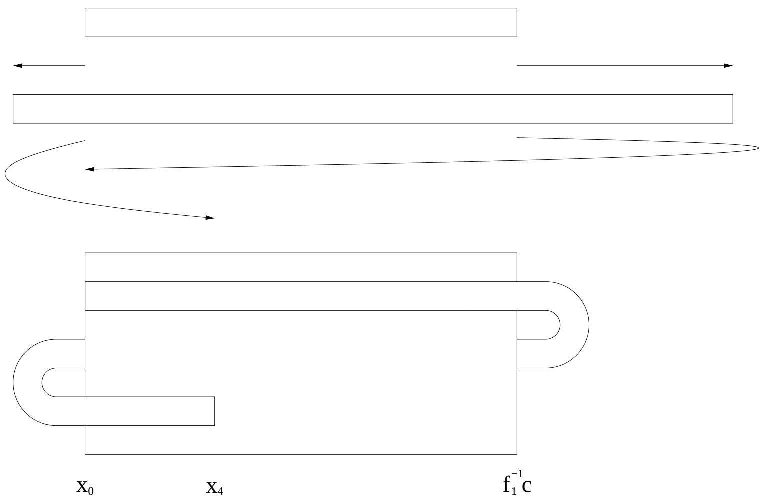

Figure 3.10: The arise of nontrivial orbits due to stretching and back folding of interval $[0, \mathbf{f}_1^{-1}]$. The interval imaged in the background is absorbed and therefore projected to $x_0 = 0$.

Some finite symbolic sequences $s_i = s_{i,1}s_{i,2}\dots s_{i,\iota_i}$ of length ι_i are defined by

$$\begin{array}{lll} s_1 = 131 & \iota_1 = 3 & \mathcal{D}(\mathbf{T}_1) = [\max(b, \mathbf{f}_1\mathbf{f}_3 a), c] \\ s_2 = 1311 & \iota_2 = 4 & \mathcal{D}(\mathbf{T}_2) = [0, x_4] \\ s_3 = 13 & \iota_3 = 2 & \mathcal{D}(\mathbf{T}_3) = [0, \mathbf{f}_1^{-1}c] \\ s_4 = 1313 & \iota_4 = 4 & \mathcal{D}(\mathbf{T}_4) = [0, \mathbf{f}_1^{-1}c] \end{array} \tag{3.15}$$

allowing a systematic investigation via the $\mathbf{T}_i$ operators

$$\mathbf{T}_i = \mathbf{f}_{s_i}^{-1} = \mathbf{f}_{s_{i,1}}^{-1}\mathbf{f}_{s_{i,2}}^{-1}\dots\mathbf{f}_{s_{i,\iota_i}}^{-1}. \tag{3.16}$$

The restrictions on a allow the iteration of $x_0 = 0$ to satisfy

$$x_4 = \mathbf{f}_1\mathbf{f}_1\mathbf{f}_3\mathbf{f}_1 x_0 = \mathbf{f}_1\mathbf{f}_1\mathbf{f}_3 a \tag{3.17}$$

by assumption. The domain of $\mathbf{T}_1$ has to be formally restricted to $\mathcal{D}(\mathbf{T}_1) = [\max(b, \mathbf{f}_1\mathbf{f}_3 a), c]$ to allow the absorption area $[b, c]$ to be mapped satisfying $\mathbf{T}_1\mathcal{D}(\mathbf{T}_1) \in [0, 1]$ in case of unrestricted a. Otherwise there will exist $x \in [b, c]$ satisfying $\mathbf{T}_1 x \in [\rho, \tilde{c}]$ with $\rho < 0$. This in fact explains the already known period $p = 4$ orbit, that is not of concern anymore.

As Figure 3.10 suggests, there exists another operator $\mathbf{T}_2$ that iterates the interval $\mathcal{D}(\mathbf{T}_2) = [0, x_4]$ backwards via $s_2 = 1311$. Figure 3.7 clearly visualizes the codomain of $\mathbf{T}_2$ to be $\mathcal{R}(\mathbf{T}_2) = [0, \mathbf{T}_1 b]$. This fact is equivalent to the statement

$$f^{(4)} : [0, \mathbf{T}_1 b] \rightarrow [0, x_4] \tag{3.18}$$

for a better understanding. Due to $\mathbf{T}_2 0 = \mathbf{T}_1 b$ and $\mathbf{T}_2 x_4 = 0$ and the linear influence of x on $\mathbf{T}_2 x$ the operator possesses another representation

$$\mathbf{T}_2 = (\mathbf{T}_1 b) \left(1 - \frac{\cdot}{x_4}\right) \tag{3.19}$$

equivalent to Definition (3.16). Obviously $\mathbf{T}_2$ is endomorph. The result obtained by application of $\mathbf{T}_2$ is demonstrated in Figure 3.12.

Because of the ambiguity of reverse iteration there exists another Operator $\mathbf{T}_3$ associated with the symbolic sequence $s_3 = 13$. Figure 3.7 shows the restrictions on a to result in the mapping process defined by

$$\mathbf{T}_3 0 = \mathbf{f}_1^{-1} c \qquad\qquad \mathbf{T}_3 \mathbf{f}_1^{-1} c = \mathbf{T}_1 c$$

with a linear influence of x on $\mathbf{T}_3 x$ yielding

$$\mathbf{T}_3 = \left(\frac{(\mathbf{T}_1 c)}{(\mathbf{f}_1^{-1} c)} - 1\right) \cdot + (\mathbf{f}_1^{-1} c) \tag{3.20}$$

featuring the domain $\mathcal{D}(\mathbf{T}_3) = [0, \mathbf{f}_1^{-1} c]$ and the codomain $\mathcal{R}(\mathbf{T}_3) = [\mathbf{T}_1 c, \mathbf{f}_1^{-1} c]$, that shows $\mathbf{T}_3$ to be endomorph, too.
By use of Transformations $\mathbf{T}_1$, $\mathbf{T}_2$ and $\mathbf{T}_3$ the whole future of all points $x \in [0, \mathbf{f}_1^{-1} c]$ can be obtained. For convenience another operator $\mathbf{T}_4 = (\mathbf{T}_3)^2$ is introduced and associated with the symbolic sequence $s_4 = 1313$. The main advantage of introducing $\mathbf{T}_4$ is revealed in the simplicity of the iteration visualized in Figure 3.14 provided by $\mathbf{T}_4$ mapping interval $[0, \mathbf{f}_1^{-1} c]$ with $\mathbf{T}_4 0 = \mathbf{T}_1 c$ and $\mathbf{T}_4 \mathbf{f}_1^{-1} c = \mathbf{T}_3 \mathbf{T}_1 c$ according to

$$\mathbf{T}_4 = \frac{(\mathbf{T}_3 \mathbf{T}_1 c) - (\mathbf{T}_1 c)}{(\mathbf{f}_1^{-1} c)} \cdot + (\mathbf{T}_1 c) \tag{3.21}$$

linearly into itself.

Gaining information

The basic idea about gaining information of the future of points $x \in [0, \mathbf{f}_1^{-1} c]$ is based on the known future of some points in the interval. Due to the restrictions on a, the image of $\mathbf{T}_1 \mathcal{D}(\mathbf{T}_1)$ with $\mathcal{D}(\mathbf{T}_1) = [b, c]$ is located completely in $[0, \mathbf{f}_1^{-1} c]$ as pictured in Figure 3.11. Hence the future of these points is known as $s_1 = 131$ followed by an absorption. For brevity, intervals containing point x will be labeled with the number of iterations to absorption

$\iota_x = \sum_\nu \iota_{i(\nu)}$, $i \in \{1,2,4\}$ instead of symbolic strings s_x in figures.

As will be shown x_4 is always located in the interval $[\mathbf{T}_1 b, \mathbf{T}_1 c]$, when period-doubling begins with $a > a_{min}$. Hence there exists an interval of known future in the domain of $\mathbf{T}_2$ resulting in the existence of an interval of known future in the codomain of $\mathbf{T}_2$.

Lemma 3.2.2. *With $x_4 < \mathbf{T}_1 c$ operator $\mathbf{T}_2$ determines the future of all points in the interval $[0, \mathbf{T}_1 b]$.*

$$\bigcup_{n=1}^{\infty} (\mathbf{T}_2)^n [0, x_4] = [0, \mathbf{T}_1 b] \tag{3.22}$$

Proof. Under forward iteration via $s_2 = 1311$ the map magnifies small intervals $\epsilon = |x_{0,1} - x_{0,2}|$ according to

$$|f^{(\iota_2)}(x_{0,1}) - f^{(\iota_2)}(x_{0,2})| = \epsilon \underbrace{\left(\frac{a}{b}\right)^3 \frac{1}{1-c}}_{>1} \tag{3.23}$$

by use of the derivatives $|\frac{df_1}{dx}| = \frac{a}{b}$ and $|\frac{df_3}{dx}| = \frac{1}{1-c}$. Using equation (2.14) to obtain the Lyapunov exponent at the fixed point $x^*_{\mathbf{T}_2}$ results in

$$\Lambda = \lim_{n\to\infty} \ln \left| \left(\left(\frac{a}{b}\right)^3 \frac{1}{1-c} \right)^{\frac{n}{4}} \right|^{\frac{1}{n}} > 0. \tag{3.24}$$

Hence the fixed point $x^*_{\mathbf{T}_2}$ is unstable and causes distances between neighboring points to increase and therefore the inverse iteration of $\mathbf{T}_2$ to converge to the fixed point. □

3.2.4 Dynamics in the interval

The main interest of this investigation is not only to examine the future of points to a given set of control parameters, but to understand the dynamics as control parameter a changes i.e. increases. So the following treatment will consider the movement of intervals provided by the $\mathbf{T}$-transformations in the interval $[0, \mathbf{f}_1^{-1} c]$ as a increases.

Assuming $a = a_{min} = \mathbf{f}_3^{-1}\mathbf{f}_1^{-1} b$ is equivalent to $0 = \mathbf{T}_1 b$ as indicated by Figure 3.7 showing that x_2 hits the $\mathbf{f}_1$-preimage of b, that is associated with period

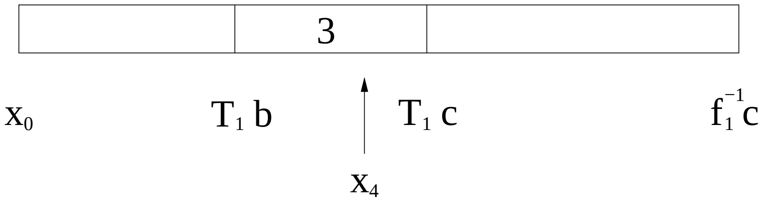

Figure 3.11: The $s_1 = 131$ preimage of $[b, c]$ with length $\iota_1 = 3$ in the interval $[0, \mathbf{f}_1^{-1}c]$.

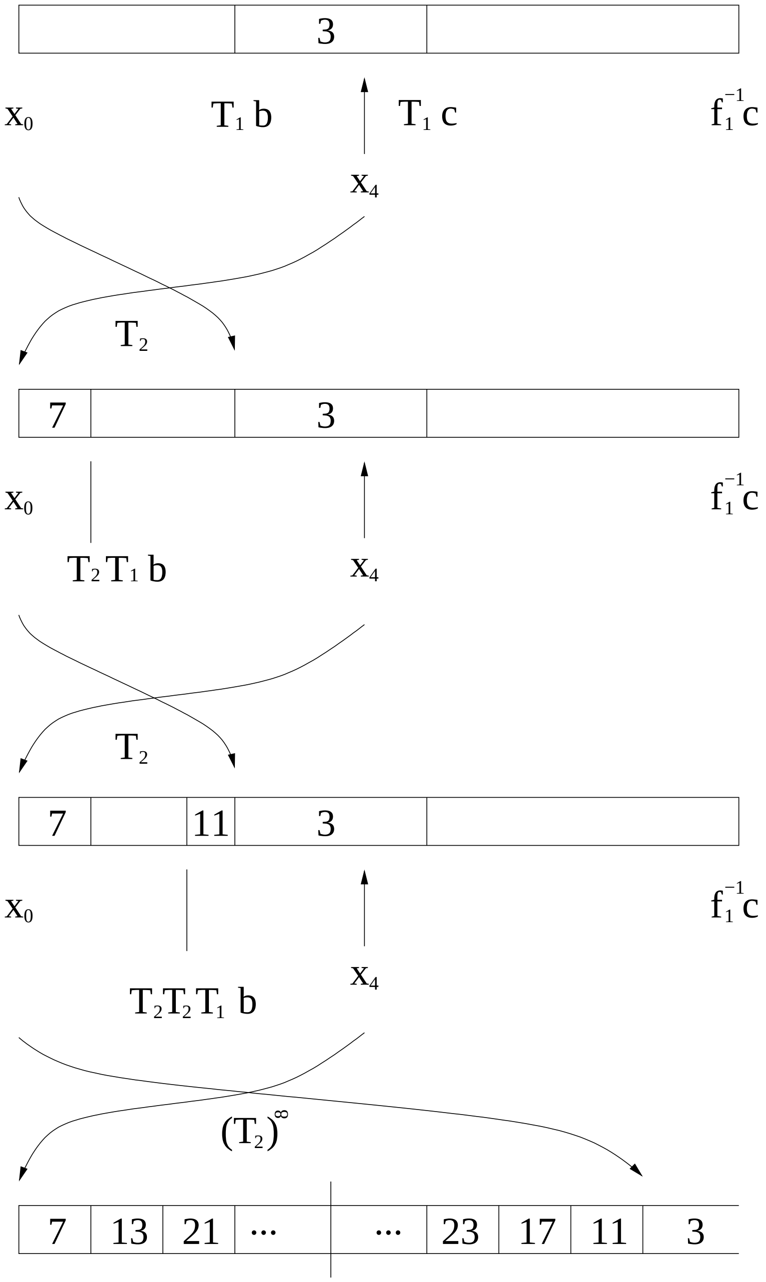

Figure 3.12: The effect of the endomorph operator $\mathbf{T}_2$. The vertical line in the lower picture represents an unstable fixed point under forward iteration.

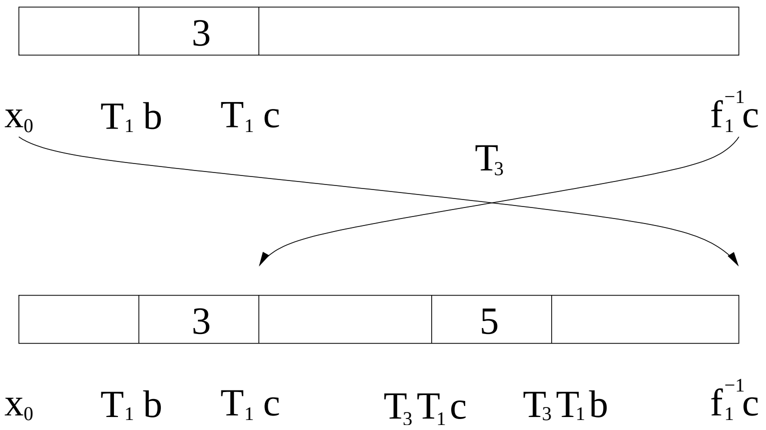

Figure 3.13: The endomorph operator $\mathbf{T}_3$ maps the whole interval twisted into itself.

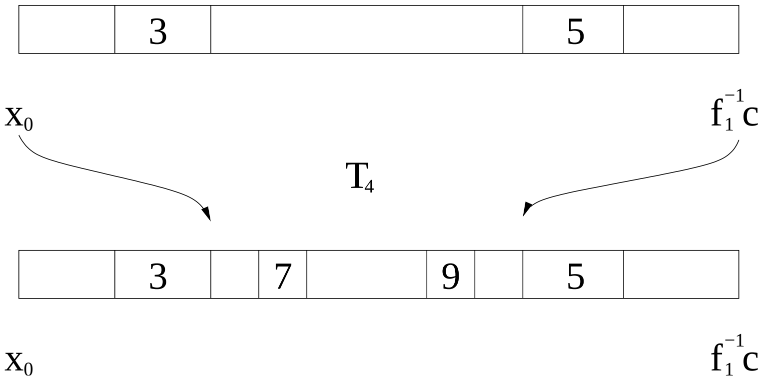

Figure 3.14: The endomorph operator $\mathbf{T}_4$ maps the whole interval conveniently into itself. Labels are spared for clarity.

$p = 2^2$. There the investigation of period-doubling starts.

Due to the continuous connection of $f_1(x)$ and $f_2(x)$ at $x \to b$, $a = a_{min}$ is also equivalent to $x_4 = 0 \in [0, \mathbf{f}_1^{-1}c]$. This ambiguous point $a = a_{min}$ represents some kind of a pitchfork bifurcation[5] in a as will be seen later. Because of $\mathcal{D}(f_2) =]b, c[$ the ambiguous point is formally associated with $x_4 = 0$ only and therefore with period $p = 2^3$ defining $a_{2^3} = a_{min}$.

Theorem 3.2.3. *The period-doubling of the linear map proceeds through all $p = 2^n$ with $n \in \mathbb{N}$ and directly connects superstable orbits at the ambiguous points if Conditions (3.25) to (3.28) are fulfilled.*

$$\frac{c}{b} > \frac{5}{2}(1-c) \tag{3.25}$$

$$\frac{c}{b} > \frac{41}{36} \tag{3.26}$$

$$0 < b < c < 1 \qquad\qquad c < a < 1 \tag{3.27}$$

$$\mathbf{T}_1 c < x_4 = \mathbf{f}_1\mathbf{f}_1\mathbf{f}_3\mathbf{f}_1 x_0 \qquad\qquad x_0 = 0 \tag{3.28}$$

In the following the $\mathbf{T}_i$-transformations with $i = \{1, 2, 4\}$ will be shown to fulfill $\frac{d}{da}\mathbf{T}_i(a)x(a) \in]0, \frac{dx_4}{da}[$ under the condition $0 < \frac{dx}{da} < \frac{dx_4}{da}$. With these properties Theorem 3.2.3 will be proven via induction. Conditions (3.25) and (3.26) are technical assumptions to obtain the proof. Their effect on the shape of the cup map is discussed in the following.

Noting the Theorem 3.2.3 and Lemma 3.2.4 to be based on Condition (3.25), the resulting restrictions to control parameters b and c and hence the shape of the map have to be discussed. Due to $0 < b < c < 1$ the left side is always greater one allowing a critical $c = c_{crit}$ to be calculated. With $c \geq c_{crit}$ Condition (3.25) is always satisfied without any further restrictions on b

$$\frac{c}{b} > 1 \geq \frac{5}{2}(1-c) \qquad \Longrightarrow \qquad c_{crit} = \frac{3}{5} = 0.6. \tag{3.29}$$

[5]The bifurcation is similar to a pitchfork bifurcation but takes place as the iteration hits the function in b or c where the function's derivative is undefined.

Another situation arises with $c \to 0$. In this case

$$c \geq \frac{5}{2} b \Big|_{c \to 0} \tag{3.30}$$

obtains a new criterion to the absorption area, demanding a minimum size of the absorption interval and therewith restricting the vanishing of b.

Condition (3.26) then simply requires another minimum width of the absorption interval by demanding $\frac{c}{b} > \frac{41}{36}$. This condition results in a restriction on b pointed out by

$$\frac{c}{b} > \frac{41}{36} \quad \Longrightarrow \quad c - b = \frac{5}{36} b \quad \Longrightarrow \quad b < b_{crit} = 0.86\overline{1}. \tag{3.31}$$

Because of the numerous but necessary simplifications performed during the proof of Lemma 3.2.4, Lemma 3.2.11 and Lemma 3.2.7 the statement of the theorem may be correct for even less restricted control parameters b and c, but under these conditions the situation is absolutely unambiguous.

Lemma 3.2.4 shows that interval $[\mathbf{T}_1 b, \mathbf{T}_1 c]$ shifts to the right in Figure 3.11 as a increases, only. Otherwise x_4 is shown to move faster to the right than $\mathbf{T}_1 x|_{x \in [b,c]}$. This fact causes $x_4 \in [\mathbf{T}_1 b, \mathbf{T}_1 c]$ for at least $\lim_{\epsilon \to 0} a = a_{min} + \epsilon$ with $\epsilon > 0$. The direct consequence is period[6] $p = \iota_{x_4} + \iota_1 + 1 = 4 + 3 + 1 = 2^3$. So the period has doubled from $p = 2^2$ to $2p = 2^3$ as a increases beyond $a_{min} = \mathbf{f}_3^{-1} \mathbf{f}_1^{-1} b$.

Figure 3.15 shows the already known future diagram of the interval $[0, \mathbf{f}_1^{-1} c]$. In the upper part x_4 approaches the end of the $\mathbf{T}_1$ transformed absorption interval of length $\iota_1 = 3$ as a increases. Following the previous discussion, the $\mathbf{T}_2$ transformation maps the length 3 interval to the length 7 interval covering $x_0 = 0$ and causing the period to be $p = 1 + \iota_2 + \iota_1 = 2^3$.

Application of transformation $\mathbf{T}_4$ causes the interval of length 7 to be mapped to the interval of length 11. If x_4 reaches the critical point $x_4 = \mathbf{T}_1 c$ as pictured, another period-doubling bifurcation takes place due to the emergence of another ambiguous point a_{2^4} formally associated to period $p = 2^4$. At the ambiguous point the period doubles. Because of Lemma 3.2.4, x_4 moves

[6] The $+1$ is due to the absorption process, that is neither included in ι_{x_4} nor ι_1.

faster than the left border of the interval of length 11 causing transformation $\mathbf{T}_2$ to create an interval of length 15 covering the seed value $x_0 = 0$. Lemma 3.2.8 will show x_4 to move directly from interval 7 into interval 11, so the doubled period is $2p = 1 + 1\iota_4 + 2\iota_2 + \iota_1 = 2^4$.

The formerly connected intervals of length 3 and 11 split, because transformation $\mathbf{T}_4$ causes another image of the length 15 interval to be joined to the length 3 interval. This process is sketched in the lower part of Figure 3.15. It is easily verified by further application of transformations $\mathbf{T}_2$ and $\mathbf{T}_4$ that the interval contains two more unstable fixed points denoted by vertical lines in Figure 3.15.

Lemma 3.2.4. *Under Condition (3.27) with $\frac{dx}{da} = 0$ derivative*

$$\frac{d\mathbf{T}_1 x}{da} = \frac{d}{da}\mathbf{f}_1\mathbf{f}_3\mathbf{f}_1 x\Big|_{x\in\mathcal{D}(\mathbf{T}_1)=[b,c]} \tag{3.32}$$

satisfies inequalities

$$\frac{\mathbf{T}_1 x}{da}\Big|_{x\in\mathcal{D}(\mathbf{T}_1)} > 0 \tag{3.33}$$

and

$$\frac{d\mathbf{T}_1 x}{da}\Big|_{x\in\mathcal{D}(\mathbf{T}_1)} < \frac{dx_4}{da}. \tag{3.34}$$

Proof. Straightforward calculation of $\mathbf{T}_1$ by using the operators (3.9) yields

$$\mathbf{T}_1 x\Big|_{x\in[b,c]} = \frac{b^2}{a^2}(1-c)x - \frac{b^2}{a}(1-c) - \frac{bc}{a} + b. \tag{3.35}$$

Differentiating with respect to a reveals

$$\frac{d\mathbf{T}_1 x}{da}\Big|_{x\in[b,c]} = -2\frac{b^2}{a^3}(1-c)x + \frac{b^2}{a^2}(1-c)\underbrace{\frac{dx}{da}}_{=0} + \frac{b^2}{a^2}(1-c) + \frac{bc}{a^2}. \tag{3.36}$$

Minorization and using Condition (3.27) proves inequality (3.33). Due to the definition of the $\mathbf{T}$-transformations x always fulfills $x \in [0, \mathbf{f}_1^{-1}c < b]$.

$$= \frac{bc}{a^2}\left[1 + \frac{b}{c}(1-c)\left(1 - 2\underbrace{\frac{x}{a}}_{<1}\right)\right] > \frac{bc}{a^2}\left[1 - \underbrace{\frac{b}{c}}_{<1}\underbrace{(1-c)}_{<1}\right] > 0$$

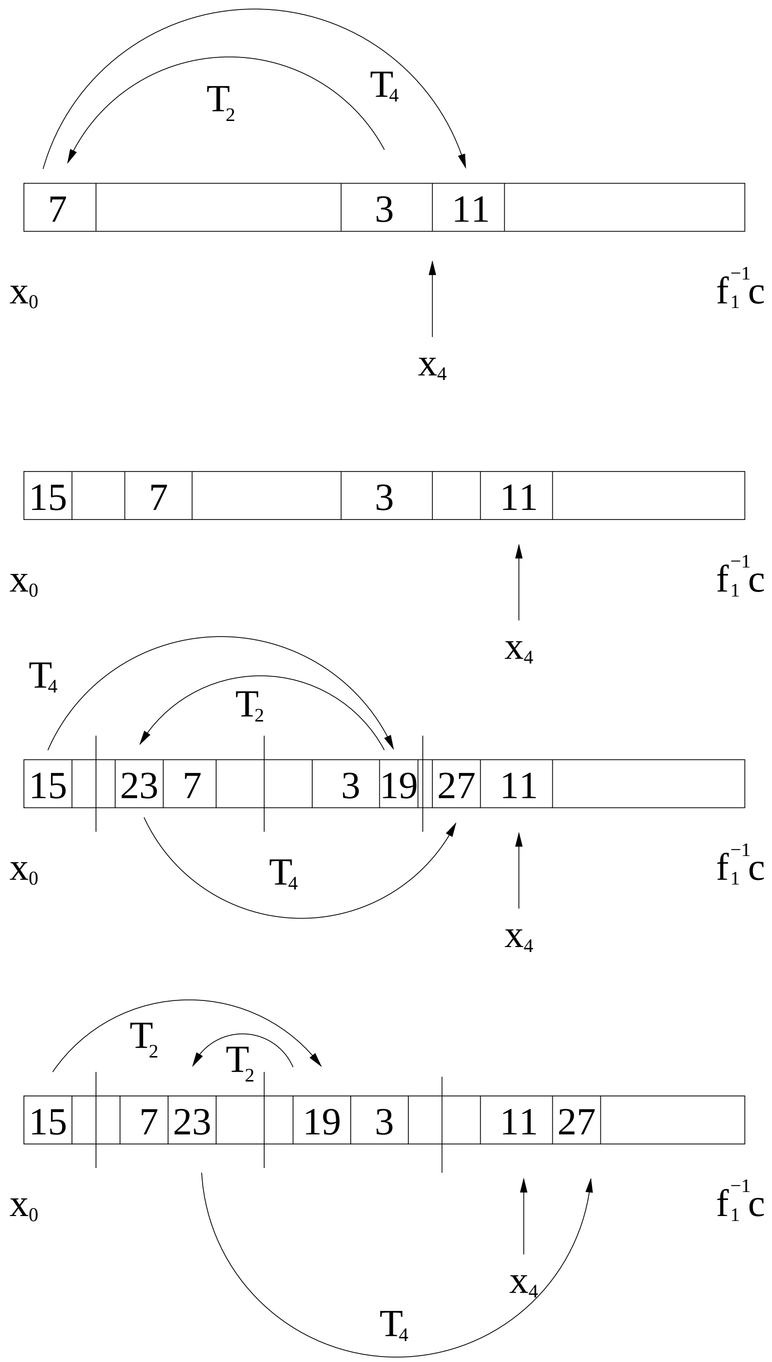

Figure 3.15: The period-doubling from period $p = 2^3$ to period $2p = 2^4$ explained by use of the **T**-transformations results in drastic changes of the future diagram. Vertical lines in the lower parts mark unstable fixed points. In the lowest sketch the emergence of the next period-doubling is visualized with x_4 sliding into interval of length 27 resulting in period $p = 2^5$.

To prove inequality (3.34) the supremum of equation (3.36) is obtained by neglecting the negative term at first.

$$\left.\frac{d\mathbf{T}_1 x}{da}\right|_{x\in[b,c]} = \underbrace{-2\frac{b^2}{a^2}(1-c)\frac{x}{a}}_{<0} + \frac{b^2}{a^2}(1-c) + \frac{bc}{a^2} \tag{3.37}$$

Thereafter other upper bonds are possible, yielding the very simple expression

$$\sup \left.\frac{d\mathbf{T}_1 x}{da}\right|_{x\in[b,c]} < (1-c)\frac{b^2}{a^2} + \underbrace{\frac{b}{a}\frac{c}{a}}_{<1} < (1-c)\underbrace{\frac{b^2}{a^2}}_{<1} + 1 < 1-c+1$$

$$\sup \left.\frac{d\mathbf{T}_1 x}{da}\right|_{x\in[b,c]} < \underbrace{2(1-c)}_{\stackrel{def}{=}F_1} + c \tag{3.38}$$

defining F_1.

Evaluating $x_4 = \mathbf{f}_1\mathbf{f}_1\mathbf{f}_3 a$ yields

$$x_4 = \frac{1}{1-c}\frac{a^3}{b^2} - \frac{c}{1-c}\frac{a^2}{b^2} - \frac{a^2}{b} + a \tag{3.39}$$

and derivative

$$\frac{dx_4}{da} = \frac{3}{1-c}\frac{a^2}{b^2} - \frac{2}{1-c}\frac{c}{b}\frac{a}{b} - 2\frac{a}{b} + 1. \tag{3.40}$$

$$= \frac{1}{1-c}\frac{a^2}{b^2} + \underbrace{\frac{2}{1-c}\frac{a^2}{b^2} - \frac{2}{1-c}\frac{c}{b}\frac{a}{b}}_{>0} - 2\frac{a}{b} + 1$$

The first term of Derivative (3.40) positively dominates at least the second term resulting in the following lower bond by use of Prerequisite (3.27).

$$\frac{dx_4}{da} > \frac{1}{1-c}\frac{a^2}{b^2} - 2\frac{a}{b} + 1 \tag{3.41}$$

Then quadratic completion reveals a more concise expression.

$$= \frac{1}{1-c}\left[\underbrace{\frac{a^2}{b^2} - 2(1-c)\frac{a}{b} + (1-c)^2}_{=\left(\frac{a}{b}-(1-c)\right)^2} - (1-c)^2\right] + 1$$

$$= \frac{1}{1-c}\left(\frac{a}{b} - (1-c)\right)^2 - (1-c) + 1$$

Finally the lower bond of Derivative (3.40) results in

$$\frac{dx_4}{da} > \underbrace{\frac{1}{1-c}\left(\frac{a}{b} - (1-c)\right)^2}_{\stackrel{def}{=} F_2} + c \tag{3.42}$$

defining F_2. To prove inequality (3.34) it is sufficient to show $F_1 < F_2$, which is equivalent to

$$(1-c)F_1 < (1-c)F_2. \tag{3.43}$$

Conditions (3.25) and (3.27) minorize the right side.

$$\frac{9}{4}(1-c)^2 = \left(\frac{5}{2}(1-c) - (1-c)\right)^2 < \left(\frac{a}{b} - (1-c)\right)^2 = (1-c)F_2 \tag{3.44}$$

$$(1-c)F_1 = 2(1-c)^2 < \frac{9}{4}(1-c)^2 \tag{3.45}$$

This minorization is correct because of $\frac{a}{b} > \frac{c}{b} > 1$ and $1 - c < 1$ that causes the bracketed and squared term in inequality (3.44) to reduce in value only. Inequalities (3.44) and (3.45) prove inequality (3.43) and therewith inequality (3.34). □

Lemma 3.2.5. *Under Condition*

$$0 < \frac{dx}{da} < \frac{dx_4}{da} \tag{3.46}$$

operator $\mathbf{T}_2$ *satisfies inequalities*

$$\frac{d\mathbf{T}_2 x}{da} > 0 \tag{3.47}$$

and

$$\frac{\mathbf{T}_2 x}{da} < \frac{dx_4}{da} \tag{3.48}$$

with $x \in \mathcal{D}(\mathbf{T}_2) = [0, x_4]$.

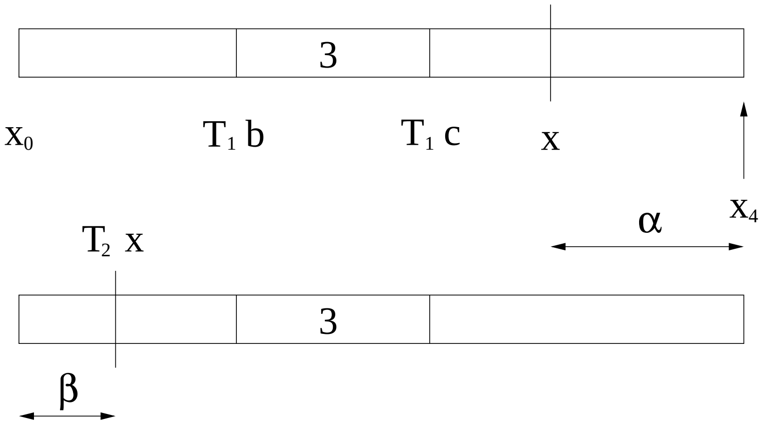

Figure 3.16: Effect of derivative $\frac{dx}{da}$ on derivative $\frac{\mathbf{T}_2 x}{da}$.

Proof. In Figure 3.16 the mapping of $\mathbf{T}_2$ applied to $x \in \mathcal{D}(\mathbf{T}_2)$ is visualized. Under Condition (3.46) distance α is easily seen to grow.

$$\frac{dx}{da} < \frac{dx_4}{da} \quad \Longrightarrow \quad \frac{d\alpha}{da} > 0 \quad \overset{\text{(eqn 3.19)}}{\Longrightarrow} \quad \frac{d\beta}{da} > 0 \quad \Longrightarrow \quad \frac{d\mathbf{T}_2 x}{da} > 0$$

Because of the linear transformation of distances by $\mathbf{T}_2$, the derivative of β conserves the sign of α's derivative and therewith proves inequality (3.47).

To prove inequality (3.48) the derivative of $\mathbf{T}_2 x$ is obtained by differentiating equation (3.19) with $x = x(a)$.

$$\begin{aligned} \frac{d\mathbf{T}_2 x}{da} &= \underbrace{\frac{d\mathbf{T}_1 b}{da}}_{\overset{\text{(lem 3.2.4)}}{<} \frac{dx_4}{da}} \underbrace{\left(1 - \frac{x}{x_4}\right)}_{\in[0,1]} - \frac{(\mathbf{T}_1 b)}{x_4}\frac{dx}{da} + \frac{(\mathbf{T}_1 b)}{x_4}\frac{x}{x_4}\frac{dx_4}{da} \\ &< \frac{dx_4}{da}\left(1 - \frac{x}{x_4} + \frac{(\mathbf{T}_1 b)}{x_4}\frac{x}{x_4}\right) - \frac{(\mathbf{T}_1 b)}{x_4}\frac{dx}{da} \end{aligned} \tag{3.49}$$

The factor $\frac{(\mathbf{T}_1 b)}{x_4}$ lies in $[0,1]$, due to Lemma 3.2.4 and the initial ambiguous point $x_4 = \mathbf{T}_1 b\Big|_{a=a_{min}} = 0$ discussed in the beginning of this section.

$$= \frac{dx_4}{da} \underbrace{\left(1 + \underbrace{\frac{x}{x_4}}_{\in[0,1]} \underbrace{\left(\frac{(\mathbf{T}_1 b)}{x_4} - 1 \right)}_{\in[-1,0]} \right)}_{\in[0,1]} - \underbrace{\frac{(\mathbf{T}_1 b)}{x_4}}_{\in[0,1]} \frac{dx}{da} \overset{\text{(eqn 3.46)}}{<} \frac{dx_4}{da}$$

□

Lemma 3.2.6. *Condition (3.26) implies*

$$\frac{a}{b} > \frac{10}{9}. \tag{3.50}$$

Proof. With $a \in [\mathbf{f}_3^{-1}\mathbf{f}_1^{-1}b, \mathbf{f}_3^{-1}\left(\mathbf{f}_1^{-1}\right)^3 c]$ the $\mathbf{T}_i$-transformations with $i \in \{1,2,3,4\}$ provide a non-empty domain according to Figure 3.7. Obviously

$$\mathbf{f}_1^{-1}b \leq \mathbf{f}_3 a \qquad \Longleftrightarrow \qquad b - \frac{b^2}{a} \leq \frac{a-c}{1-c} \tag{3.51}$$

is satisfied. Rearranging and substituting of $x = \frac{a}{b} \in]1, \infty[$ yields

$$0 \geq x^2 - \frac{7}{a}\frac{c}{b}x + \frac{c}{b} \overset{def}{=} F(x) \tag{3.52}$$

according to Condition (3.27). Function $F(x)$ possesses a minimum at $x_E = \frac{7}{10}\frac{c}{b}$. Inserting x_E in $F(x)$ reveals, that the function is negative at its minimum by use of Condition (3.27)

$$F(x_E) = -\left(\frac{7}{10} \underbrace{\frac{c}{b}}_{>1} \right)^2 + \frac{7}{10} \underbrace{\frac{c}{b}}_{>1} < 0.$$

To obtain a lower limit for x satisfying inequality (3.52) the limiting case is solved as a quadratic equation, giving

$$x_{limit} = \frac{7}{10}\frac{c}{b} + \sqrt{\left(\frac{7}{10}\frac{c}{b}\right)^2 - \frac{2}{5}\frac{c}{b}}.$$

Substitution of $\frac{c}{b} = 1 + \epsilon$ with $\epsilon > 0$ reveals solution

$$x_{limit} = \frac{7}{10}(1+\epsilon)+\frac{1}{10}\sqrt{9 + 18\epsilon + 49\epsilon^2} > \frac{7}{10}(1+\epsilon)+\frac{1}{10}\underbrace{\sqrt{9 + 6\epsilon + \epsilon^2}}_{=3+\epsilon}. \quad (3.53)$$

Use of Condition (3.26) in equation (3.53) yields

$$\frac{a}{b} \geq x_{limit} > \frac{7}{10}(1 + \epsilon) + \frac{1}{10}(3 + \epsilon) = 1 + \frac{8}{10}\epsilon \quad (3.54)$$

concluding the proof by

$$1 + \epsilon = \frac{c}{b} > \frac{41}{36} \qquad \Longrightarrow \qquad \epsilon > \frac{5}{36} \qquad \Longrightarrow \frac{a}{b} > \frac{10}{9}.$$

□

Lemma 3.2.7. *(1) Inequality*

$$0 < \alpha_{\mathbf{T}_4} < \frac{4}{25} \quad (3.55)$$

is valid.

(2)Under Conditions (3.25), (3.26) and

$$0 < \frac{dx}{da} < \frac{dx_4}{da} \quad (3.56)$$

the following inequalities are satisfied.

(a)

$$\frac{d}{da}\mathbf{T}_4 x > 0 \quad (3.57)$$

(b)

$$\frac{d}{da}\mathbf{T}_4 x < \frac{dx_4}{da} \quad (3.58)$$

Proof. (1) Definition of $\mathbf{T}_4$ in equation (3.16) offers the opportunity to use the derivatives $\frac{d\mathbf{f}_1^{-1}}{dx} = -\frac{b}{a}$ and $\frac{d\mathbf{f}_3^{-1}}{dx} = 1 - c$ to calculate $\alpha_{\mathbf{T}_4}$ explicitly as a simple function of the control parameters shown in

$$\alpha_{\mathbf{T}_4} = \left(\frac{d\mathbf{f}_1^{-1}x}{dx}\right)^2 \left(\frac{d\mathbf{f}_3^{-1}x}{dx}\right)^2 = \left(\frac{b}{a}\right)^2 (\underbrace{1 - c}_{\overset{\text{eqn 3.25}}{>} \frac{2}{5}\frac{c}{b}})^2 < 1 \quad (3.59)$$

according to $s_4 = 1313$. Obviously $\alpha_{\mathbf{T}_4}$ is positive. Using Condition (3.25) results in inequality

$$\alpha_{\mathbf{T}_4} \overset{\text{(eqn 3.25)}}{<} \left(\frac{b}{a}\right)^2 \left(\frac{c}{b}\right)^2 \frac{4}{25} \overset{\text{(eqn 3.27)}}{<} \frac{4}{25} \tag{3.60}$$

proving the assertion.

(2a) Inequality (3.57) is proved by the fact, that operator $\mathbf{T}_4$ maps its domain linearly into interval $[\mathbf{T}_1 c, \mathbf{T}_3\mathbf{T}_1 c]$ with a positive $\alpha_{\mathbf{T}_4}$. The derivative of $\alpha_{\mathbf{T}_4}$ is calculated to

$$\frac{d\alpha_{\mathbf{T}_4}}{da} = -\frac{2}{a}\alpha_{\mathbf{T}_4} < 0 \tag{3.61}$$

that implies the movement of the interval borders $[\mathbf{T}_1 c, \mathbf{T}_3\mathbf{T}_1 c]$ to obey

$$\frac{d\mathbf{T}_1 c}{da} > \frac{d\mathbf{T}_3\mathbf{T}_1 c}{da} \tag{3.62}$$

due to the alternate Definition (3.21) of $\mathbf{T}_4$. Derivative $\frac{d\mathbf{T}_3\mathbf{T}_1 c}{da}$ will be shown to be positive so that the whole codomain will move to the right while it is shrinking as a increases. So, no point x with $\frac{dx}{da} > 0$ can satisfy $\frac{d\mathbf{T}_4 x}{da} < 0$. Evaluating the derivative $\frac{d}{da}\mathbf{T}_3\mathbf{T}_1$ according to Definition (3.20) yields

$$\frac{d}{da}\mathbf{T}_3\mathbf{T}_1 c = \left(2\frac{\mathbf{T}_1 c}{\mathbf{f}_1^{-1} c} - 1\right)\frac{d\mathbf{T}_1 c}{da} + \left(1 - \left(\frac{\mathbf{T}_1 c}{\mathbf{f}_1^{-1} c}\right)^2\right)\frac{d\mathbf{f}_1^{-1} c}{da}. \tag{3.63}$$

By differentiating $\alpha_{\mathbf{T}_3} = -\frac{b}{a}(1-c)$, $\frac{d}{da}\alpha_{\mathbf{T}_3} = \frac{b}{a^2}(1-c) > 0$ is obtained. Following Definition (3.20), relationship

$$\frac{d\mathbf{T}_1 c}{da} < \frac{d\mathbf{f}_1^{-1} c}{da} \tag{3.64}$$

is obtained, which is shown minorize equation (3.63).

$$\frac{d}{da}\mathbf{T}_3\mathbf{T}_1 c = \left(2\underbrace{\frac{\mathbf{T}_1 c}{\mathbf{f}_1^{-1} c}}_{\in[0,1]} - \left(\underbrace{\frac{\mathbf{T}_1 c}{\mathbf{f}_1^{-1} c}}_{\in[0,1]}\right)^2\right)\underbrace{\frac{d\mathbf{T}_1 c}{da}}_{\overset{\text{(lem 3.2.4)}}{>}0} > 0 \tag{3.65}$$

Because of the faster and positive movement of the left interval border by equation (3.62) and Lemma 3.2.4 as a increases, the derivative $\frac{d}{da}\mathbf{T}_4 x$ can not be negative unless $\frac{dx}{da} < 0$ that is prohibited by Assumption (3.56).

(2b) To prove inequality (3.58) the derivative of $\mathbf{T}_4 x$ is rewritten to

$$\frac{d}{da}\mathbf{T}_4(a)x(a) = \frac{d}{da}\left[\alpha_{\mathbf{T}_4}(a)x(a) + \beta(a)\right] \tag{3.66}$$

making use of the operator group representation. Because of inequality (3.61) $\frac{d\alpha_{\mathbf{T}_4}}{da}$ is negative and can be neglected.

$$\frac{d}{da}\mathbf{T}_4(a)x(a) = \underbrace{\frac{d\alpha_{\mathbf{T}_4}}{da}}_{\overset{(\text{eqn } 3.61)}{<} 0} x + \underbrace{\alpha_{\mathbf{T}_4}}_{\overset{(\text{lem } 3.2.7(1))}{<} \frac{4}{25}} \frac{dx}{da} + \underbrace{\frac{d\beta}{da}}_{\overset{(\text{eqn } 3.21)}{=} \frac{d\mathbf{T}_1 c}{da}} \tag{3.67}$$

By assuming the limiting case $\frac{dx}{da} = \frac{dx_4}{da}$, it is sufficient to show

$$\frac{d\mathbf{T}_1 c}{da} < \frac{21}{25}\frac{dx_4}{da} \tag{3.68}$$

to be valid to prove inequality (3.58). Starting with equation (3.37) and $x = c$ yields

$$\frac{d\mathbf{T}_1 c}{da} = \underbrace{-2\frac{b^2}{a^2}(1-c)\frac{c}{a}}_{<0} + \frac{b^2}{a^2}(1-c) + \frac{bc}{a^2} \tag{3.69}$$

$$\frac{d\mathbf{T}_1 c}{da} < \frac{b^2}{a^2}\underbrace{(1-c)}_{\overset{(\text{eqn } 3.25)}{<} \frac{2}{5}\frac{c}{b}} + \frac{bc}{a^2} < \frac{2}{5}\frac{b^2}{a^2}\frac{c}{b} + \frac{bc}{a^2} = \frac{7}{5}\underbrace{\frac{b}{a}}_{\overset{(\text{lem } 3.2.6)}{<} \frac{9}{10}}\underbrace{\frac{c}{a}}_{<1} < \frac{63}{50}. \tag{3.70}$$

Using inequality (3.41) offers a minorization of expression $\frac{21}{25}\frac{dx_4}{da}$ resulting in inequality (3.72).

$$\frac{21}{25}\frac{dx_4}{da} > \frac{21}{25}\left[\underbrace{\frac{1}{1-c}}_{\substack{(\text{eqn } 3.27)\\(\text{eqn } 3.25)\\ >}\ \frac{5}{2}\frac{b}{a}}\frac{a^2}{b^2} - 2\frac{a}{b} + 1\right] \tag{3.71}$$

$$> \frac{21}{25}\left[\frac{5}{2}\frac{a}{b} - 2\frac{a}{b} + 1\right]$$

$$\frac{21}{25}\frac{dx_4}{da} > \frac{21}{25}\left[\frac{1}{2}\underbrace{\frac{a}{b}}_{>1} + 1\right] > \frac{63}{50} \tag{3.72}$$

Inequality (3.72) and inequality (3.70) prove inequality (3.68) and therefore inequality (3.58).

□

Lemma 3.2.8 (Conclusions). *The period-doubling from period $p = 2^3$ to $2p = 2^4$ happens without gap due to the validity of*
(1)

$$0 < \frac{d}{da}\mathbf{T}_4\mathbf{T}_2\mathbf{T}_1 x\bigg|_{x\in\mathcal{D}(\mathbf{T}_1)} < \frac{dx_4}{da} \tag{3.73}$$

and Lemma 3.2.4. Another consequence is the validity of inequalities
(2)

$$0 < \frac{d}{da}\mathbf{T}_4\mathbf{T}_2\mathbf{T}_2\mathbf{T}_2 x\bigg|_{x\in\mathcal{D}(\mathbf{T}_2),0<\frac{dx}{da}<\frac{dx_4}{da}} < \frac{dx_4}{da} \tag{3.74}$$

and (3)

$$0 < \frac{d}{da}\mathbf{T}_4\mathbf{T}_2\mathbf{T}_4\mathbf{T}_2 x\bigg|_{x\in\mathcal{D}(\mathbf{T}_2),0<\frac{dx}{da}<\frac{dx}{da}} < \frac{dx_4}{da}. \tag{3.75}$$

Proof. (1)

$$0 \overset{\substack{\text{(eqn 3.73)}\\\text{(lem 3.2.4)}}}{<} \frac{d}{da}\mathbf{T}_1 x \overset{\substack{\text{(eqn 3.73)}\\\text{(lem 3.2.4)}}}{<} \frac{dx_4}{da} \overset{\text{(lem 3.2.5)}}{\Longrightarrow} 0 < \frac{d}{da}\mathbf{T}_2\mathbf{T}_1 x < \frac{dx_4}{da}$$

$$\overset{\text{(lem 3.2.7)}}{\Longrightarrow} 0 < \frac{d}{da}\mathbf{T}_4\mathbf{T}_2\mathbf{T}_1 x < \frac{dx_4}{da}$$

(2)

$$0 \overset{\substack{\text{(eqn 3.74)}\\\text{(lem 3.2.5)}}}{<} \frac{d}{da}\mathbf{T}_2 x \overset{\substack{\text{(eqn 3.74)}\\\text{(lem 3.2.5)}}}{<} \frac{dx_4}{da} \overset{\text{(lem 3.2.5)}}{\Longrightarrow} 0 < \frac{d}{da}\mathbf{T}_2\mathbf{T}_2 x < \frac{dx_4}{da}$$

$$\overset{\text{(lem 3.2.5)}}{\Longrightarrow} 0 < \frac{d}{da}\mathbf{T}_2\mathbf{T}_2\mathbf{T}_2 x < \frac{dx_4}{da} \overset{\text{(lem 3.2.7)}}{\Longrightarrow} 0 < \frac{d}{da}\mathbf{T}_4\mathbf{T}_2\mathbf{T}_2\mathbf{T}_2 x < \frac{dx_4}{da}$$

(3)

$$0 \overset{\substack{\text{(eqn 3.75)}\\\text{(lem 3.2.5)}}}{<} \frac{d}{da}\mathbf{T}_2 x \overset{\substack{\text{(eqn 3.75)}\\\text{(lem 3.2.5)}}}{<} \frac{dx_4}{da} \overset{\text{(lem 3.2.7)}}{\Longrightarrow} 0 < \frac{d}{da}\mathbf{T}_4\mathbf{T}_2 x < \frac{dx_4}{da}$$

$$\overset{\text{(lem 3.2.5)}}{\Longrightarrow} 0 < \frac{d}{da}\mathbf{T}_2\mathbf{T}_4\mathbf{T}_2 x < \frac{dx_4}{da} \overset{\text{(lem 3.2.7)}}{\Longrightarrow} 0 < \frac{d}{da}\mathbf{T}_4\mathbf{T}_2\mathbf{T}_4\mathbf{T}_2 x < \frac{dx_4}{da}$$

□

Theorem 3.2.9. *The inverse period-doubling iteration of the absorption interval by using* $\mathbf{T}$*-transformations is expressed by the period-doubling operator*

$$\mathbf{P}_{2^n} = \mathbf{T}_2(\mathbf{T_4T_2T_2T_2})(\mathbf{T_4T_2T_2T_2T_4T_2T_2T_2})^{k(n)}\mathbf{T_4T_2T_1} \qquad n \geq 5$$
$$k(n) = 2^{n-5} - 1. \tag{3.76}$$

Proof. Analyzing the symbolic period-doubling sequences σ_{2p} defined in equation (3.5) on page 30 period-doubling Operator $\mathbf{P}_{2^n}$ is recognized to possess a non-empty domain. Therefore Table 3.2.4 shows the period-doubled sequences explicitly, showing exponent k to fulfill the recurrence relation

$$k(n+1) = 2k(n) + 1 \qquad n \geq 5, k(5) = 0 \tag{3.77}$$

that is easily identified to equation

$$k(n) = 2^{n-5} - 1 \qquad n \geq 5. \tag{3.78}$$

□

Proof of Theorem 3.2.3. The period-doubling operator

$$\mathbf{P}_{2^n} = \mathbf{T}_2(\mathbf{T_4T_2T_2T_2})(\mathbf{T_4T_2T_2T_2T_4T_2T_2T_2})^{k(n)}\mathbf{T_4T_2T_1} \qquad n \geq 5$$

is composed of operator sequences of $\mathbf{T}$-transformations

$$\mathbf{T}_4\mathbf{T}_2\mathbf{T}_2\mathbf{T}_2 \tag{3.79}$$

and

$$\mathbf{T}_4\mathbf{T}_2\mathbf{T}_4\mathbf{T}_2. \tag{3.80}$$

n	σ_{2n}
0	1
1	$\underbrace{131}_{\mathbf{T}_1}$
3	$\underbrace{1311}_{\mathbf{T}_2}\ \underbrace{131}_{\mathbf{T}_1}$
4	$\underbrace{1311\ 1313\ 1311\ 131}_{\mathbf{T}_2\mathbf{T}_4\mathbf{T}_2\mathbf{T}_1}$
5	$\underbrace{1311\ 1313\ 1311\ 1311\ 1311\ 1313\ 1311\ 131}_{\mathbf{T}_2(\mathbf{T}_4\mathbf{T}_2\mathbf{T}_2\mathbf{T}_2)(...)^0\mathbf{T}_4\mathbf{T}_2\mathbf{T}_1}$
6	$\underbrace{1311\ 1313\ 1311\ 1311\ 1311\ 1313\ 1311\ 1313}_{\mathbf{T}_2\mathbf{T}_4\mathbf{T}_2\mathbf{T}_2\mathbf{T}_2\mathbf{T}_4\mathbf{T}_2\mathbf{T}_4}$ $\underbrace{1311\ 1313\ 1311\ 1311\ 1311\ 1313\ 1311\ 131}_{\mathbf{T}_2\mathbf{T}_4\mathbf{T}_2\mathbf{T}_2\mathbf{T}_2\mathbf{T}_4\mathbf{T}_2\mathbf{T}_1}$
	$\Longrightarrow \mathbf{T}_2(\mathbf{T}_4\mathbf{T}_2\mathbf{T}_2\mathbf{T}_2)(\mathbf{T}_4\mathbf{T}_2\mathbf{T}_4\mathbf{T}_2\mathbf{T}_4\mathbf{T}_2\mathbf{T}_2\mathbf{T}_2)^1\mathbf{T}_4\mathbf{T}_2\mathbf{T}_1$
7	$\underbrace{1311\ 1313\ 1311\ 1311\ 1311\ 1313\ 1311\ 1313}_{\mathbf{T}_2\mathbf{T}_4\mathbf{T}_2\mathbf{T}_2\mathbf{T}_2\mathbf{T}_4\mathbf{T}_2\mathbf{T}_4}$ $\underbrace{1311\ 1313\ 1311\ 1311\ 1311\ 1313\ 1311\ 1311}_{\mathbf{T}_2\mathbf{T}_4\mathbf{T}_2\mathbf{T}_2\mathbf{T}_2\mathbf{T}_4\mathbf{T}_2\mathbf{T}_2}$ $\underbrace{1311\ 1313\ 1311\ 1311\ 1311\ 1313\ 1311\ 1313}_{\mathbf{T}_2\mathbf{T}_4\mathbf{T}_2\mathbf{T}_2\mathbf{T}_2\mathbf{T}_4\mathbf{T}_2\mathbf{T}_4}$ $\underbrace{1311\ 1313\ 1311\ 1311\ 1311\ 1313\ 1311\ 131}_{\mathbf{T}_2\mathbf{T}_4\mathbf{T}_2\mathbf{T}_2\mathbf{T}_2\mathbf{T}_4\mathbf{T}_2\mathbf{T}_1}$ $\Longrightarrow \mathbf{T}_2(\mathbf{T}_4\mathbf{T}_2\mathbf{T}_2\mathbf{T}_2)\underbrace{\mathbf{T}_4\mathbf{T}_2\mathbf{T}_4\mathbf{T}_2\mathbf{T}_4\mathbf{T}_2\mathbf{T}_2\mathbf{T}_2\mathbf{T}_4\mathbf{T}_2\mathbf{T}_2\mathbf{T}_2\mathbf{T}_4\mathbf{T}_2\mathbf{T}_2\mathbf{T}_2\mathbf{T}_4\mathbf{T}_2\mathbf{T}_4\mathbf{T}_2\mathbf{T}_4\mathbf{T}_2\mathbf{T}_2\mathbf{T}_2}_{(\mathbf{T}_4\mathbf{T}_2\mathbf{T}_4\mathbf{T}_2\mathbf{T}_4\mathbf{T}_2\mathbf{T}_2\mathbf{T}_2)^3}\mathbf{T}_4\mathbf{T}_2\mathbf{T}_1$
8	$\Longrightarrow \mathbf{T}_2(\mathbf{T}_4\mathbf{T}_2\mathbf{T}_2\mathbf{T}_2)(\mathbf{T}_4\mathbf{T}_2\mathbf{T}_4\mathbf{T}_2\mathbf{T}_4\mathbf{T}_2\mathbf{T}_2\mathbf{T}_2)^7\mathbf{T}_4\mathbf{T}_2\mathbf{T}_1$
9	$\Longrightarrow \mathbf{T}_2(\mathbf{T}_4\mathbf{T}_2\mathbf{T}_2\mathbf{T}_2)(\mathbf{T}_4\mathbf{T}_2\mathbf{T}_4\mathbf{T}_2\mathbf{T}_4\mathbf{T}_2\mathbf{T}_2\mathbf{T}_2)^{15}\mathbf{T}_4\mathbf{T}_2\mathbf{T}_1$

Table 3.2: The period-doubling sequences σ_{2n} and the representation in **T**-transformations.

By Lemma 3.2.8 Derivative (3.73) is known to be positive and limited in value. As a consequence the derivative of Operator (3.79) with respect to a fulfills the same properties and so does the derivative of (3.80). By induction

$$\mathbf{T}_2^{-1}\mathbf{P}_{2^n} < \frac{dx_4}{da} \tag{3.81}$$

is valid and proves all periods $p_n = 2^n$, $n \in \mathbb{N}$ to exist, because x_4 slides through interval $[0, \mathbf{f}_1^{-1}c]$ faster than any $\mathbf{T}_2^{-1}\mathbf{P}_{2^n}$ image of the absorption interval $[b, c]$, giving successive rise to bifurcations as illustrated in Figure 3.15.

Due to the vanishing derivative of function f in the interval $]bc[$ the orbits are superstable according to equation (2.9) on page 12 with $x_4 \in]\mathbf{T}_2^{-1}\mathbf{P}_{2^n}y_1$, $\mathbf{T}_2^{-1}\mathbf{P}_{2^n}y_2[$, y_1, $y_2 \in \{b, c\}$. Just in case of x_4 hitting the border between connected intervals, ambiguous points exist, associated to degenerate non-superstable periodic points of period p and $2p$ simultaneously.

□

An interesting difference to period-doubling in unimodal maps and the cup-map is the opposite dominance of orbits regarding superstability. In unimodal maps there are single points in the control parameter's period p interval associated with superstability surrounded by stable intervals. The linear cup map features superstability in the whole range of the interval except for the ambiguous points at the borders of the parameter's period p interval.

3.2.5 Implicit period-doubling operator

In the previous section the period-doubling operator has been defined as backward iteration resembling the symbolic period-doubling sequences defined for $a > b$ that cause fixed point x_1^* to be unstable and give rise to period-doubling as a increases. The sequences of period-doubled orbits have been excessively generated by use of equations (3.5) and (3.6).

Finally the period-doubling operator has been defined via the $\mathbf{T}$-transformations in its operator representation and therewith period-doubling could be shown to pass all $p = 2^n$, $n \in \mathbb{N}$ periods. Because of the necessity to numerically investigate the period-doubling behavior in order to obtain the period-doubling function, a more convenient representation of the period-doubling operator is desirable. The main advantage is due to the group nature of the operators $\mathbf{f}_i$, $i \in \{1, 2, 3\}$ (3.3) allowing to calculate $\alpha_{\mathbf{P}_{2^n}}$ and $\beta_{\mathbf{P}_{2^n}}$ once and perform arbitrary many iterations by use of

$$\mathbf{P}_{2^n} = \alpha_{\mathbf{P}_{2^n}} \cdot + \beta_{\mathbf{P}_{2^n}} \overset{def}{=} \mathbf{P}_{2^n}(a,b,c) = \alpha_{\mathbf{P}_{2^n}}(a,b,c) \cdot + \beta_{\mathbf{P}_{2^n}}(a,b,c) \tag{3.82}$$

thereafter instead of iterating each point $x \in \mathcal{D}(\mathbf{P}_{2^n})$ by use of successive and time consuming application of $\mathbf{T}$-transformations to each point under iteration.

The well behaved Operators (3.3) and (3.9) with their group structure allow to derive an analytical expression for any admissible sequence s_p to make arbitrary forward as well as backward iterations possible in a single operation. Operator (3.82) will be derived as a function of n, and the control parameters a, b and c to the sequence σ_{2^n}. The backward iteration on $x \in [b,c]$ due to sequence $s_{2^n} = \sigma_{2^n} s_{2^n,2^n}$ is performed by application of the operator $\mathbf{P}_{2^n}$, which resembles the the backward iteration according to the reverse read σ_{2^n} sequence. By solving equation

$$0 = \mathbf{P}_{2^n}(a)x \Big|_{x\in\{b,c\}} \tag{3.83}$$

for a, period-doubling bifurcations a_{2^n} and $a_{2^{n+1}}$ can be located in order to study the period-doubling function[7].
The period-doubling sequences can be rewritten by introducing operator $\mathbf{A}_{2^n}$ and $\mathbf{B}_n$ According to Table 3.3.

$$\mathbf{P}_{2^n} = \mathbf{A}_{2^n}\mathbf{f}_1^{-1} \tag{3.84}$$

$$\mathbf{A}_{2^n} = \mathbf{A}_{2^{n-1}}\mathbf{B}_n\mathbf{A}_{2^{n-1}} \qquad\qquad n \geq 2, \mathbf{A}_{2^1} = \mathbf{id} \tag{3.85}$$

$$\mathbf{A}_{2^1} = \mathbf{id} \qquad \Longleftrightarrow \qquad \alpha_{\mathbf{A}_{2^1}} = 1, \quad \beta_{\mathbf{A}_{2^1}} = 0 \tag{3.86}$$

$$\mathbf{B}_n = \begin{cases} \mathbf{B}_e = \mathbf{f}_1^{-1}\mathbf{f}_3^{-1} & n \text{ even} \\ \mathbf{B}_o = \mathbf{f}_1^{-1}\mathbf{f}_1^{-1} & n \text{ odd} \end{cases} \tag{3.87}$$

Operator $\mathbf{B}_n$ can be expressed by

$$\mathbf{B}_n = \frac{1}{2}(1+(-1)^n)\mathbf{B}_e + \frac{1}{2}(1-(-1)^n)\mathbf{B}_o \tag{3.88}$$

yielding the final expression

[7]The period-doubling function is the exponentially growing equivalent to the *Feigenbaum constant* δ in unimodal maps for the cup map.

n	σ_{2^n}	$\mathbf{P}_{2^n}$
1	1	1
2	131	$\mathbf{B}_e 1$
3	1311131	$\mathbf{B}_e\mathbf{B}_o\mathbf{B}_e 1$
4	131113131311131	$\mathbf{B}_e\mathbf{B}_o\mathbf{B}_e\mathbf{B}_e\mathbf{B}_e\mathbf{B}_o\mathbf{B}_e 1$
$\vdots$	$\vdots$	$\vdots$

Table 3.3: The period-doubling sequences rewritten in another operator representation.

$$\mathbf{B}_n = \alpha_{\mathbf{B}_n} \cdot + \beta_{\mathbf{B}_n} \tag{3.89}$$

by using equations (3.9). Operator $\mathbf{B}_n$ is just dependent on n and the control parameters a, b and c.

$$\alpha_{\mathbf{B}_n} = \frac{1}{2}\frac{b}{a}\left[(1-(-1)^n)\frac{b}{a} - (1+(-1)^n)(1-c)\right] \tag{3.90}$$

$$\beta_{\mathbf{B}_n} = \frac{1}{2}\frac{b}{a}\left[(1+(-1)^n)(a-c) + (1-(-1)^n)(a-b)\right] \tag{3.91}$$

Operator $\mathbf{A}_{2^n}$ can be expressed by

$$\mathbf{A}_{2^n} = \alpha_{\mathbf{A}_{2^n}} \cdot + \beta_{\mathbf{A}_{2^n}} \tag{3.92}$$

due to the group nature of the operators. The identity between equation (3.85) and (3.92) results in the recurrence relations

$$\alpha_{\mathbf{A}_{2^n}} = (\alpha_{\mathbf{A}_{2^{n-1}}})^2 \alpha_{\mathbf{B}_n} \tag{3.93}$$

and

$$\beta_{\mathbf{A}_{2^n}} = \alpha_{\mathbf{A}_{2^{n-1}}} \alpha_{\mathbf{B}_n} \beta_{\mathbf{A}_{2^{n-1}}} + \alpha_{\mathbf{A}_{2^{n-1}}} \beta_{\mathbf{B}_n} + \beta_{\mathbf{A}_{2^{n-1}}}. \tag{3.94}$$

$$\mathbf{A}_{2^n} = \underbrace{(\alpha_{\mathbf{A}_{2^{n-1}}})^2 \alpha_{\mathbf{B}_n}}_{=\alpha_{\mathbf{A}_{2^n}}} \cdot + \underbrace{\alpha_{\mathbf{A}_{2^{n-1}}} \alpha_{\mathbf{B}_n} \beta_{\mathbf{A}_{2^{n-1}}} + \alpha_{\mathbf{A}_{2^{n-1}}} \beta_{\mathbf{B}_n} + \beta_{\mathbf{A}_{2^{n-1}}}}_{=\beta_{\mathbf{A}_{2^n}}} \qquad n \geq 2 \tag{3.95}$$

Using Condition (3.86) on recurrence relation (3.93) yields an implicit formula

$$\alpha_{\mathbf{A}_{2^n}} = \prod_{\nu=2}^{n} (\alpha_{\mathbf{B}_\nu})^{2^{n-\nu}} \tag{3.96}$$

to obtain $\alpha_{\mathbf{A}_{2^n}}$. The recurrence relation (3.94) can be rewritten to

$$\beta_{\mathbf{A}_{2^n}} = \beta_{\mathbf{A}_{2^{n-1}}} \underbrace{(1 + \alpha_{\mathbf{A}_{2^{n-1}}} \alpha_{\mathbf{B}_n})}_{\stackrel{\text{def}}{=} \chi_n} + \underbrace{\alpha_{\mathbf{A}_{2^{n-1}}} \beta_{\mathbf{B}_n}}_{\stackrel{\text{def}}{=} \lambda_n} \tag{3.97}$$

introducing purposeful substitutions χ_n and λ_n. Starting with $n = 2$ yielding $\beta_{\mathbf{A}_{2^2}} = \lambda_2 = \beta_{\mathbf{B}_2}$ the recurrence relation (3.97) reveals its identity to

$$\beta_{\mathbf{A}_{2^n}} = \sum_{\nu=2}^{n} \lambda_\nu \prod_{\mu=\nu+1}^{n} \chi_\mu. \tag{3.98}$$

The period-doubling operator represented by equation (3.84) therefore yields

$$\mathbf{P}_{2^n} = \underbrace{-\frac{b}{a}\alpha_{\mathbf{A}_{2^n}}}_{=\alpha_{\mathbf{P}_{2^n}}} \cdot + \underbrace{b\alpha_{\mathbf{A}_{2^n}} + \beta_{\mathbf{A}_{2^n}}}_{=\beta_{\mathbf{P}_{2^n}}} \tag{3.99}$$

$$\alpha_{\mathbf{P}_{2^n}} = -\frac{b}{a} \prod_{\nu=2}^{n} (\alpha_{\mathbf{B}_\nu})^{2^{n-\nu}}$$

$$\beta_{\mathbf{P}_{2^n}} = b \prod_{\nu=2}^{n} (\alpha_{\mathbf{B}_\nu})^{2^{n-\nu}} + \sum_{\nu=2}^{n} \beta_{\mathbf{B}_\nu} \left(\prod_{r=2}^{\nu-1} (\alpha_{\mathbf{B}_\nu})^{2^{\nu-1-r}} \right) \prod_{\mu=\nu+1}^{n} \left[1 + \alpha_{\mathbf{B}_\nu} \left(\prod_{r=2}^{\mu-1} (\alpha_{\mathbf{B}_\mu})^{2^{\mu-1-r}} \right) \right]$$

that is dependent on $\alpha_{\mathbf{B}_\nu}$ and $\beta_{\mathbf{B}_\nu}$, which are directly dependent on the control parameters a, b and c and even directly known by equations (3.90) and (3.91) to switch between two values according to n even or odd. Equation (3.83) offers a complicated analytical expression, that does not show its dependency on a easily. But further study of $\mathbf{P}_{2^n} x\Big|_{x\in\{b,c\}}$ as a function of control parameter a and n with $b = const$ and $c = const$ are shown to be well behaved for root finding in Figure 3.17. When solving equation (3.83) numerically, a_n and a_{n+1} is obtained with $a_n < a_{n+1}$.

Calculation of a_∞

The period-doubling operator $\mathbf{P}_{2^n}$ shows its dependency on $\alpha_{\mathbf{A}_{2^n}}$ and $\beta_{\mathbf{A}_{2^n}}$ in equation (3.99), that is most easily used to calculate a_∞ as a solution to

$$0 = \lim_{n\to\infty} \mathbf{P}_{2^n}(a_n)x\Big|_{x\in\mathcal{D}(\mathbf{P}_{2^n})}. \tag{3.100}$$

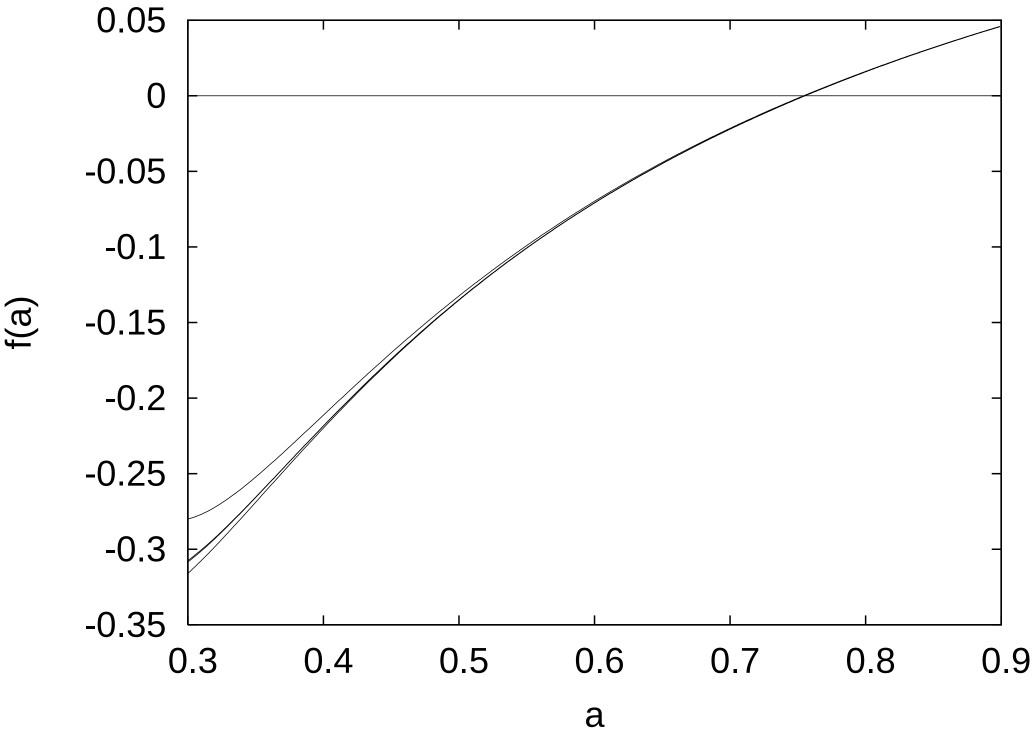

Figure 3.17: The period-doubling operator $f(a) = \mathbf{P}_{2^n}(a)x$ applied to $x = c = 0.7$ (upper curve) and $x = b = 0.3$ (lower curve) with $n = 3$ as a function of control parameter a. The center curves with $n = 4$ are yet almost indistinguishable. With increasing n the functions converge to $\lim_{n\to\infty} \beta_{\mathbf{A}_{2^n}}(a)$. By increasing n the roots of $f(a)$ slide leftwards to their limiting value a_∞.

By using Lemma 3.2.10 in (3.99), equation (3.100) simplifies to

$$0 = \lim_{n\to\infty} \beta_{\mathbf{A}_{2^n}}(a_n). \tag{3.101}$$

To obtain a_∞, the root of (3.101) has to be calculated. This can be done by using the *bisection method* with n sufficiently high, due to the well behaved $\beta_{\mathbf{A}_{2^n}}(a_n)$.

Lemma 3.2.10. *As n approaches ∞, $\alpha_{\mathbf{A}_{2^n}}$ vanishes:*

$$0 = \lim_{n\to\infty} \alpha_{\mathbf{A}_{2^n}}$$

Proof. By prerequisite Condition (3.2) on page 29 is valid as well as $a > c$ implied by $p > 2$ resulting in $|\alpha_{\mathbf{B}_n}| < 1$ shown by evaluating equation (3.90) for even and odd n. Equation (3.96) serves the proof.

$$|\alpha_{\mathbf{B}_n}| = \begin{cases} \left| -\underbrace{\frac{b}{a}}_{<1}\underbrace{(1-c)}_{<1} \right| < 1 & n \text{ even} \\[2em] \left| \underbrace{\left(\frac{b}{a}\right)^2}_{<1} \right| < 1 & n \text{ odd} \end{cases}$$

□

3.2.6 Period-doubling function

In the previous sections period-doubling of map $f(x)$ under increase of control parameter a has been shown to continue ad-infinitum in Theorem 3.2.3 as it is found in unimodal maps, too. The implicit representation of the period-doubling operator has been derived to a short analytical representation (3.82) in direct dependence of the control parameters.

Now that the existence of period $p = 2^n$, $n \in \mathbb{N}$ is certain and the convenient representation of operator $\mathbf{P}_{2^n}$ is present, the way is free to study the behavior of equation (2.5) with $n \to \infty$. This equation can be rewritten to

$$\lim_{n\to\infty} \delta_n = \frac{a_{2^n} - a_{2^{n-1}}}{a_{2^{n+1}} - a_{2^n}} \qquad n \geq 2, a_{2^1} = b, a_{2^2} = c \tag{3.102}$$

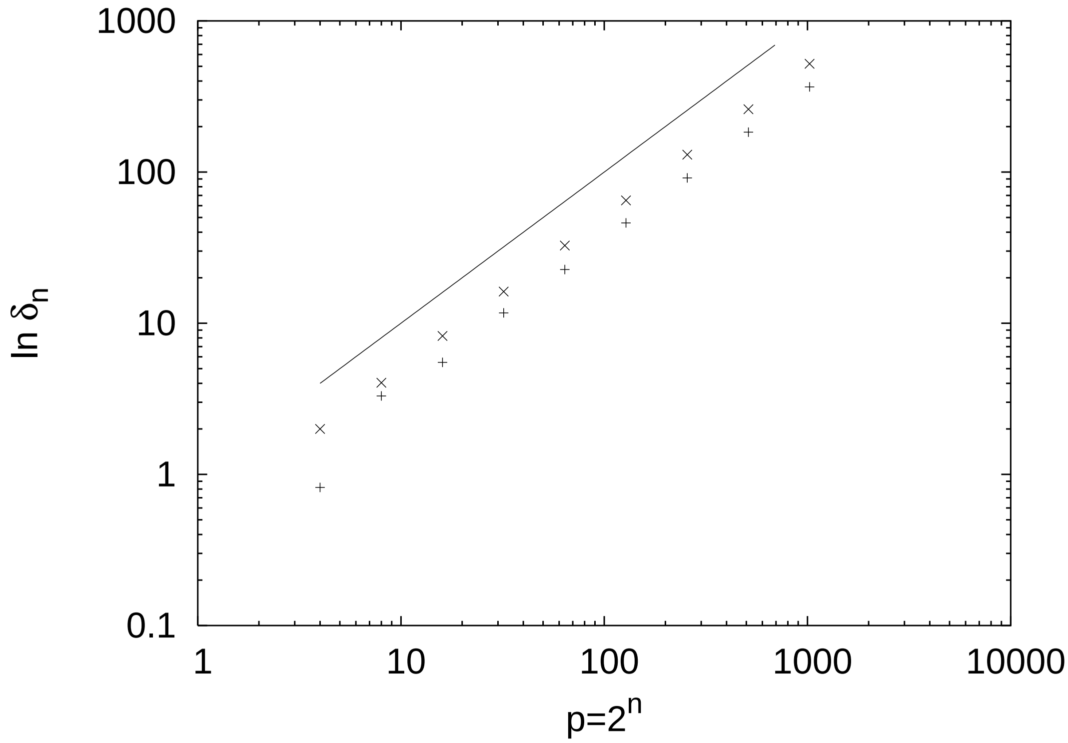

Figure 3.18: The period-doubling function with $n \in \{2, 3, \ldots, 10\} \subset \mathbb{N}$ of the symmetric case $b = 0.3$ and $c = 0.7$ denoted by $\times$ and of a rather asymmetric and less fast converging case denoted by $+$ featured by $b = 0.1$ and $c = 0.21$ still fulfilling Condition (3.25). The straight line represents e^x for comparison.

utilizing the control parameter under variation with $a = a_{2^n}$ the ambiguous point between period $p = 2^{n-1}$ and $2p = 2^n$ identifying the bifurcation in a. Numerical evaluation and root finding via the *bisection method* of equation (3.83) leads to the period-doubling function in Figure 3.18. Obviously the period-doubling function does not converge to a constant with $n \to \infty$ as found for unimodal maps. The function reveals an exponential growth instead.

As it is easily verified in Figure 3.18 the exponential growth is dependent of the control parameters b and c. New questions arise about the functional dependence of $\delta_n(b, c)$ inspiring further analytical investigations.

n	sequence
2	$\mathbf{T}_1[b,c]$
3	$\mathbf{T}_2 \underbrace{\mathbf{T}_1}_{\Delta_3 I}[b,c]$
4	$\mathbf{T}_2 \underbrace{\mathbf{T}_4\mathbf{T}_2}_{\Delta_4 I=\alpha_{\mathbf{T}_2}\alpha_{\mathbf{T}_4}\Delta_3 I} \mathbf{T}_1[b,c]$
5	$\mathbf{T}_2 \underbrace{\mathbf{T}_4\mathbf{T}_2\mathbf{T}_2\mathbf{T}_2}_{\Delta_5 I=\alpha_{\mathbf{T}_2}{}^3\alpha_{\mathbf{T}_4}{}^1\Delta_4 I} \mathbf{T}_4\mathbf{T}_2\mathbf{T}_1[b,c]$
6	$\mathbf{T}_2 \underbrace{\mathbf{T}_4\mathbf{T}_2\mathbf{T}_2\mathbf{T}_2\mathbf{T}_4\mathbf{T}_2\mathbf{T}_4\mathbf{T}_2}_{\Delta_6 I=\alpha^5_{\mathbf{T}_2}\alpha^3_{\mathbf{T}_4}\Delta_5 I} \mathbf{T}_4\mathbf{T}_2\mathbf{T}_2\mathbf{T}_2\mathbf{T}_4\mathbf{T}_2\mathbf{T}_1[b,c]$

Table 3.4: The shrinking of successive intervals of $\mathbf{T}_2^{-1}\mathbf{P}_{2^n}x$, $x \in \mathcal{D}(\mathbf{T}_1)$ by multiplication with $\alpha_{\mathbf{T}_2}$ and $\alpha_{\mathbf{T}_4}$.

Analytical explanation

Rewriting equation (3.102) and skipping the limits yields another representation of δ_n in

$$\delta_n = \frac{\Delta_n a}{\Delta_{n+1} a} \qquad n \geq 2 \tag{3.103}$$

with

$$\Delta_n a = a_{2^n} - a_{2^{n-1}}.$$

Due to the supposed exponential growth of δ_n in $p = 2^n$ the intervals $\Delta_n a$ have to shrink quite fast as n increases. This is equivalent to a fast approach of a to a_∞ when the considering higher periods. If n is sufficiently high a_{2^n} will no longer change significantly by increasing of n, resulting in transformations $\mathbf{T}_2(a_\infty)$ and $\mathbf{T}_4(a_\infty)$ almost independent of a_{2^n}. Equations (3.19) and (3.21) can be expressed in the common group representation

$$\mathbf{T}_i = \alpha_{\mathbf{T}_i}(a) \cdot + \beta_{\mathbf{T}_i}(a) \qquad i \in \{2,4\} \tag{3.104}$$

with

$$\alpha_{\mathbf{T}_i}(a) \overset{n\to\infty}{\longrightarrow} \alpha_{\mathbf{T}_i}(a_\infty)$$

and

$$\beta_{\mathbf{T}_i}(a) \overset{n\to\infty}{\longrightarrow} \beta_{\mathbf{T}_i}(a_\infty).$$

The basic idea is, that derivative $\lim_{a\to a_\infty} \frac{dx_4}{da}(a)$ becomes constant too, causing x_4 to move with constant *speed* through interval $[\mathbf{T}_2^{-1}\mathbf{P}_{2^n}y_1, \mathbf{T}_2^{-1}\mathbf{P}_{2^n}y_2]$

with $y_1, y_2 \in \{b, c\}$. Beginning with interval $\Delta_3 I = |\mathbf{T}_1 b - \mathbf{T}_1 c|$ supposed to be stationary as a increases equation

$$\Delta_n I = \left(\frac{dx_4}{da}\right)(a_\infty)\Delta_{n+1} a \tag{3.105}$$

is valid with $n = 3$. The movement of x_4 then is estimated by the constant derivative $\left(\frac{dx_4}{da}\right)(a_\infty)$ and the change $\Delta_n a$ in a, that describes the width of the interval in a of period $p = 2^n$. Of course equation (3.105) is a good approximation for $n \gg 1$ only, resulting in $\Delta_n a \to 0$ with $\Delta_n a > 0$. Rewriting equation (3.103) by use of (3.105) results in

$$\delta_n = \frac{\Delta_{n-1} I}{\Delta_n I} \tag{3.106}$$

expressing δ_n by the widths of intervals of images of $\mathbf{T}_2^{-1}\mathbf{P}_{2^n}[b, c]$. Table 3.4 shows the period-doubling sequences another time emphasizing the shrinking of images of interval $[\mathbf{T}_1 b, \mathbf{T}_1 c]$ caused by numerous applications of $\mathbf{T}_2$ and $\mathbf{T}_4$. As this investigation is concerned with the shrinking of intervals only, just the $\alpha_{\mathbf{T}_i}$ have to be taken into account. Table 3.4 shows the exponent $h(n)$ of

$$\Delta_n I = {\alpha_{\mathbf{T}_2}}^{h(n)} {\alpha_{\mathbf{T}_4}}^{h(n-1)} \Delta_{n-1} I \tag{3.107}$$

to follow recurrence relation

$$h(n) = \begin{cases} 2h(n-1) - 1 & n \text{ even} \\ 2h(n-1) + 1 & n \text{ odd} \end{cases} \tag{3.108}$$

when considering $\alpha_{\mathbf{T}_2}$ at first. As it is easily verified the recurrence relation is valid for $\alpha_{\mathbf{T}_4}$ with $h(n-1)$, too.
Starting with $h(4) = 1$ for treating the recurrence relation and writing down the recurrence relation for a few $n > 4$ reveals an implicit law for generating $h(n)$ in

$$h(n) = 2^{n-4} h(4) + \sum_{\nu=0}^{n-5} (-1)^\nu 2^{n-\nu-5} \tag{3.109}$$

and therewith

$$h(n) = 2^{n-5}\left[2 + \sum_{\nu=0}^{n-5}\left(-\frac{1}{2}\right)^\nu\right]. \tag{3.110}$$

Using formula $S_n = \frac{1-q^{n+1}}{1-q}$ for calculating partial sums of kind $S_n = \sum_{\nu=0}^{n} q^\nu$ with $|q| < 1$ in equation (3.110) yields

$$h(n) = \frac{2^{n-2} - (-1)^n}{3} \tag{3.111}$$

after some trivial algebra. Now using equation (3.107) in equation (3.106) reveals δ_n's dependence on the $\alpha_{\mathbf{T}_i}$

$$\delta_n = \alpha_{\mathbf{T}_2}^{-h(n)} \alpha_{\mathbf{T}_4}^{-h(n-1)}. \tag{3.112}$$

Remembering equation (3.59) on page 51 and calculating $\alpha_{\mathbf{T}_2}$ in the same way, gives way to equation (3.114) by insertion into equation (3.112) under the condition $n \gg 1$ and $a \to a_\infty$.

$$\alpha_{\mathbf{T}_4} = \left(\frac{b}{a}\right)^2 (1-c)^2$$

$$\alpha_{\mathbf{T}_2} = \left(\frac{b}{a}\right)^3 (1-c)^1 \tag{3.113}$$

$$\delta_n = \left(\frac{a_\infty}{b}\right)^{3h(n)+2h(n-1)} \left(\frac{1}{1-c}\right)^{h(n)+2h(n-1)} \qquad n \gg 1 \tag{3.114}$$

Evaluating the exponents simplifies the terms to

$$3h(n) + 2h(n-1) = 2^{n-2} - (-1)^n + 2\frac{2^{n-3} - (-1)^{n-1}}{3} = \frac{2^n - (-1)^n}{3}$$

$$h(n) + 2h(n-1) = \frac{2^{n-2} - (-1)^n}{3} + 2\frac{2^{n-3} - (-1)^{n-1}}{3} = \frac{2^{n-1} + (-1)^n}{3}$$

and reveals a more obvious functional dependence of δ_n on the control parameters

$$\delta_n = \left(\frac{a_\infty}{b}\right)^{\frac{2^n - (-1)^n}{3}} \left(\frac{1}{1-c}\right)^{\frac{2^{n-1} + (-1)^n}{3}} \tag{3.115}$$

and

$$\ln \delta_n = \frac{2^n - (-1)^n}{3} \ln\left(\frac{a_\infty}{b}\right) - \frac{2^{n-1} + (-1)^n}{3} \ln(1-c). \tag{3.116}$$

Re-substitution of $p = 2^n$ results in

$$\delta_n = e^{-\frac{(-1)^n}{3}\left[\ln \frac{a_\infty}{b} + \ln(1-c)\right]} e^{\frac{p}{3}\left[\ln \frac{a_\infty}{b} - \frac{1}{2}\ln(1-c)\right]} \tag{3.117}$$

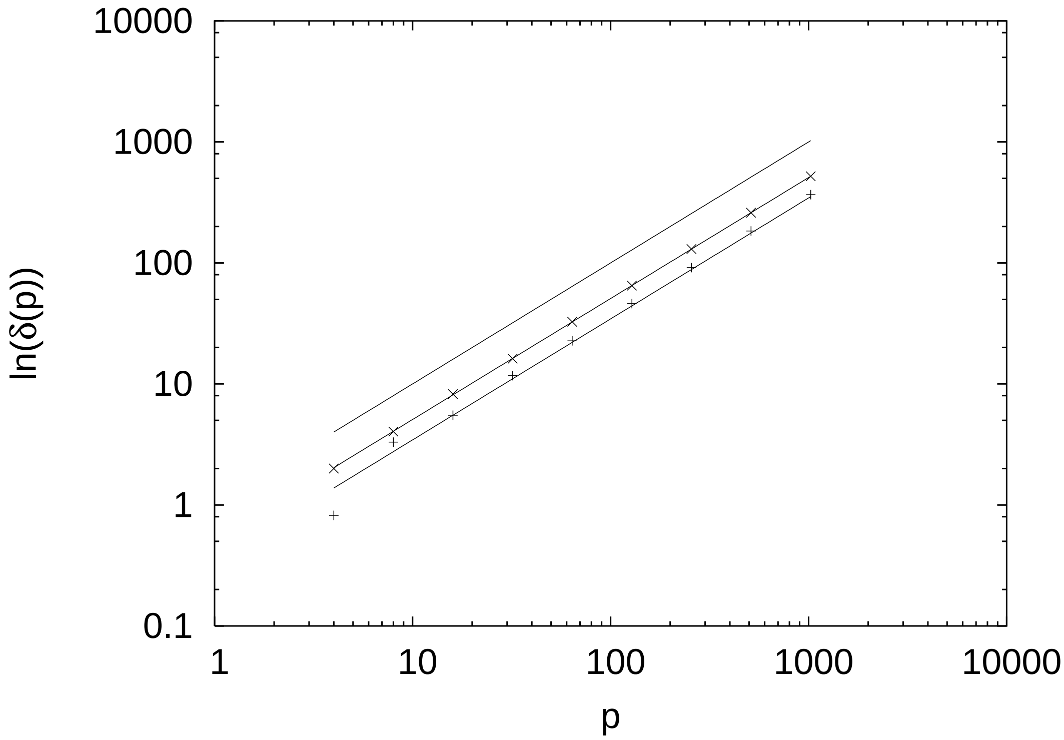

Figure 3.19: The period-doubling function of Figure 3.18 asymptotically resembled by use of equation (3.118).

directly revealing the functional dependence of the period-doubling function on the control parameters b, c and the period $p = 2^n$. Parameter $a_\infty(b, c)$ is already defined by b and c according to the previous section. By using $p = 2^n$ a direct relationship between δ_n and the period p is obtained.

Because of $n \gg 1$ in the assumption to the derivation of equation (3.115) the small oscillating $\frac{1}{3}(-1)^n$ term in equation (3.116) can be waived, offering the asymptotic behavior

$$\delta(p) \sim e^{\frac{p}{3}\left[\ln \frac{a_\infty}{b} - \frac{1}{2}\ln(1-c)\right]} \tag{3.118}$$

of the period-doubling function. Evaluation of equation (3.118) explains the numerically obtained data of Figure 3.18 in Figure 3.19. Even coarse estimations of a_∞ lead to useful results.

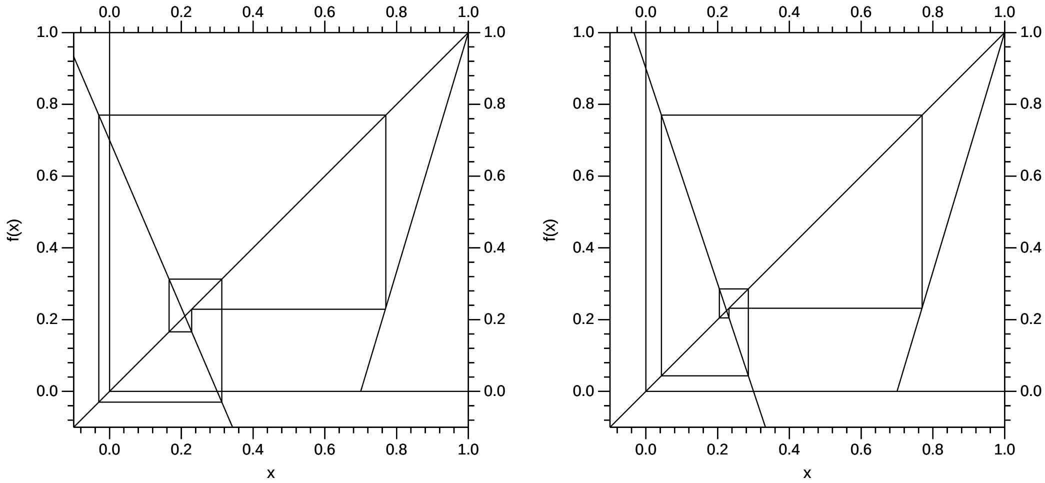

Figure 3.20: An example of the failing word lifting technique.

3.2.7 Admissibility of orbits

In Section 3.2.5 the implicit period-doubling operator has been derived under the assumption of the admissibility of the orbit under investigation. The word lifting technique offered the possibility to do so in analogy to the treatment of the logistic map shown in Section 2.2.2. But in general the word lifting technique fails, when applied to the cup map. This fact is illustrated in Figure 3.20. Apparently the word lifting technique allows the periodic orbit $s_x = \overline{11113}$ of point $x = 0.77$ to be of ambiguous origin in the control parameter with $a_1 \approx 0.7$ and $a_2 \approx 0.9$. The first solution a_1 obviously violates the domain $\mathcal{D}(\mathbf{f}_1^{-1})$ and is therefore no admissible solution.

Admissibility of orbits in maps under iteration are well studied and led to the development of the *kneading theory* [5, 8, 10]. Referring to the unimodal logistic map, the main statement of this theory is, that orbits are admissible in case of validity of

$$\sup_k \sigma^k s_x \leq \kappa_{uni} \qquad x \in [0,1], k \in \mathbb{Z}_+ \tag{3.119}$$

with

$$\kappa_{uni} = \sigma s_x \Big|_{x=c=\frac{1}{2}} . \tag{3.120}$$

The *kneading sequence* κ_{uni} defined by equation (3.120) and σ the *Bernoulli*

shift operator[8] defined by equation (2.31) are tools to check the validity of inequality (3.119) for a given orbit s_x in the unimodal map with critical point c in order to investigate the admissibility of $s_x = \prod_{i=0}^{n} s_{x,i}$ usually featured by $n \to \infty$. To compare symbolic sequences in inequality (3.119) Order (2.18) on page 14 is used.
As mentioned in Section 2.2.1 the period-doubling in unimodal maps leads to successively greater symbolic representations s_p with respect to Order (2.18) unlike the cup map's period-doubling that always decreases the symbolic value as the period doubles with respect to Order (3.7) on page 30. This inverse behavior is a consequence of the swapped slopes in the cup map's partitions.

The set of admissible orbits $\mathcal{O}_{cup}$ of points x in the cup map is defined by

$$\mathcal{O}_{cup} = \{s_x | x \in [0,1], \kappa_{cup} \leq \inf_k \sigma^k s_x \leq \overline{3}\} \tag{3.121}$$

by use of the kneading sequence $\kappa_{cup} = s_{x_0}$, with $x_0 = 0$ and $k \in \mathbb{Z}_+$ in contrast to admissible orbits

$$\mathcal{O}_{uni} = \{s_x | x \in [0,1], \overline{L} \leq \sup_k \sigma^k s_x \leq \kappa_{uni}\} \tag{3.122}$$

in unimodal maps. By definition of κ_{cup} the period-doubling operator $\mathbf{P}_{2^n}$ is obviously valid featuring a non-empty domain $\mathcal{D}(\mathbf{P}_{2^n}) \neq \varnothing$ in case of the existence of an $x \in [b,c]$ satisfying $\inf_k \sigma^k s_x \geq \kappa_{cup}$ with $\sigma s_x = s_{2^n}$. Otherwise the domain $\mathcal{D}(\mathbf{P}_{2^n})$ is declared empty. The consequence is, that all $\mathbf{P}_{2^\nu}$ with $\nu < n$ map the absorption interval $[b,c]$ into the interval $]0,b]$, where the interval is free to be mapped according to recurrence relation (3.85), which causes the whole mapped interval to be located closer to $x_0 = 0$. In case of $\sigma s_x = s_{2^n} < \kappa_{cup}, \forall x \in [b,c]$ the implicit period-doubling operator $\mathbf{P}_{2^n}$ would map the whole absorption area $[b,c]$ into the interval $[\rho_1, \rho_2]$ with $\rho_1, \rho_2 < 0$. Therefore the domain of $\mathbf{P}_{2^n}$ is declared empty.

In more accessible terms the period-doubling operator $\mathbf{P}_{2^n}$ is admissible for a non-empty set of points $x \in [b,c]$ as long as all its predecessors $\mathbf{P}_{2^\nu}$, $\nu < n$ map interval $[b,c]$ completely into interval $]0,b]$.

For use in Section 3.3 it has to be pointed out that Theorem 3.2.3 asserts that period-doubling in the linear cup map proceeds gap-less through all periods

[8]Application of the Bernoulli shift operator in the symbolic representation s_x of x is equivalent to iteration of x.

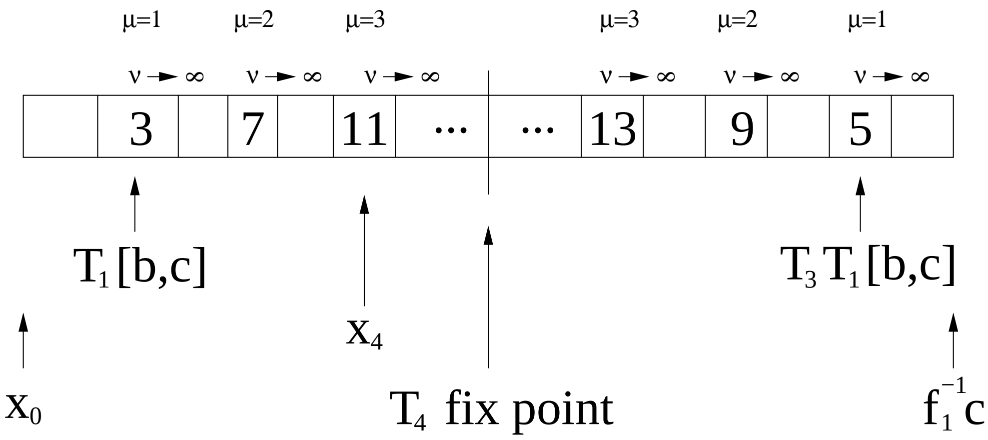

Figure 3.21: After the well studied period-doubling x_4 also hits intervals $\mathbf{T}_4^{\mu-1}\mathbf{T}_1[b,c]\ \forall\mu \in \mathbb{N}$ followed by hitting intervals $\mathbf{T}_4^{\mu-1}\mathbf{T}_3\mathbf{T}_1[b,c]\ \forall\mu \in \mathbb{N}$ with μ decreasing from ∞ to 1.

$p = 2^n$. As a consequence of this fact the kneading sequence decreases monotonically through the symbolic sequences

$$\kappa = \overline{\left(\overset{n}{\underset{\nu=1}{*}} 1\right) s_{p,p}} \qquad s_{p,p} \in \{1,2,3\}, p = 2^n \tag{3.123}$$

with n and p respectively, according to equations (3.5) and (3.6) as a increases.

3.2.8 Total period-doubling

The situation sketched in Figure 3.7 on page 36 denoted by $a \in [\mathbf{f}_3^{-1}\mathbf{f}_1^{-1}b,$ $\mathbf{f}_3^{-1}\left(\mathbf{f}_1^{-1}\right)^3 c]$ gave rise to period-doubling that runs through all $p = 2^n$, $n \in \mathbb{N}$. Due to the exponentially fast growing period-doubling function the whole Feigenbaum scenario reaches $p_\infty = \infty$ fast. By calculating a_∞ via the method mentioned in Section 3.2.5 $a_\infty < \mathbf{f}_3^{-1}\left(\mathbf{f}_1^{-1}\right)^3 c$ is easily verified emphasizing the question for the processes following the Feigenbaum scenario as a further increases.

Figure 3.21 shows the primary intervals $\mathbf{T}_1[b,c]$ and $\mathbf{T}_3\mathbf{T}_1[b,c]$ in the left and in the right. In case of $x_4 \in [\mathbf{T}_1 b, \mathbf{T}_1 c]$ the already known period-doubling sets in as a increases. Application of operator $\mathbf{T}_4$ to the whole interval $[0, \mathbf{f}_1^{-1}c]$ causes further images of the primary intervals to emerge.
By assuming $x_4 \in \mathbf{T}_4^{\mu-1}\mathbf{T}_1[b,c]$ and $x_4 \in \mathbf{T}_4^{\mu-1}\mathbf{T}_3\mathbf{T}_2[b,c]$ respectively for $\mu \in$

$\mathbb{N}$ other period-doublings set in, satisfying the generalized period-doubling operator

$$\mathbf{P}_{\mu,\nu} = \mathbf{A}_{\mu,\nu}\mathbf{T}_1 \tag{3.124}$$

resembling equation (3.84) on page 58 with $\mu = 1$ and $n \geq 3$. So the identity $\mathbf{P}_{1,\nu} \equiv \mathbf{P}_{2^n}$ is obtained with $n = \nu + 2$.
In strict analogy to the period-doubling described in Section 3.2.4 the following definitions are generalizations for arbitrary μ and can be verified easily by performing successive iterations in $[0, \mathbf{f}_1^{-1}c]$ by hand the same way as demonstrated in Figure 3.15 on page 46.

$$\mathbf{A}_{\mu,\nu} = \mathbf{A}_{\mu,\nu-1}\mathbf{T}_i\mathbf{A}_{\mu,\nu-1} \tag{3.125}$$

$$\mathbf{A}_{\mu,1} = \mathbf{T}_2\left(\mathbf{T}_4\right)^{\mu-1}\mathbf{T}_3 \tag{3.126}$$

$$\mathbf{T}_i = \begin{cases} \mathbf{T}_4 & \nu \text{ even (odd)} \\ \mathbf{T}_2 & \nu \text{ odd (even)} \end{cases} \text{left (right) of } \mathbf{T}_4 \text{ fixed point}$$

$$\mathbf{A}_{\mu,1} = \begin{cases} \mathbf{T}_2\left(\mathbf{T}_4\right)^{\mu-1} & \text{left of } \mathbf{T}_4 \text{ fixed point} \\ \mathbf{T}_2\left(\mathbf{T}_4\right)^{\mu-1}\mathbf{T}_3 & \text{right of } \mathbf{T}_4 \text{ fixed point} \end{cases} \tag{3.127}$$

$$\left(\mathbf{T}_4\right)^0 \stackrel{def}{=} \mathbf{id}$$

The symbolic length of operator $\mathbf{A}_{\mu,1}$ is obtained by

$$\iota_{\mathbf{A}_{\mu,1}} = \begin{cases} (\mu-1)\iota_4 + \iota_2 & \text{left of } \mathbf{T}_4 \text{ fixed point} \\ (\mu-1)\iota_4 + \iota_3 + \iota_2 & \text{right of } \mathbf{T}_4 \text{ fixed point} \end{cases} \tag{3.128}$$

and the period of the periodic orbit[9] is obtained by

$$p = \iota_{\mathbf{P}_{\mu,\nu}} + 1 = \iota_{\mathbf{A}_{\mu,\nu}} + \iota_1 + 1. \tag{3.129}$$

Equations (3.128) and (3.125) give rise to recurrence relation

$$\iota_{\mathbf{A}_{\mu,\nu}} = 2\iota_{\mathbf{A}_{\mu,\nu-1}} + \iota_i \qquad \iota_i = 4 = \begin{cases} \iota_2 & \nu \text{ even} \\ \iota_4 & \nu \text{ odd} \end{cases} \tag{3.130}$$

that yields the implicit length $\iota_{\mathbf{A}_{\mu,\nu}}$ defined by

[9]Note the length of the period-doubling operator to be $\iota_{\mathbf{P}_{\mu,\nu}} = p - 1$ due to sparing the inversion of f_2.

$$\iota_{\mathbf{A}_{\mu,\nu}} = 2^{\nu-1}\iota_{\mathbf{A}_{\mu,1}} + \iota_i\left(2^{\nu-1} - 1\right). \tag{3.131}$$

Solving equation (3.131) by using equation (3.128) yields the implicit formula for the symbolic length of $\mathbf{A}_{\mu,\nu}$

$$\iota_{\mathbf{A}_{\mu,\nu}} = \begin{cases} 2^{\nu+1}(\mu+1) - 4 & \text{left of fixed point} \\ 2^{\nu+1}(\mu+\frac{3}{2}) - 4 & \text{right of fixed point.} \end{cases} \tag{3.132}$$

Then using equation (3.132) in equation (3.129) yields the length of all countable infinite period-doubling sequences (3.133) depicted in Figure 3.21 that occur as a increases within its interval of restriction. Table 3.5 shows some of the period-doubling sequences to be read row by row from top to bottom resembling their appearances as a increases.

$$p = 2^{\nu+1}(\mu+k) \qquad k = \begin{cases} 1 & \text{left of } \mathbf{T}_4 \text{ fixed point} \\ \frac{3}{2} & \text{right of } \mathbf{T}_4 \text{ fixed point} \end{cases} \tag{3.133}$$

It should be mentioned, that Lemma 3.2.4, Lemma 3.2.5 and Lemma 3.2.7 also prove the existence of infinite periods in the period-doubling sequences appearing left of the $\mathbf{T}_4$ fixed point due to the definition of $\mathbf{A}_{\mu,\nu}$ (3.125) and (3.127). The conclusion is exactly analogous to the proof of Theorem 3.2.3 found on page 55.

The more interesting question is if the situation right of the $\mathbf{T}_4$ fixed point featuring $\mathbf{A}_{\mu,1} = \mathbf{T}_2\mathbf{T}_4^{\mu-1}\mathbf{T}_3$ also proceeds through all periods as described by equation (3.133).
The derivatives of $\mathbf{T}_1$, $\mathbf{T}_2$ and $\mathbf{T}_4$ have well defined properties worked out in Lemmas 3.2.4, 3.2.5 and 3.2.7 resulting in a reduction of the overall derivative's value that finally allowed to conclude the existence of all periods $p = 2^n$ in Theorem 3.2.3.

The situation considered here is different, due to $\mathbf{T}_3x$ reversing the sign of derivative $\frac{dx}{da}$ in its image. This fact might cause the derivative of $\mathbf{T}_2\mathbf{T}_3x$ with respect to a to violate Condition (3.46) or (3.47) resulting in undefined motion of the interval $\mathbf{T}_2^{-1}\mathbf{P}_{\mu,\nu}[b,c]$. Lemma 3.2.13 proves that the derivative of $\mathbf{T}_2\mathbf{T}_3x$ is never greater than $\frac{dx_4}{da}$ so the already known procedure shown in Figure 3.22 is applicable.

Lemma 3.2.11. *Under Assumption*

$$0 < \frac{dx}{da} < \frac{dx_4}{da} \tag{3.134}$$

μ,ν	1	2	3	4	5	...	∞
1	8	16	32	64	128	...	∞
2	12	24	48	96	192	...	∞
3	16	32	64	128	256	...	∞
4	20	40	80	160	320	...	∞
5	24	48	96	192	384	...	∞
6	28	56	112	224	448	...	∞
7	32	64	128	256	512	...	∞
$\vdots$	$\vdots$	$\vdots$	$\vdots$	$\vdots$	$\vdots$	$\vdots$	$\vdots$
∞	∞	∞	∞	∞	∞	∞	∞
∞	∞	∞	∞	∞	∞	∞	∞
$\vdots$	$\vdots$	$\vdots$	$\vdots$	$\vdots$	$\vdots$	$\vdots$	$\vdots$
7	34	68	136	272	544	...	∞
6	30	60	120	240	480	...	∞
5	26	52	104	208	416	...	∞
4	22	44	88	176	352	...	∞
3	18	36	72	144	288	...	∞
2	14	28	56	112	224	...	∞
1	10	20	40	80	160	...	∞

Table 3.5: The period-doubling sequences according to equation 3.133 arising as a increases in order of appearance from upper left to lower right. Where all periods are $p_\infty = \infty$, x_4 hits the $\mathbf{T}_4$ fixed point and so no absorption occurs.

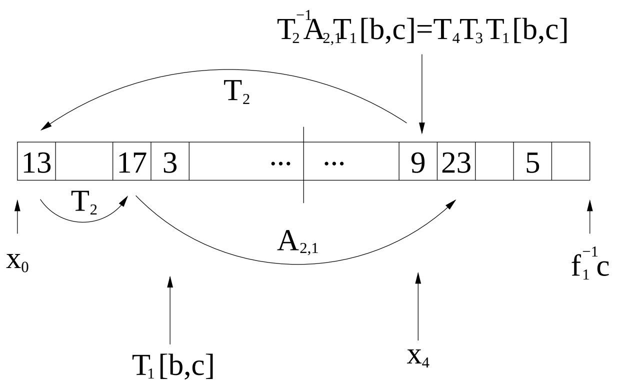

Figure 3.22: The process of period-doubling with $\mathbf{A}_{\mu,1}$ as specified in equation (3.126), $\mu = 2$ and $\nu = 1$ in analogy to the previous section. Lemma 3.2.13 shows the interval labeled 23 to move less fast to the right than x_4, giving rise to period-doubling ad-infinitum.

inequality

$$\left.\frac{d\mathbf{T}_3 x}{da}\right|_{x\in\mathcal{D}(\mathbf{T}_3)} < \frac{dx_4}{da} \tag{3.135}$$

is satisfied.

Proof. Straightforward calculation of $\mathbf{T}_3 x = \mathbf{f}_1^{-1}\mathbf{f}_3^{-1}x$ results in equation

$$\mathbf{T}_3 x = -\frac{b}{a}(1-c)x + b - \frac{bc}{a} \tag{3.136}$$

and its derivative

$$\frac{d\mathbf{T}_3 x}{da} = \frac{b}{a^2}(1-c)x - \underbrace{\frac{b}{a}(1-c)}_{\in[0,1]}\frac{dx}{da} + \frac{bc}{a^2}. \tag{3.137}$$

Because of $x \in [0, \mathbf{f}_1^{-1}c]$ and $x < b$ the derivative is majorized with $x \to b$ and the neglect of the negative term. The proof follows from inequalities (3.70) and (3.72) found in the proof of Lemma 3.2.7 on page 53.

$$\frac{d\mathbf{T}_3 x}{da} < \frac{b^2}{a^2}(1-c) + \frac{bc}{a^2} \overset{\substack{\text{(eqn 3.72)}\\ \text{(eqn 3.70)}}}{<} \frac{21}{25}\frac{dx_4}{da} < \frac{dx_4}{da}$$

$\square$

Lemma 3.2.12. *Under condition* $0 < \frac{dx}{da} < \frac{dx_4}{da}$ *derivative* $\frac{d\mathbf{T}_2\mathbf{T}_3 x}{da}$ *satisfies*

$$\frac{d}{da}\mathbf{T}_2\mathbf{T}_3 x < \frac{dx_4}{da}. \tag{3.138}$$

Proof. Following the definition of $\mathbf{T}_2$ and $\mathbf{T}_3$ (3.16,3.15) the symbolic string for the operator product is $s_{\mathbf{T}_2\mathbf{T}_3} = 131113$. The resulting transformation can be expressed in the operator group representation

$$\mathbf{T}_2\mathbf{T}_3 = \alpha_{\mathbf{T}_2\mathbf{T}_3}(a)x(a) + \beta_{\mathbf{T}_2\mathbf{T}_3}(a). \tag{3.139}$$

Differentiating with respect to a yields

$$\frac{d}{da}\mathbf{T}_2\mathbf{T}_3 = \underbrace{\frac{\alpha_{\mathbf{T}_2\mathbf{T}_3}}{da}}_{<0}\underbrace{x}_{\in[0,\mathbf{f}_1^{-1}c]} + \underbrace{\alpha_{\mathbf{T}_2\mathbf{T}_3}}_{\in[0,\frac{4}{25}]}\frac{x}{da} + \frac{\beta_{\mathbf{T}_2\mathbf{T}_3}}{da}. \tag{3.140}$$

According to $s_{\mathbf{T}_2\mathbf{T}_3} = 131113$ factor $\alpha_{\mathbf{T}_2\mathbf{T}_3}$ is

$$\alpha_{\mathbf{T}_2\mathbf{T}_3} = \left(\frac{b}{a}\right)^4 (1-c)^2 \overset{\text{(eqn 3.25)}}{<} \frac{4}{25}\left(\frac{b}{a}\right)^2 < \frac{4}{25}. \tag{3.141}$$

Its derivative with respect to a is

$$\frac{d}{da}\alpha_{\mathbf{T}_2\mathbf{T}_3} = -\frac{4}{a}\alpha_{\mathbf{T}_2\mathbf{T}_3} < 0. \tag{3.142}$$

Finally equation (3.140) is majorized by

$$\frac{d}{da}\mathbf{T}_2\mathbf{T}_3 < \frac{4}{25}\frac{dx_4}{da} + \frac{\beta_{\mathbf{T}_2\mathbf{T}_3}}{da}. \tag{3.143}$$

To prove inequality (3.138) it is sufficient to show

$$\frac{d\beta_{\mathbf{T}_2\mathbf{T}_3}}{da} < \frac{21}{25}\frac{dx_4}{da}. \tag{3.144}$$

Evaluating $\beta_{\mathbf{T}_2\mathbf{T}_3}$ according to $s_{\mathbf{T}_2\mathbf{T}_3} = 131113$ yields

$$\beta_{\mathbf{T}_2\mathbf{T}_3} = b - \frac{bc}{a} - \frac{b^2}{a}(1-c) + \frac{b^3}{a^2}(1-c) - \frac{b^4}{a^3}(1-c) + \frac{b^4}{a^4}c(1-c). \tag{3.145}$$

Differentiating with respect to a obtains

$$\frac{d}{da}\beta_{\mathbf{T}_2\mathbf{T}_3} = \frac{bc}{a^2} + \frac{b^2}{a^2}(1-c) - 2\frac{b^3}{a^3}(1-c) + 3\frac{b^4}{a^4}(1-c) - 4\frac{b^4}{a^4}\frac{c}{a}(1-c). \tag{3.146}$$

The derivative can be majorized by making the last term less negative via $c \to b$. Then rewriting the the sum yields

$$\frac{d}{da}\beta_{\mathbf{T}_2\mathbf{T}_3} < \frac{bc}{a^2} - \frac{b}{a}(1-c)\sum_{\nu=1}^{4} \nu \left(-\frac{b}{a}\right)^{\nu}, \tag{3.147}$$

which can be rewritten another time

$$\frac{d}{da}\beta_{\mathbf{T}_2\mathbf{T}_3} < \frac{bc}{a^2} - \frac{b}{a}(1-c)\sum_{\nu=1}^{4} q\frac{d}{dq}(q)^{\nu}\bigg|_{q=-\frac{b}{a}}. \tag{3.148}$$

Due to the finite sum, the differential operator may be swapped with the sum

$$\frac{d}{da}\beta_{\mathbf{T}_2\mathbf{T}_3} < \frac{bc}{a^2} - \frac{b}{a}(1-c)q\frac{d}{dq}\sum_{\nu=1}^{4}(q)^{\nu}\bigg|_{q=-\frac{b}{a}}. \tag{3.149}$$

Calculating the partial sum via $S_n = \sum_{\nu=1}^{n} q^n = \frac{q-q^{n+1}}{1-q}$ yields

$$\frac{d}{da}\beta_{\mathbf{T}_2\mathbf{T}_3} < \frac{bc}{a^2} - \frac{b}{a}(1-c)q\frac{d}{dq}\frac{q-q^5}{1-q}\bigg|_{q=-\frac{b}{a}}. \tag{3.150}$$

Differentiating and re substitution of $q = \frac{b}{a}$ yields the final representation of inequality (3.148) in

$$\frac{d}{da}\beta_{\mathbf{T}_2\mathbf{T}_3} < \frac{bc}{a^2} + \frac{b^2}{a^2}(1-c)\frac{1-5\left(\frac{b}{a}\right)^4 - 4\left(\frac{b}{a}\right)^5}{(1+\frac{b}{a})^2}. \tag{3.151}$$

Inequality (3.151) is majorized another time by neglecting the negative terms and by making the denominator as small as possible by $1 + \frac{b}{a} \to 1$

$$\frac{d}{da}\beta_{\mathbf{T}_2\mathbf{T}_3} < \frac{bc}{a^2} + \frac{b^2}{a^2}(1-c). \tag{3.152}$$

To show inequality (3.144) and therewith inequality (3.138) it is sufficient to show

$$\frac{d}{da}\beta_{\mathbf{T}_2\mathbf{T}_3} < \frac{bc}{a^2} + \frac{b^2}{a^2}(1-c) < \frac{21}{25}\frac{dx_4}{da} \tag{3.153}$$

that has already been proven to be fulfilled under Conditions (3.25) and (3.27) in the proof of Lemma 3.2.7 via inequalities (3.70) and (3.72) on page 53. □

Lemma 3.2.13 (Conclusion). *Under condition*

$$0 < \frac{dx}{da} < \frac{dx_4}{da} \tag{3.154}$$

the derivative of $\mathbf{A}_{\mu,1}$ *with respect to* a *complies inequality*
(1)

$$\frac{d}{da}\mathbf{A}_{\mu,1} = \frac{d}{da}\mathbf{T}_2\left(\mathbf{T}_4\right)^{\mu-1}\mathbf{T}_3 < \frac{dx_4}{da} \tag{3.155}$$

and therewith the derivative of $\mathbf{T}_2\mathbf{A}_{\mu,\nu}$ *with respect to* a *results in the validity of inequality*
(2)

$$0 < \frac{d}{da}\mathbf{A}_{\mu,1}\mathbf{T}_i\mathbf{A}_{\mu,1}x\bigg|_{i\in\{2,4\}} < \frac{dx_4}{da} \tag{3.156}$$

and allows period-doubling ad-infinitum by the validity of
(3)

$$\frac{d}{da}\mathbf{T}_2^{-1}\mathbf{P}_{\mu,\nu}x < \frac{dx_4}{da}. \tag{3.157}$$

Proof. (1) Due to the property of $\mathbf{T}_4$ to be endomorph and its property to conserve the relative shift of points in the preimage, it is sufficient to show equation (3.155) with $\mu = 1$, only.

$$0 < \frac{d}{da}x < \frac{dx_4}{da} \quad \overset{\text{(lem 3.2.12)}}{\Longrightarrow} \quad 0 < \frac{d}{da}\mathbf{T}_2\mathbf{T}_3 < \frac{dx_4}{da}$$
$$\Longrightarrow \quad 0 < \frac{d}{da}\mathbf{A}_{\mu,1} < \frac{dx_4}{da}$$

(2)

$$0 < \frac{d}{da}\mathbf{A}_{\mu,1} < \frac{dx_4}{da} \quad \overset{\substack{\text{(lem 3.2.7)}\\ \text{(lem 3.2.5)}}}{\Longrightarrow} \quad 0 < \frac{d}{da}\mathbf{T}_i\mathbf{A}_{\mu,1}x\bigg|_{i\in\{2,4\}} < \frac{dx_4}{da}$$
$$\overset{\text{(lem 3.2.13(1))}}{\Longrightarrow} \quad 0 < \frac{d}{da}\mathbf{A}_{\mu,1}\mathbf{T}_i\mathbf{A}_{\mu,1}x < \frac{dx_4}{da}$$

By recurrently concluding this way, inequality (3.156) is proved.
(3)

$$0 < \frac{d}{da}x < \frac{dx_4}{da} \quad \overset{\text{(lem 3.2.4)}}{\Longrightarrow} \quad 0 < \frac{d}{da}\mathbf{T}_1x < \frac{dx_4}{da}$$
$$\overset{\substack{\text{(lem 3.2.7)}\\ \text{(lem 3.2.11)}\\ \text{(lem 3.2.13(2))}}}{\Longrightarrow} \frac{d}{da}\underbrace{\mathbf{T}_2^{-1}\mathbf{T}_2}_{\mathbf{id}}\mathbf{T}_4^{\mu-1}\mathbf{T}_3\mathbf{A}_{\mu,1}\mathbf{T}_i\mathbf{A}_{\mu,1}\ldots\mathbf{A}_{\mu,1}\mathbf{T}_i\mathbf{A}_{\mu,1}\mathbf{T}_1x < \frac{dx_4}{da}$$

□

3.3 Convex case

After the period-doubling mechanism has been understood by using the **T**-transformations in the linear case, this section is concerned about the transfer of knowledge to the nonlinear convex case implying $1 < \rho$.

The functions (3.1) and (3.3) respectively defined on page 27 possess the same kneading sequence with $\rho = 1$ and $\rho > 1$ for suitable control parameters a. This fact is analog to the logistic map, sharing all orbits associated to symbolic sequences of the tent map if they posses the same kneading sequence, as pointed out in Section 2.2.3 by treating the logistic map as a deformed tent map under maintenance of continuity and monotonicity.

Due to the continuous and strictly monotonic branch f_1 of the function f and the same kneading sequence κ_{cup}, orbits with the symbolic representations s_x and $\sigma_k s_x \in [\kappa_{cup}, \overline{3}]$, $k \in \mathbb{Z}_+$ are admissible.

> For clarity, the monotonically decreasing kneading sequence could be imagined not to proceed through all periodic sequences as a increases, resulting in a break down of period-doubling at a finite period $p_0 = 2^{n_0}$.
> Assuming the kneading sequence to stop decreasing at $\kappa = s_{2^{n_0}}$ followed by a jump to an even lower sequence for example $\kappa = 131112$, that is a smaller sequence than any period-doubling sequence according to equation (3.6).
> Under this assumption the kneading theory with respect to equation (3.121) asserts that points $x \in [0, 1]$ exist, providing
>
> $$s_x = \overline{\left(\overset{n}{\underset{\nu=1}{*}} 1\right) s_{x,p}} \qquad\qquad \forall n \in \mathbb{N},\ s_{x,p} \in \{1, 2, 3\}.$$
>
> This fact implies, that the **T**-transformations according to the inverse period-doubling operator (3.76) worked out in Section 3.2.4 feature a non-empty domain for every $\mathbf{P}_{2^n}$, with $n \in \mathbb{N}$. Hence the period-doubling did proceed through all periods $p = 2^n$, $n \in \mathbb{N}$ as in the linear case. This is a contradiction to the assumption, resulting in the fact that the kneading sequence κ has to run through all the period-doubling sequences (3.123) as a increases.

The kneading-value proceeds to lower values as control parameter a increases until f_1 becomes surjective too, allowing all symbolic sequences $s_x = \prod_\nu s_{x,\nu}$ with $s_{x,\nu} \in \{1, 2, 3\}$ to exist as long as digit 2 leads to periodic behavior.

The monotonicity and continuity of f_1 implies, that the same orbits exist in maps with different ρ and associated control parameter a_ρ.
Therefore the kneading-value asserts that these orbits exist, while monotonicity and continuity of f_1 keep the order of appearance valid as ρ increases. It follows that any orbit found in the iteration of $f_{\rho=1}$ will be found in $f_{\rho>1}$, too. Due to the convexity the period-doubling does no longer proceed directly from superstable orbit p to superstable orbit $2p$ as will be shown later.

Figure 3.23 shows the effect of the three different kinds of ρ to the period $p(a)$ as a function of a. In the convex case featured by $\rho = 2$ there exist areas e.g. $[0.7, 0.71]$, where there is no period $p(a)$ defined. These areas correspond to non-absorbing attractive orbits to be discussed in the following. Given a control parameter a e.g. $a < b$ in Figure 3.26(b) an increase in ρ results in a pitchfork bifurcation, because of the transition of a stable fixed point to a non-absorbing attractive period $p = 2$ orbit.

The dependence of the structures on control parameter a observed in the $p(a)$ diagram in Figure 3.23 is easily understood by discerning Figure 3.24. When ρ increases, the preimages located around the fixed point become more closely located near the fixed point and less dependent on a. In the concave case this process is reversed. In general changes in ρ lead to changes in the behavior of fixed points e.g. an increase in ρ causes the degenerate ambiguous points in the period-doubling sequence to become whole intervals as a basin of attraction to non-absorbing periodic orbits, that will be investigated in the following.

Comparison between Figure 3.25 and 3.7 shows the $\mathbf{T}$-transformations to make sense according to their Definition (3.16) and (3.15) on page 38 by use of the generalized Operators (3.3).

$$\mathbf{T}_i = \mathbf{f}_{s_i}^{-1} = \mathbf{f}_{s_{i,1}}^{-1}\mathbf{f}_{s_{i,2}}^{-1} \dots \mathbf{f}_{s_{i,\iota_i}}^{-1} \tag{3.158}$$

$$\begin{array}{lll} s_1 = 131 & \iota_1 = 3 & \mathcal{D}(\mathbf{T}_1) = [\max(b, \mathbf{f}_1\mathbf{f}_3 a), c] \\ s_2 = 1311 & \iota_2 = 4 & \mathcal{D}(\mathbf{T}_2) = [0, x_4] \\ s_3 = 13 & \iota_3 = 2 & \mathcal{D}(\mathbf{T}_3) = [0, \mathbf{f}_1^{-1}c] \\ s_4 = 1313 & \iota_4 = 4 & \mathcal{D}(\mathbf{T}_4) = [0, \mathbf{f}_1^{-1}c] \end{array} \tag{3.159}$$

$$\begin{array}{ll} \mathbf{f}_1^{-1} = b\left(1 - \frac{\cdot}{a}\right)^{\frac{1}{\rho}} & \mathcal{D}(\mathbf{f}_1) = [0, a] \\ \mathbf{f}_3^{-1} = (1-c)\cdot + c & \mathcal{D}(\mathbf{f}_3) = [0, 1] \end{array} \tag{3.160}$$

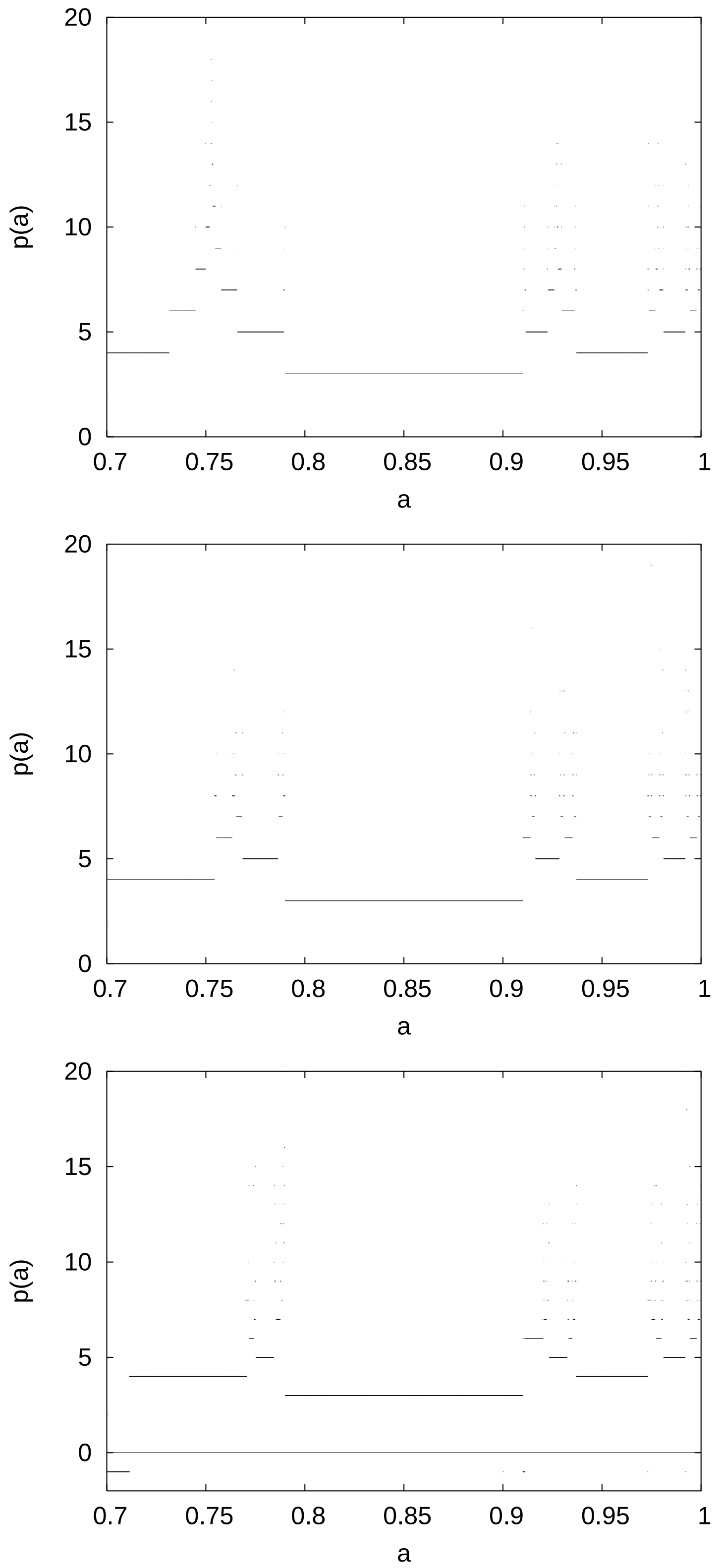

Figure 3.23: The complicated structures of periods $p(a)$ versus a are shortened as ρ increases. The period $p(a)$ is shown for $\rho = \frac{1}{2}$, $\rho = 1$ and $\rho = 2$ respectively. Period $p = -1$ in the convex case below is associated with an attractive non-absorbing periodic orbit.

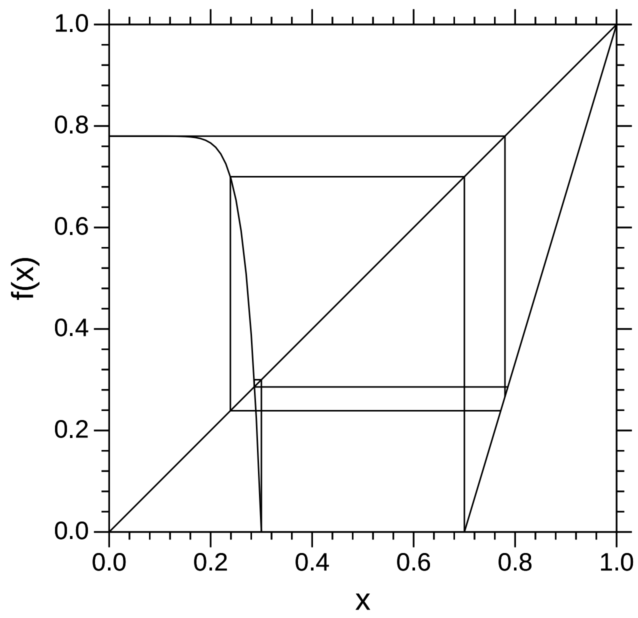

Figure 3.24: With $\rho = 10$ preimages located around the fixed point e.g. interval $[\mathbf{f}_1^{-1}c, \mathbf{f}_1^{-1}b]$ are easily verified to become almost invariant under a change of a.

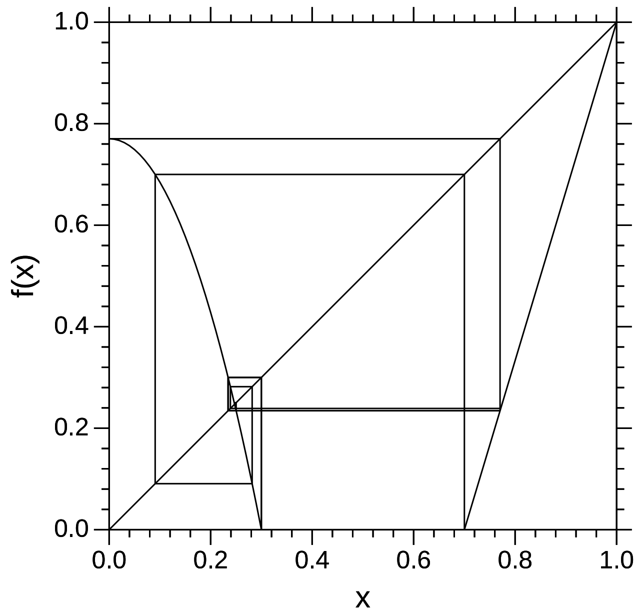

Figure 3.25: The arise of non-trivial orbits in the convex map allows to use the same $\mathbf{T}$-transformations again just in their nonlinear representation due to their dependence on ρ.

$$\begin{aligned}\tfrac{d}{da}\mathbf{f}_1^{-1}x &= \tfrac{b}{a\rho}\left(1-\tfrac{x}{a}\right)^{\frac{1-\rho}{\rho}}\left(\tfrac{x}{a}-\tfrac{dx}{da}\right)\\ \tfrac{d}{da}\mathbf{f}_3^{-1}x &= (1-c)\tfrac{dx}{da}\end{aligned} \tag{3.161}$$

Equations (3.158), (3.159) and (3.160) resemble these definitions under the general condition of non-trivial orbits $a \in [\mathbf{f}_3^{-1}\mathbf{f}_1^{-1}b, \mathbf{f}_3^{-1}\left(\mathbf{f}_1^{-1}\right)^3 c]$.
Figure 3.26 shows Lamerey diagrams of the period-doubling as a increases. Due to the expansive parts of the map, the Lamerey diagrams scarcely allow to distinguish situations for higher period's a parameters i.e. period $p = 4$ possesses non-superstable attractive periodic orbits too, that are however hardly visible in Lamerey diagrams similar to Figure 3.26 (e).

To focus on period-doubling, beginning with the superstable orbit of period $p = 2$ is useful, because of its trivial nature characterized by $x_0 \in [\mathbf{f}_1^{-1}c, \mathbf{f}_1^{-1}b]$ and $x_2 = x_0 = 0$. Figure 3.27 (a) gives a hint to the situation concerning interval $[0, \mathbf{f}_1^{-1}b]$ in concordance with Figure 3.26 (c). As a increases the superstable period $p = 2$ orbit becomes a non-superstable attractive periodic orbit depicted in Figure 3.26 (d) and is explained in Figure 3.27 (b).
This attractive periodic orbit occurs due to Lemma 3.3.1, that shows $\mathbf{f}_1^{-1}c$ to move to the right with infinite rate as a increases just in the moment $x_2 = \mathbf{f}_3\mathbf{f}_1 x_0 = x_0$ appears in the interval $[0, \mathbf{f}_1^{-1}c]$. So the resulting orbit is non superstable but an attractive periodic orbit of period $p = 2$ and sequence $s_{lc} = 13$. Therewith the convex map is shown to exhibit attractive periodic orbits without an absorption. Due to the missing absorption Figures 3.23 and 2.8 on page 26 display these orbits with $p_\infty = \infty$ that are almost invisible because of their small width. The degenerate ambiguous points b and c of the linear map turn to real intervals of finite basins of attraction to $x_0 = 0$ in a as they are in unimodal maps without hitting partition 2.

Lemma 3.3.1 explains that all derivatives of $\mathbf{T}$-transformations defined in equation (3.159) diverge when mapped to a point x to 0, because of the final operation of the $\mathbf{f}_1$ operator.

Lemma 3.3.1. *Every point x imaged to the neighborhood of $x_0 = 0$ by operator $\mathbf{f}_1^{-1}$ shifts to the right in Figure 3.27 with a diverging derivative as $\rho > 1$ is fulfilled.*

Proof. Validity of

$$\lim_{\mathbf{f}_1^{-1}x\to 0} \frac{d}{da}\mathbf{f}_1^{-1}x\bigg|_{\frac{dx}{da}<1} = \pm\infty \tag{3.162}$$

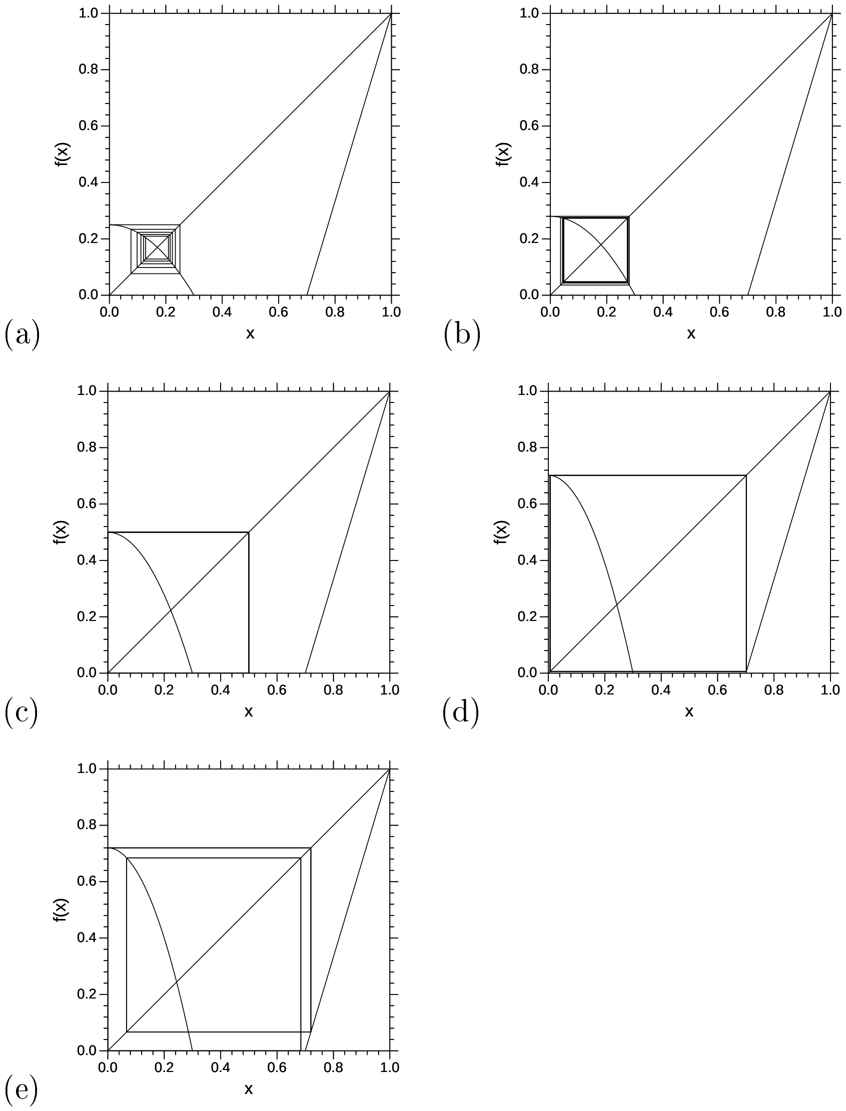

Figure 3.26: Period-doubling as a increases from (a) stable fixed point of period $p = 1$ to (b) period $p = 2$ attractive orbit featuring $a < b$ to (c) superstable period $p = 2$ orbit to (d) attractive orbit of period $p = 2$ (e) and attractive period $p = 4$ orbit.

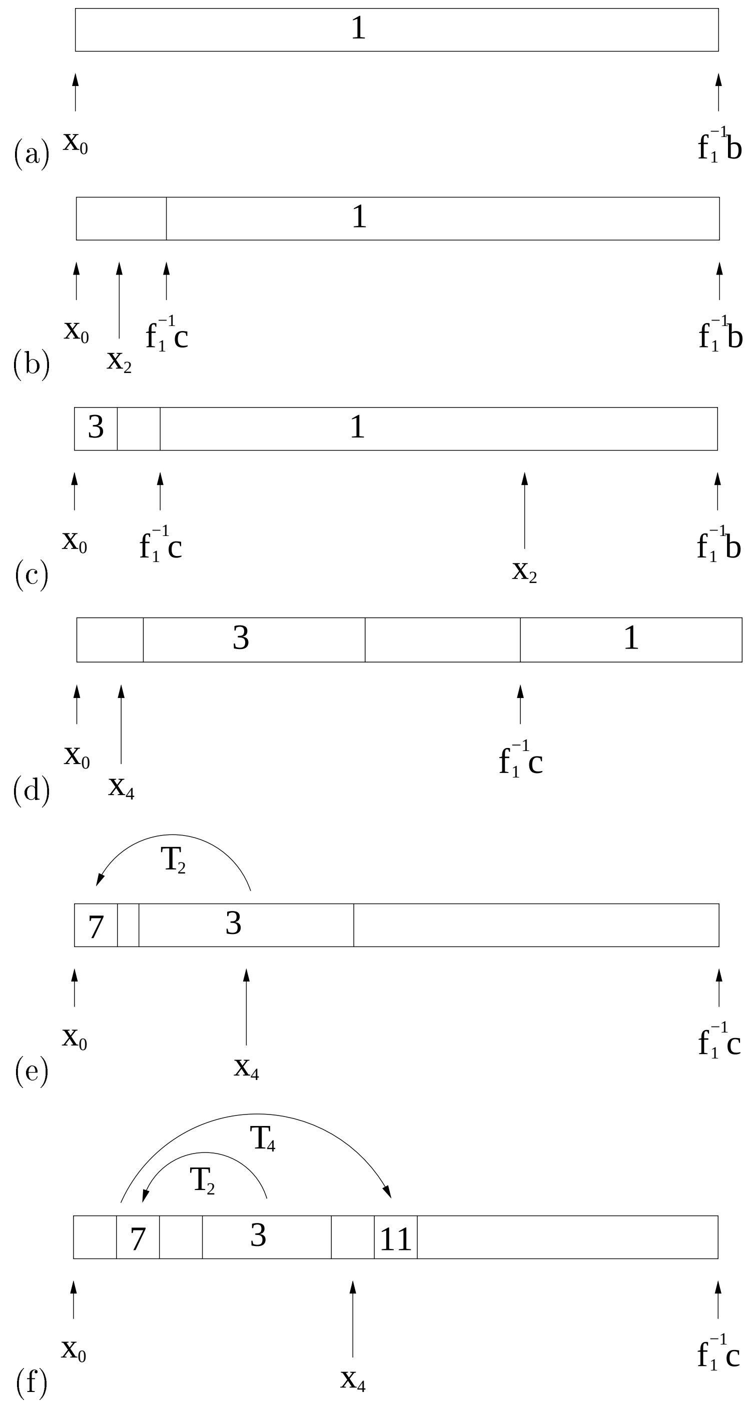

Figure 3.27: Starting with the superstable period $p = 2$ orbit (a) period-doubling proceeds via the period $p = 2$ attractive orbit (b) followed by period $p = 4$ superstable orbit (c) indicated by $x_2 \in [\mathbf{f}_1^{-1}c, \mathbf{f}_1^{-1}b]$. Then non-trivial period-doubling sets in with attractive orbit $x_4 \notin \mathbf{T}_1[b, c]$ (d) followed by superstable period $p = 8$ orbit (e) and another non-superstable attractive orbit (f).

has to be shown. By using equation (3.161) expression (3.162) can be evaluated to yield equation

$$\lim_{\mathbf{f}_1^{-1}x \to 0} \frac{d}{da}\mathbf{f}_1^{-1}x = \lim_{x \to a} \frac{d}{da}\mathbf{f}_1^{-1}x = \frac{b}{\rho} \lim_{x \to a} \left(1 - \frac{x}{a}\right)^{\frac{1-\rho}{\rho}} \left(\frac{x}{a^2} - \frac{1}{a}\frac{dx}{da}\right) = \pm\infty. \tag{3.163}$$

Performing the limit results in a diverging derivative because of the negative exponent of the vanishing factor in the left parenthesis. The right parenthesis stays almost constant and determines the sign.

□

3.4 Relationship to unimodal maps & Scenario

In this section the relationship between the cup map and unimodal maps is pointed out. The orbits of the cup map in Figure 3.28 (a) do not change in their symbolic representation under transformation $x \longrightarrow 1 - x$ and $f(x) \longrightarrow 1 - f(x)$ illustrated in Figure 3.28(a), (b). This transformation results in an unchanged but rotated Lamerey diagram of orbits, which is equivalent to a rotation of the Lamerey diagram about the angle $\varphi = \pi$ and a rescaling of the axes.

In the center interval the function $f(x)$ is equal to 1 and still possesses a vanishing derivative. Taking the limiting case $c, b \to \frac{1}{2}$ reveals the function depicted in Figure 3.28(c).

Claiming the derivative to be zero and continuous in the degenerate point $x = \frac{1}{2}$ and by using the kneading-value and the admissibility criterion (3.121) the function $f_{uni}(x)$ depicted in Figure 3.28(d) is obtained that will be proven S-unimodal by Lemma 3.4.1.
Equation 3.165 is a cubic parabola shown in Figure 3.28(d) satisfying boundary Conditions (3.164) for all $a \in [0, 1]$ and matches the definition of unimodality (2.2) on page 8 unless $a < \frac{4}{5}$. Otherwise the minimum of $f_{uni}(x)$ will be located in the interval $[0, 1]$ destroying the necessary monotonicity in the right branch of $f(x)$.

$$f(0) = 0, \qquad f\left(\frac{1}{2}\right) = 1, \qquad f(1) = a, \qquad \left(\frac{df}{da}\right)\left(\frac{1}{2}\right) = 0 \tag{3.164}$$

$$f_{uni}(x) = 4ax^3 - 4(a+1)x^2 + (a+4)x \qquad\qquad a \in [0, \frac{4}{5}[\tag{3.165}$$

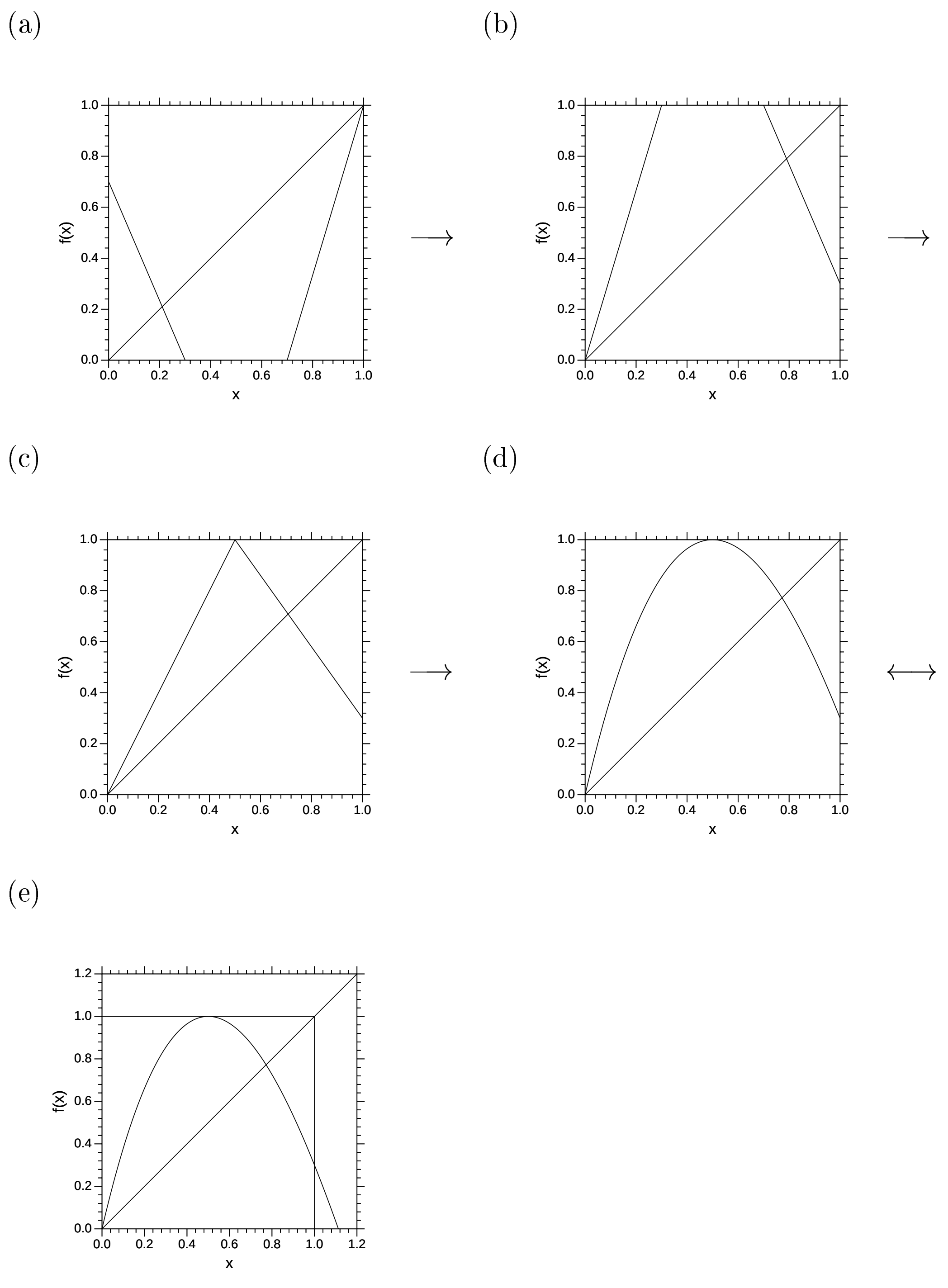

Figure 3.28: The cup map becomes S-unimodal under the invariant transformation $x \longrightarrow 1-x$ and $f(x) \longrightarrow 1-f(x)$ (a), (b), degenerating the center partition to a point (c), using the admissibility theorem (3.121) and claiming the derivative to become continuous (d). By extending the domain and the codomain (e) the relationship to the parameterization of the logistic map becomes obvious.

This transformation scarcely stresses imagination and relates many features of the cup map to the well understood unimodal maps and their Feigenbaum scenario into chaos. Especially the emergence of period-doubling is obvious due to the same fixed point becoming unstable, giving rise to period-doubling.

The parameterization of unimodal maps usually employs their maximum to increase in a linear dependence of the control parameter used to obtain the Feigenbaum constant δ. By using the S-unimodal map $f_{uni}(x)$ the control parameter a is another parameterization for the mechanism of the fixed point becoming unstable, leading to the period-doubling function derived in Section 3.2.6.

Lemma 3.4.1. *The function $f_{uni}(x)$ is S-unimodal in $[0,1]$ with $a \in [0, \frac{4}{5}[$.*

Proof. At first the function $f_{uni}(x)$ has to be shown to match unimodality Condition (2.2) on page 8. The derivative

$$\frac{df_{uni}}{da} = 12ax^2 - 8(a+1) + a + 4$$

yields two extremes x_{E1} and x_{E2} with

$$x_{E1} = \frac{1}{2}, \qquad x_{E2} = \frac{1}{6} + \frac{2}{3a} \qquad \Longrightarrow \qquad x_{E2} > 1\Big|_{a<\frac{4}{5}} .$$

As long as $a \in [0, \frac{4}{5}[$, there exist 2 monotonous branches with critical point $c = x_{E1} = \frac{1}{2}$ and the unimodality condition is fulfilled.
To show S-unimodality equation (2.1) has to be shown to be negative for all $x \in [0,1]$ and $a \in [0, \frac{4}{5}[$. It is sufficient to show equation

$$g(x) = \frac{d^3 f_{uni}}{dx^3}\frac{df_{uni}}{dx} - \frac{3}{2}\left(\frac{d^2 f_{uni}}{dx^2}\right)^2 \tag{3.166}$$

to be negative under these conditions.
Evaluating equation (3.166) by use of equation (3.165) results in a polynomial $g(x)$.

$$g(x) = -576a^2x^2 + 384a(a+1)x - 72a^2 - 96a - 96$$

Calculating the extremum of $g(x)$ yields a maximum at

$$x_{g_E} = \frac{1}{3}\left(1 + \frac{1}{a}\right)$$

with

$$g(x_{g_E}) = -8a^2 + 32a - 32 < 0.$$

Therefore the function $f_{uni}(x)$ is S-unimodal in $[0,1]$ for $a \in [0, \frac{4}{5}[$ by Definition (2.2). $\square$

The period-doubling scenario of the linear cup map is quite different to the scenario undergone by unimodal maps despite all the similarities of the mechanism already pointed out. Figure 3.29 shows the period-doubling scenario of the linear cup map in the asymmetric case featuring $b = 0.1$ and $c = 0.21$. The scenario differs drastically from the universal U-sequence in Figure 2.1 on page 11. From left to right in the interval $[0.21, \approx 0.3]$ that will be called a *band* in the following, Figure 3.29 shows the period-doubling sequence as a increases. Due to the exponential growing period-doubling function there are very few periods visible.
After the period-doubling the total period-doubling sets in as discussed in section 3.2.8. Finally all trivial orbits of kind $s = 13(1)^n 2$ appear divided by areas of complex behavior. At first n takes all odd values increasingly from $n = 1$ to $n = \lim_{\mu\to\infty} 2\mu + 1$ until the fixed point visible in Figure 3.7 is hit by $x_2 = \mathbf{f}_3 a$. Then n decreases from $n = \lim_{\mu\to\infty} 2\mu$ to $n = 2$. After all these trivial orbits and the complex behaviors between them have been passed, trivial orbits of kind $s = 132$ appear at $a \approx 0.3$ in a wide window.

As it is easily verified by the left part of Figure 3.4 on page 33 generation of $\mathbf{f}_3$ preimages of interval $[b, c]$ results in countable infinite $\mathbf{f}_3$ preimages that are successively hit by $x_1 = \mathbf{f}x_0 = a$ as a increases. These intervals are the silent windows in the orbit diagram shown in Figure 3.29 that divide the bands of trivial orbits and the complex behaviour.

Figure 3.30 focuses on the primary period-doubling and the successive band, where the skeleton of the linear cup map resembles the orbit diagram in wide intervals due to the superstability caused by the absorption interval $[b, c]$.

(a)

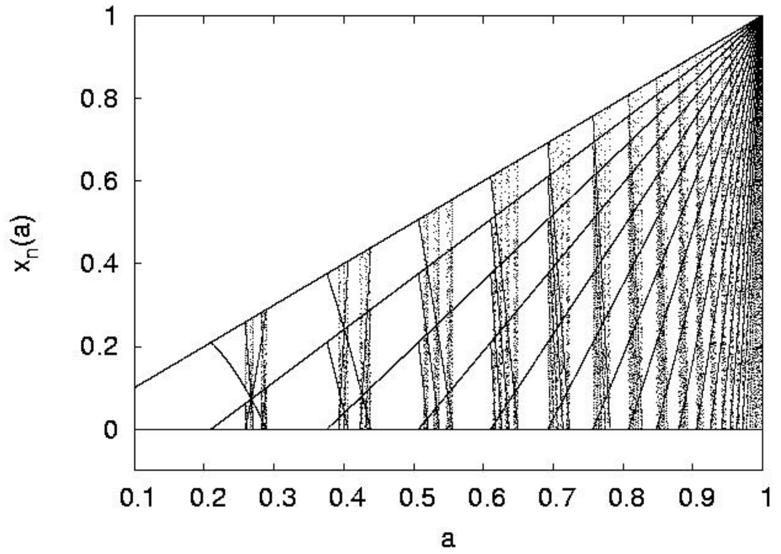

(b)

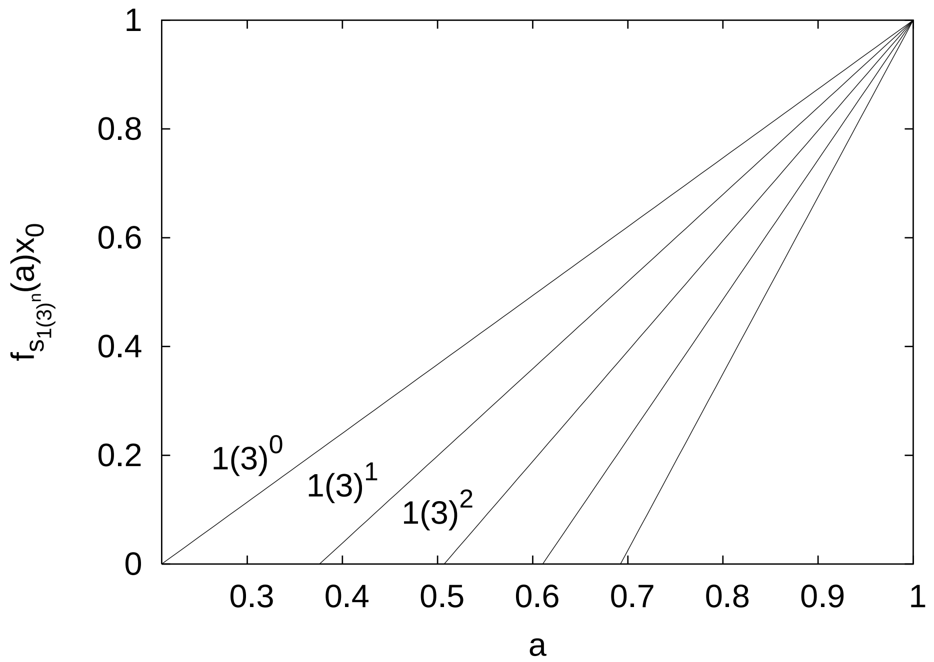

Figure 3.29: (a) Orbit diagram of the linear cup map with $b = 0.1$ and $c = 0.21$ shows the different Feigenbaum scenario to unimodal maps. With $a \in [0.2, 0.3]$ from left to right period-doubling sets in followed by total period-doubling. Thereafter trivial orbits $s_{t_1} = 13(1)^n 2$ exist separated by other complex behaviors. With $0.3 < a < 0.4$ trivial s_{t_2} orbit 132 dominates the diagram. The simple lines in (b) represent the skeleton of orbits of kind $s_{x_0} = 1(3)^n$.

(a)

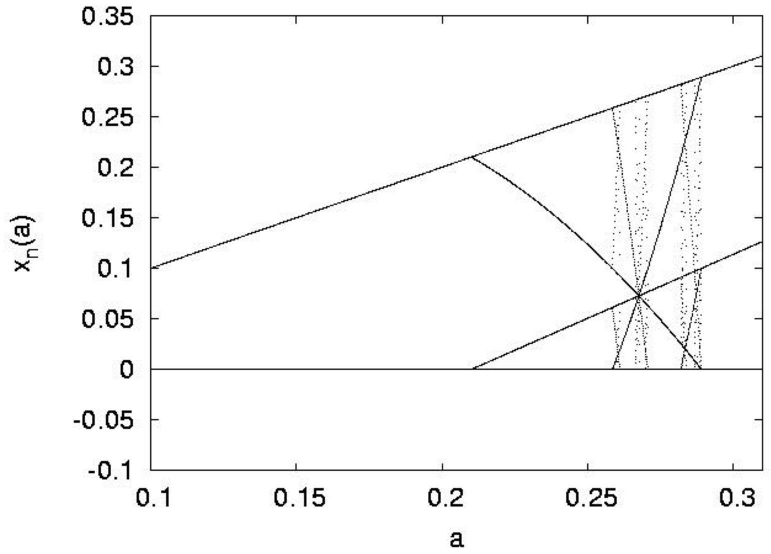

(b)

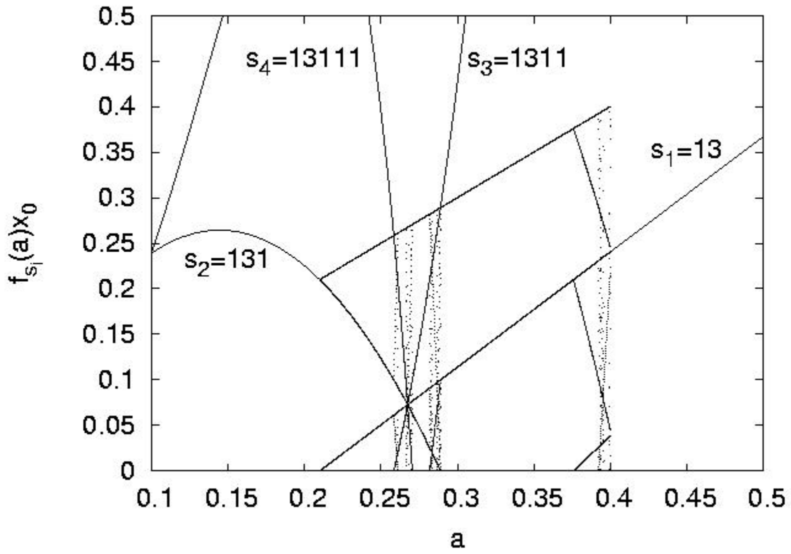

Figure 3.30: The detail of the orbit diagram (a) and parts of the skeleton to the linear cup map are shown to resemble the orbit diagram in whole intervals due to superstability for all possible orbits (b).

Chapter 4

The original map

The model of a particle in a horizontally shaken box discussed in Section 2.4 led to a complicated iterated map. Chapter 3 dealt with a theoretical explanation of the period-doubling observed in numerical simulations of the generic cup map, which was designed to capture the essential features of the original map concerning period-doubling. Structures in the right of the iterated map depicted in Figure 2.7 on page 26 deserve study as well to characterize the whole system's behavior. They will be referred to as the *maze*.

In Section 4.1 an analytically solveable approximation of the oscillating box is developed in order to investigate the behavior of the maze-like structure of the map in Section 4.2 by using standard techniques. Therefore the *Perron-Frobenius Operator* is used to obtain the leading invariant density and to quantify the escape rate of the artificial maze. This way the transient behavior of the system is characterized.

4.1 Generic maze

Neglecting friction, the harmonic motion of the shaken box leads in direct consequence to solution (2.43) found on page 22 as a transcendent equation in ϕ complying the equation of motion (2.42). Figure 2.6 shows the walls in their harmonic sine motion. To obtain an analytically solvable model, the sine function can be approximated by parabolas shown in Figure 4.1 and represented by

$$f_n(x) = (x - 4n + 1)^2 + \alpha - 1 \qquad x \in [4n-2, 4n],\ n \in \mathbb{N} \tag{4.1}$$

and

$$g_k(x) = -(x - 4k + 3)^2 + 1 \qquad x \in [4k - 4, 4k - 2],\ k \in \mathbb{N}. \tag{4.2}$$

The abscissa has been rescaled to unity according to $\phi = \frac{\pi}{2} \longrightarrow x = 1$ to simplify the following quadratic equations.

Slowly moving particles colliding with the wall of the shaken box hit the wall at phases close to $\phi \to \frac{\pi}{2}$ that corresponds with $x \to 1$ in the iterated map. The parabola approximation resembles the original sinusoidal motion best in case of $x \to 1$ and allows to estimate the width of the function's branches as a function of n.

Figure 4.2 gives a hint to possible trajectories of the particle with point X associated to abscissa coordinate $x = \frac{\phi_0}{\frac{\pi}{2}} \to 1$. The points Y, Z are associated to their abscissa coordinates y, z. To obtain the next point of iteration

$$x' = z - (4n + 2) \tag{4.3}$$

is used. For simplicity $k = 1$ will be used all the time unless otherwise stated. Treating the next collision $z = \frac{\phi_1}{\frac{\pi}{2}}$ to a given rescaled starting phase $x = \frac{\phi_0}{\frac{\pi}{2}}$ its dependence is illustrated in Figure 4.2(a) to result in a continuous increase in z until the minimum of function $f_n(x)$ is reached at $z = 4n - 1$ with $n = 2$ in Figure 4.1 associated with $x' = 1$ the next starting phase obtained by equation (4.3).

Thereafter a collision with the upper wall i.e. function $f_n(x)$ results in a jump of point Z to the next f_{n+1} minimum at the second collision with the upper wall illustrated in Figure 4.2(b), giving birth to the point Y that indicates the first collision with the upper wall.
A further increase in x therefore is associated with a decrease in z and therewith in x' that results in a negative slope in the map that is scarcely to be seen in Figure 2.7 at $a \approx 0.75$. The conclusion of this fact is, that the original iterated map $f(x) : [0, 1] \to [0, 1]$ is continuous.

As x increases further, point Y moves to the right and therefore Z moves from $z = 4(n + 1) - 1$ to the left, and so does x' until the limiting case depicted in Figure 4.1 and 4.2(c) is reached.

In the limiting case no longer a collision occurs in Y, resulting in an increase in z as x increases. Coordinate z is continuous, but derivative $\frac{dz}{dx}$ is discon-

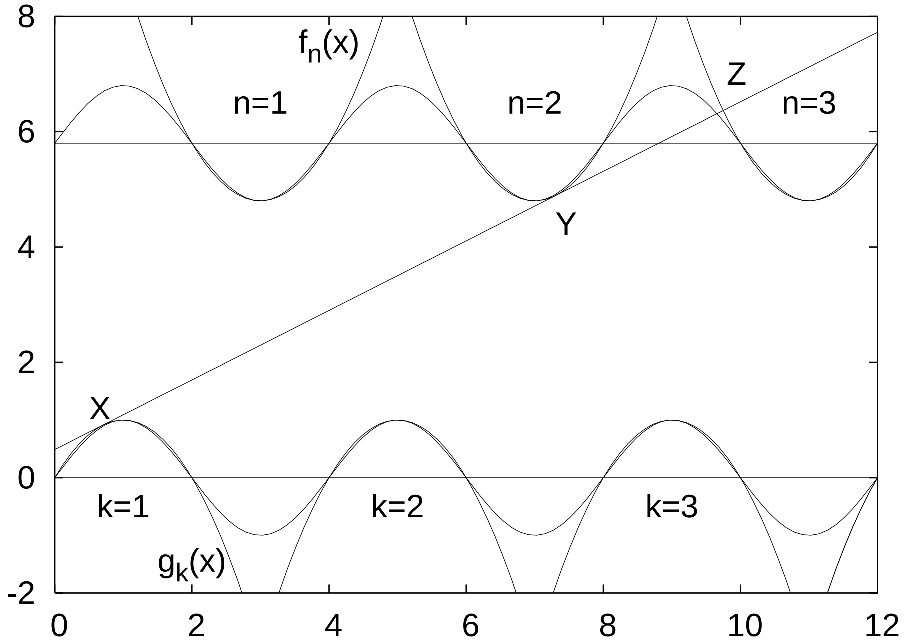

Figure 4.1: An analytically solvable model of the particle in a horizontally shaken box. The sloped line represents a trajectory starting at point X passing point Y without touching the wall and finally hitting the wall at point Z.

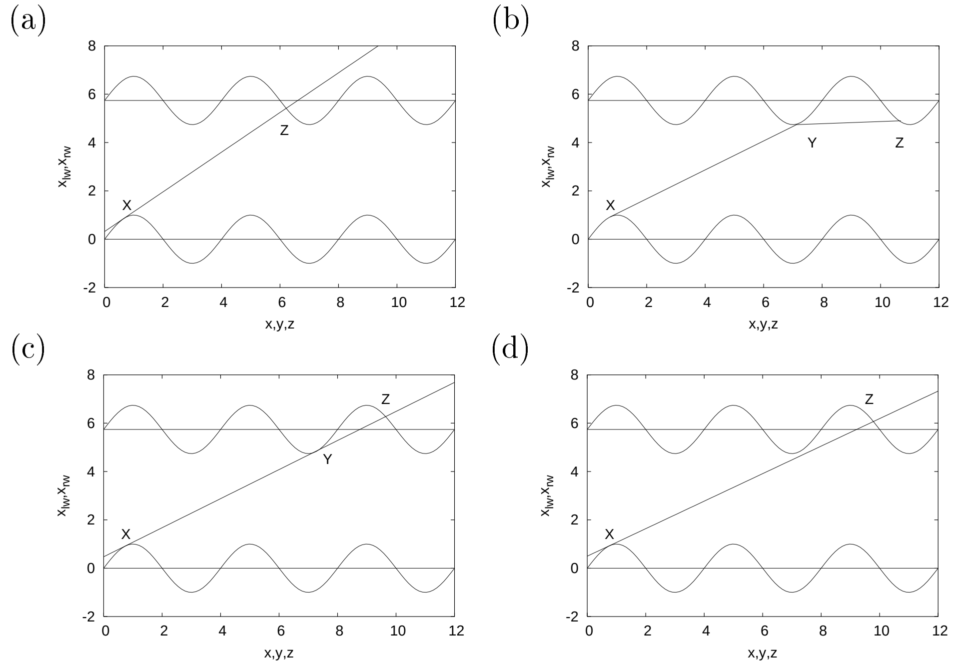

Figure 4.2: Subsequent types of trajectories as x increases. First z grows monotonically with x (a), then z decreases (b) until the limiting case (c) is reached and then grows again (d).

tinuous in the limiting case, because it suddenly switches from negative to positive values. Condition

$$\left(\frac{dg_k}{dx}\right)(x_n) = \left(\frac{df_n}{dx}\right)(y_n) \tag{4.4}$$

identifies this kind of discontinuities in the derivative of z, allowing to calculate the associated x_n and y_n explicitly as a function of n. Apparently the x_n monotonically converge to 1 with $n \to \infty$ and satisfy $x_n > 0$, $n \in \mathbb{N}$.

As equation (4.3) and Figure 4.1 suggest, x' becomes negative in special cases with small n like the one shown in Figure 4.2(d), because the particle hits the wall in the positive sine wave leading to absorption. The absorption is identical to the absorption discussed in Section 2.4. Therefore collisions yielding $x' < 0$ lead to the next starting value $x = 0$ in the iterated map, because of the system's reset due to absorption. For an explanation of the original map's shape $x' < 0$ is useful for identifying other intervals of absorption in the artificial iteration function depicted in Figure 4.4 at $x \approx 0.7$ and $x \approx 0.8$, where the function is identical to zero due to absorption. As a consequence

$$x_{c_n} = z_n - (4n + 2) \tag{4.5}$$

defines rescaled phases of collision x_{c_n} in the limiting case with y_n located at function $f_n(x)$ and z_n located at $f_{n+1}(x)$. Absorptions after a collision at $x_{c_n} < 0$ yield the next starting phase $x = 0$. Therefore there exist

$$\tilde{x}_{c_n} = \begin{cases} x_{c_n} & x_{c_n} > 0 \\ 0 & x_{c_n} < 0 \end{cases} \tag{4.6}$$

defining an interval of collision phases $[x_{c_n}, \tilde{x}_{c_n}]$ resulting in the same following starting phase $x = 0$. This interval in the collision phase is connected to an interval in the associated starting phases $[x_n, \tilde{x}_n]$ that result in an absorption and therewith a following starting phase $x = 0$, with $x_n \overset{\text{eqn. of motion}}{\longrightarrow} x_{c_n}$ and $\tilde{x}_n \overset{\text{eqn. of motion}}{\longrightarrow} \tilde{x}_{c_n}$.

To prevent the codomain of the iteration function from becoming negative

$$\tilde{x}_n = \begin{cases} x_{c_n} & x_{c_n} > 0 \\ x_{c_n} - \frac{x_{n+1} - x_n}{1 - x_{c_n}} x_{c_n} & x_{c_n} < 0 \end{cases} \tag{4.7}$$

is defined by using linear interpolation. The additional absorption intervals are specified by $[x_n, \tilde{x}_n]$ as long as the interval borders differ. By using linear

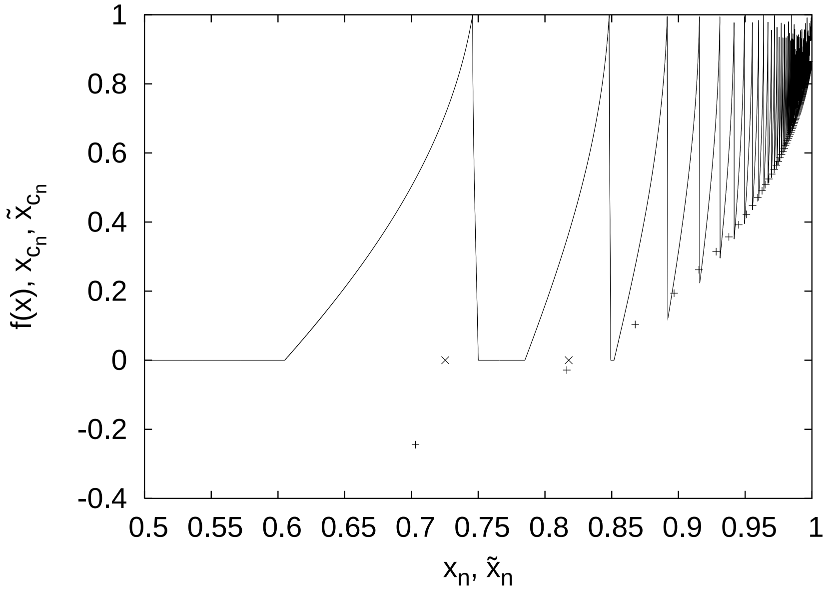

Figure 4.3: Comparison between the points (x_n, x_{c_n}) denoted by $+$ and $(\tilde{x}_n, \tilde{x}_{c_n})$ denoted by $\times$. Their horizontal distance between them are new absorption intervals. The dots are shifted to the left with respect to the original iteration function's absorption areas due to the parabola approximation.

interpolation to obtain $\tilde{x}_n$, the artificial maze designed in Section 4.2 by use of $\tilde{x}_n$ will become very simple due to linearization of the function's branches.

To summarize the terminology used in the following, the limiting case determines the associated point of departure x_n resulting in a collision at phase x_{c_n}. Contingent absorptions yield $\tilde{x}_{c_n}$ and their associated linearly interpolated starting phase $\tilde{x}_n$.

$$\text{limiting case} \longrightarrow x_n \longrightarrow x_{c_n}$$

$$x_{c_n} \xrightarrow{\text{lin. interpol.}} \begin{cases} (\tilde{x}_n, \tilde{x}_{c_n}) & \text{Function branch starting points} \\ [x_n, \tilde{x}_n] & \text{Adittional absorption intervals} \end{cases}$$

In Figure 4.3 the difference between points (x_n, x_{c_n}) and points $(\tilde{x}_n \tilde{x}_{c_n})$ is seen to lead to another two absorption intervals. The two new absorption intervals are associated with the abscissa difference between the leftmost $+$ and $\times$.

Small n cause x_n to be most affected by error made by the parabola approximation. The artificial parabola model resembles the map's absorption intervals more left than in the original map due to higher values of the parabolas derivatives as $x \ll 1$. With $n \gg 1$ and $x \to 1$ respectively the approximation converges and allows to study the original maze by use of the artificial maze instead, because the behavior of interest is the behavior of $f(x)$ with $x \to 1$.

To calculate an analytical expression for x_n the limiting case (4.4) of the parabola approximation illustrated in Figure 4.1 can be evaluated by the derivatives of equations (4.1) and (4.2)

$$\frac{df_n}{dx} = 2(x - 4n + 1) \tag{4.8}$$

and

$$\frac{dg_k}{dx} = -2(x - 4k + 3). \tag{4.9}$$

By evaluating equation (4.4) relationship

$$y_n = -x_n + 4(k + n - 1) \tag{4.10}$$

is obtained in general with arbitrary $k < n$. Equation

$$f_n(y_n) = g_k(x_n) + \left(\frac{dg_k}{dx}\right)(x_n)(y_n - x_n) \tag{4.11}$$

is a consequence of the linear motion of the particle satisfying Condition (4.4). By use of Relationship (4.10) in equation (4.11) a quite simple quadratic equation

$$0 = {x_n}^2 - 4(k + n - 1)x_n - 4k + 16kn - 12n + 4 - \frac{\alpha}{2} \tag{4.12}$$

is obtained. Solving the quadratic equation (4.12) with $k = 1$ and choosing the correct branch yields the final solution

$$x_n = 2n - 2\sqrt{\left(n - \frac{1}{2}\right)^2 + \frac{\alpha - 2}{8}} \tag{4.13}$$

describing the sequence x_n. Equation (4.13) is easily verified to reproduce the convergence $\lim_{n\to\infty} x_n = 1$.
To obtain the phase of collision for a given starting point x_n associated with the n'th limiting process, Figure 4.1 suggests to calculate $z_n(x_n)$ by

$$f_{n+1}(z_n) = f_n(y_n) + \left(\frac{df_n}{dx}\right)(y_n)(z_n - y_n). \tag{4.14}$$

Using Relationship (4.10) and $k = 1$, another simple quadratic equation

$$0 = {z_n}^2 - 2(4(n+1) - x_n)z_n + (4n+3)^2 - (1-x_n)^2 - 2(1-x_n)(x_n - 4n) \tag{4.15}$$

is obtained that offers a useful solution by choosing the physically relevant solution

$$z_n(x_n) = 4(n+1) - x_n - \sqrt{8(1-x_n)}. \tag{4.16}$$

By use of equation (4.16) in equation (4.5) the simple expression

$$x_{c_n} = 2 - x_n - \sqrt{8(1-x_n)} \tag{4.17}$$

gives the points (x_n, x_{c_n}) depicted in figure 4.3 as +.

To summarize, by using the parabola approximation simple analytical expressions x_n and x_{c_n} allow to construct a generic model with the same convergence property as the original map as x approaches 1. The original iteration function is only accessible by numerically solving the transcendent solution to the equation of motion while x_n and x_{c_n} are accessible by quite simple expressions.

4.2 Stochastic investigation of the maze

The complicated maze structure in the iteration function depicted in Figure 4.3 makes a deterministic approach in understanding the systems behavior difficult. There exist countably infinite unstable fixed points. The function's branches become almost linear with a diverging slope as $n \to \infty$ and $x \to 1$ respectively. Because of the function's branches codomain extending from below the bisector up to 1 there exists a tendency to map all trajectories to smaller x and finally to enter the part of the map already studied deterministically in chapter 3. The codomain of each function's branch reaching up to 1 causes another set of trajectories to step deeper into the maze again. It is of great interest to know which process dominates at last and how to quantify the resulting behavior. To investigate this behavior standard techniques involving the Perron-Frobenius Operator [3] are utilized.

Because equation (4.17) represents an envelope with $x_n \to x \in [0,1]$ to the maze it can be continued to

$$h(x) = 2 - x - \sqrt{8(1-x)} \qquad x \in [0,1]. \tag{4.18}$$

The maze will be modeled by function $f(x)$ consisting of linear functions $f_n(x)$ defined by

$$f_n(x) = \frac{1-h(\tilde{x}_n)}{x_{n+1}-\tilde{x}_n}(x-\tilde{x}_n)+h(\tilde{x}_n) \qquad \mathcal{D}(f_n) =]\tilde{x}_n, x_{n+1}] \tag{4.19}$$

and

$$f_n(x) = \alpha_n x + \beta_n \qquad \mathcal{D}(f_n) =]\tilde{x}_n, x_{x+1}] \tag{4.20}$$

respectively with

$$\alpha_n = \frac{df_n}{dx} = \frac{1-h(\tilde{x}_n)}{x_{n+1}-\tilde{x}_n} = const \neq 0 \tag{4.21}$$

and

$$\beta_n = -\alpha\tilde{x}_n + h(\tilde{x}_n). \tag{4.22}$$

The resulting artificial maze $f(x)$ is represented by

$$f(x) = \sum_{\nu=1}^{\infty} [\Theta(x-\tilde{x}_n) - \Theta(x-x_{n+1})] \left[(x-\tilde{x}_n)\frac{df_n}{dx} + h(\tilde{x}_n)\right] \tag{4.23}$$

using the Heaviside function to take the domain of $f_n(x)$ into account. By doing so the less relevant case (b) of Figure 4.2 is neglected completely. Using the familiar representation of linear functions equation (4.19) appears in another representation (4.20) directly revealing its inverse function $f_n^{-1}(x)$ defined by

$$f_n^{-1}(x) = \alpha_n^i x + \beta_n^i \qquad \mathcal{D}(f_n^{-1}) =]h(\tilde{x}), 1] \tag{4.24}$$

with

$$\alpha_n^i = \frac{1}{\alpha_n} \tag{4.25}$$

and

$$\beta_n^i = \tilde{x}_n - \frac{h(\tilde{x}_n)}{\alpha_n}. \tag{4.26}$$

As it is obvious by definition of $\tilde{x}_n$ (4.7) via (4.5), that x_n and $\tilde{x}_n$ differ only for small n, their difference is of great importance in the formal Definition (4.23) of $f_n(x)$ reproducing the two additional absorption intervals for the

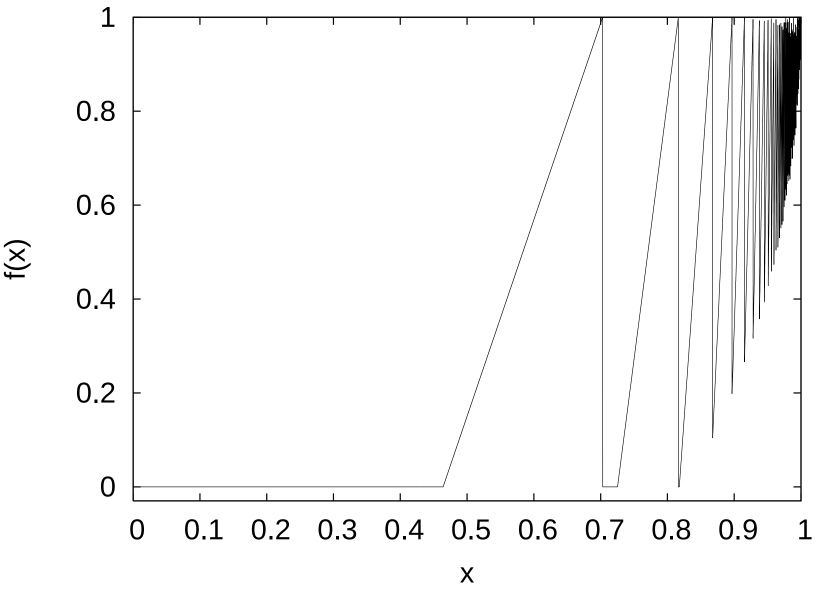

Figure 4.4: The generic linear model of the maze with the same α as figure 4.3 by use of x_n, $\tilde{x}_n$ and x_{c_n}.

given $\alpha = 5.74$ due to the cut off of function f_n at x_{n+1} and the function f_{n+1} switched on at $\tilde{x}_{n+1} \geq x_{n+1}$.

Using the Perron-Frobenius operator $\mathbf{L}$ defined by equation (2.34) on page 20 the evolution of a probability distribution $\rho_0(x)$ defined in the interval $[0,1]$ can be investigated.

$$\rho_{\nu+1} = \mathbf{L}\rho_\nu(x) = \sum_\sigma \frac{\rho_\nu(f_\sigma^{-1}(x))}{|\left(\frac{df}{dx}\right)(f_\sigma^{-1}(x))|}$$

Rewriting the Perron-Frobenius operator for the maze by use of equation (4.24) with respect to the domain of $\mathcal{D}(f_n^{-1})$ and the derivative (4.21) of the function f_n results in

$$\rho_{\nu+1}(x) = \sum_{n=1}^{\infty} \Theta(x - h(\tilde{x}_n))\alpha_n^i \rho_\nu(\alpha_n^i x + \beta_n^i) \qquad \mathcal{D}(\rho_i) = [0,1]. \tag{4.27}$$

Equation (4.27) can be rewritten to equation

$$\rho_{\nu+1}(x) = \sum_{n=1}^{\infty} \Theta(x - h(\tilde{x}_n)) \frac{x_{n+1} - \tilde{x}_n}{1 - h(\tilde{x}_n)} \rho_\nu \left(\frac{x_{n+1} - \tilde{x}_n}{1 - h(\tilde{x}_n)} (x - h(\tilde{x}_n)) + \tilde{x}_n \right), \tag{4.28}$$

that is used as a starting point for numerical investigation.

Figure 4.5 shows the numerically evaluated equation (4.28) beginning with $\rho_0(x) = 1$ up to $\rho_{10}(x)$ on a logarithmic scale. The logarithmic scale directly shows the asymptotically equidistant and for higher ν almost equishaped distributions. The successive application of the Perron-Frobenius operator quickly revealed the leading invariant distribution of the maze and allows to estimate the Eigenvalue χ of the Perron Frobenius operator according to equation

$$\rho_{\nu+1}(x) = \mathbf{L}\rho_\nu(x) \sim \chi_\nu \rho_\nu(x) \qquad\qquad \lim_{\nu\to\infty} \chi_{\nu+1} = \chi = e^\kappa. \tag{4.29}$$

Equation (4.29) becomes an equality in case of $\rho_\nu(x)$ being an invariant distribution. Because $\rho_0(x) = 1$ is not an invariant distribution of the map, but converges toward it, the sequence χ_ν will converge toward the Eigenvalue of the invariant distribution to the Perron-Frobenius Operator of the map as the distribution $\rho_\nu(x)$ converges to the invariant distribution.

Due to the systems absorption intervals, Eigenvalue χ is unequal to 1 and can be represented as $\chi = e^\kappa$ introducing the escape rate κ.

$$\rho_{\nu+\mu}(x) = \mathbf{L}^\mu \rho_\nu(x) \sim e^{\kappa\mu} \rho_\nu(x) \qquad\qquad \nu \gg 1 \tag{4.30}$$

For numerical treatment the notation is modified to

$$\rho_{\nu+\mu}(x_0) = \mathbf{L}^\mu \rho_\nu(x_0) = \chi_{\nu+\mu}(x_0) \rho_\nu(x_0) \tag{4.31}$$

introducing $\chi_{\nu+\mu}(x_0) \overset{\nu\gg 1}{\approx} const$ to allow the quotient

$$\frac{\chi_{\nu+1}(x_0)}{\chi_\nu(x_0)} \qquad \overset{\nu\to\infty}{\longrightarrow} \qquad \chi = e^\kappa \tag{4.32}$$

to be calculated for a single point $x_0 \in [0, 1]$. This way the small differences in the distributions become negligible and useful assertions on the system's escape rate can be made.

Figure 4.6 shows the quotient defined in equation (4.32) versus ν. It converges very fast, so the escape rate κ shows the process of convergence in

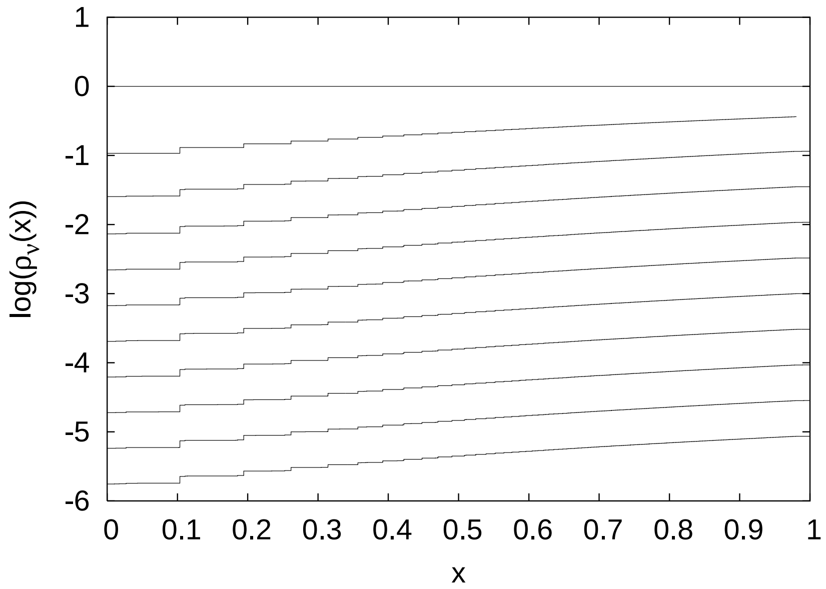

Figure 4.5: Successive application of $\mathbf{L}$ to $\rho_0(x) = 1$ quickly converges toward the leading invariant distribution of the maze.

more detail in Figure 4.7 because of the logarithmic scale.

Due to this investigation the dynamics on the maze are completely understood. A very slowly moving particle in the model of the horizontally shaken box approaches the wall and hits it in a phase ϕ_0 close to $\frac{\pi}{2}$ represented by $x \to 1$. This is inevitably correct, because the wall is estimated to oscillate much faster than the slow particle moves. Then iteration of the maze-map will show the particle to leave the maze with the probability

$$W_\nu = 1 - e^{\kappa\nu} \tag{4.33}$$

in the ν'th step without paying attention to the deterministic orbit. Due to $\kappa \approx -0.516 < 0$ and the instability of all the fixed points in the maze a real physical system will cause any orbit to leave the maze with $\nu \to \infty$ and to enter the deterministic system discussed in Chapter 3.

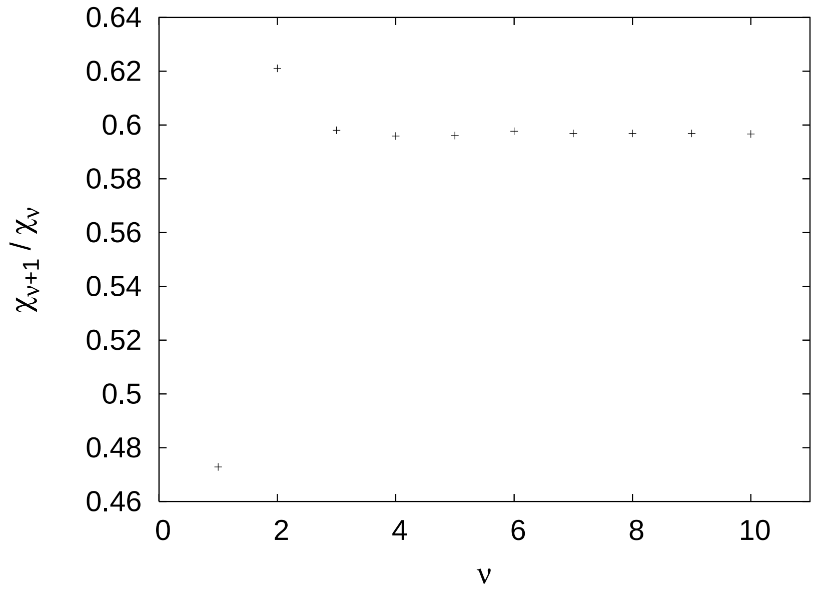

Figure 4.6: The quotient $\frac{\chi_{\nu+1}}{\chi_\nu}$ versus ν represents the share of the remaining distribution, that has not left the maze at step ν via absorption.

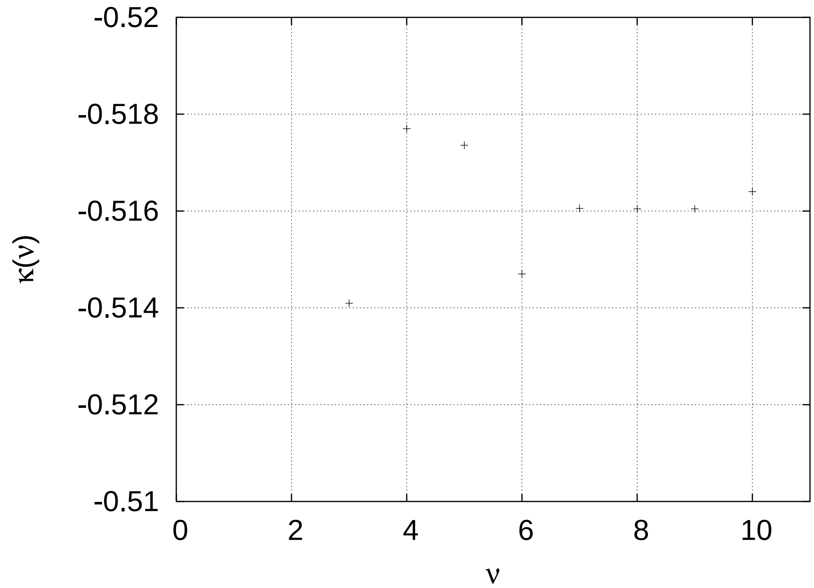

Figure 4.7: The escape rate of the maze in dependence of ν shows the fast convergence toward the invariant distribution and measures the tendency of the system to leave the maze.

Chapter 5

Conclusions

This work is dedicated to the understanding of non-standard period-doubling in an approximately piecewise continuous dynamical system given by a particle in a horizontally shaken box. The original problem emerged out of transcendent equations in shape of a non-unimodal iterated map. This complicated map offered two areas of interest. The first was of rather deterministic nature and concerned with non-standard period-doubling. The second area of interest was a maze-like structure associated with slowly moving particles in a sinusoidal, horizontally shaken box.

At first the period-doubling problem has been made accessible by construction of a generic *cup map*, that resembles the original map's properties and is open to numerical analysis via the implicit $\mathbf{P}_{2^n}$ operator by using techniques of symbolic dynamics. The numerically observed *period-doubling function* as an exponentially growing equivalent to the *Feigenbaum constant* of unimodal maps demanded an analytical explanation that could be achieved in Section 3.2.6 via the $\mathbf{T}$-transformation introduced in Section 3.2.3. These transformations are an ultimate tool to determine the future of every point in the cup map under iteration in non-trivial cases. Non-trivial orbits encircling the fixed point more often than the ones considered in this work will be described by analog definitions of the $\mathbf{T}$-transformations. The process is always the same.

Finally an interesting relationship between the *cup map* and unimodal maps was indicated, revealing the period-doubling phenomenon to be of the same origin as period-doubling in unimodal maps. The emergence of the period-doubling function is inevitably a consequence of the restraints of the cup map. The absorption interval of the cup map enforces a parametrization different to the common parametrization of unimodal maps making application of renormalisation theory to the cup map a lost cause. So the period-doubling function is a direct equivalent to the Feigenbaum constant that characterizes the same period-doubling simply due to another parametrization.

After the deterministic period-doubling had been understood, the maze structure was investigated using a stochastic process. An analytical solveable piecewise continuous generic model of the maze has been developed, resembling the rate of convergence of the maze's function branches. This generic model allowed to find one of the maze's *invariant distributions* and the estimation of *escape rate* via the *Perron-Frobenius operator* under endurable numerical efforts.

After these two processes have been investigated, the dynamical system of the particle in the harmonically, horizontally shaken box can be considered to be understood. Every trajectory except sets of measure zero will lead into the absorption interval and therewith into the deterministic part of the map after sufficient iteration.

The deterministic part of the map offers a wide range of stable homeostatic as well as very sensitive areas of behavior under the variation of the control-parameter a. Even the exponentially growing period-doubling function could be of engineering interest in optical or nano-mechanical computers, where logarithms of signals are of interest for calculation i.e. multiplication via addition purposes.

Maybe one day there are devices in nano-mechanics, optical-computing, control-theory or communication-theory that employ results of this work.

Appendix A

Nomenclature

Common notation

$\mathbb{N}$	set of natural numbers
$\mathbb{N}_0$	$\mathbb{N} \cup \{0\}$
$\mathbb{Z}$	set of whole numbers
$\mathbb{Z}_+ = \mathbb{N}_0$	set of non-negative whole numbers
$\mathbb{R}$	set of real numbers
$\mathbb{C}$	set of complex numbers
$\Theta(x) = \begin{cases} 0 & x < 0 \\ \frac{1}{2} & x = 0 \\ 1 & x > 1 \end{cases}$	Heaviside function
$\delta(x) = \frac{d}{dx}\Theta(x)$	Dirac's delta distribution
$f \circ g(x)$	$\equiv f(g(x))$
$\left(\frac{df}{dx}\right)(x_0)$	derivative of $f(x)$ evaluated at x_0
$\mathbf{A}$	operator $\mathbf{A}$
$\mathcal{D}(\mathbf{A})$	domain of operator $\mathbf{A}$
$\mathcal{R}(\mathbf{A})$	codomain of operator $\mathbf{A}$
$\mathbf{A} = \alpha_{\mathbf{A}} \cdot + \beta_{\mathbf{A}}$	$\equiv \mathbf{A}x = \alpha_{\mathbf{A}} x + \beta_{\mathbf{A}}$
$\mathbf{id}$	identity
$\mathbf{L}$	Perron-Frobenius operator
σ	Bernoulli shift operator
κ	kneading sequence, escaperate
$\rho(x)$	density/probability distribution

Specific notation

$Sf(x)$	Schwarzian derivative of function $f(x)$
$f_r(x), g_\mu(x)$	the discrete logistic map
Λ	Lyapunov exponent
$f^{(n)}(x)$	n'th iterate of function $f(x)$
$x_n = f^{(n)}(x_0)$	point x_n after n iterations of x_0.
s_{x_0}	symbolic sequence of point x_0 under iteration
$s_{x_0,n}$	n'th digit of sequence s_x
$\iota_{s_{x_0}}$	length of symbolic sequence s_{x_0}
x^*	fixed point satisfying $x^* = f(x^*)$
a,b,c	control parameters of the cup map
ρ	convexity parameter of the cup map
$\mathbf{P}_{2^n}$	period-doubling operator

Bibliography

[1] B. Drossel, T. Prellberg, *Dynamics of a single particle in a horizontally shaken box*, The European Physical Journal B, Springer Verlag, 1998.

[2] Stephen H. Strogatz, *Nonlinear Dynamics and Chaos*, Westview Press, 2000.

[3] C. Beck, F. Schlögl, *Thermodynamics of chaotic systems - an introduction*, Cambridge University Press, 1993.

[4] H. G. Schuster, *Deterministic Chaos*, John Wiley and sons Ltd. 1994.

[5] Kai T. Hansen, *Symbolic dynamics in chaotic systems*, Dissertation University of Oslo, 1993.

[6] Hao Bai Lin, *Elementary symbolic dynamics*, World Scientific Publishing Co. Pte. Ltd. 1989.

[7] Jean Collet, Jean-Pierre Eckmann, *Iterated maps on the interval as dynamical systems*, Birkhäuser 1986.

[8] Robert L. Devaney, *An introduction to chaotic Dynamical Systems*, Perseus Books Publishing L.L.C 1989.

[9] Vladimir I. Arnold, *Gewöhnliche Differentialgleichungen*, Springer Verlag, 2001.

[10] Wolfgang Metzler, *Nichtlineare Dynamik und Chaos - Eine Einführung*, B. G. Teubner Stuttgart, Leipzig 1998.

[11] Michael F. Barnsley, *Fraktale: Theorie und Praxis der deterministischen Geometrie*, Spektrum Verlag Heidelberg, Berlin, Oxford 1995.

[12] Fumio Inaba, *Optische Computer*, Springer-Verlag Berlin, Heidelberg 1992.

[13] Heinz Georg Schuster, *Complex adaptive systems - an introduction*, Scator Verlag, 2001.

[14] Stuart Kauffman, *Der Öltropfen im Wasser*, Piper Verlag München Zürich, 1995.

[15] Warren Brisley, *Grundbegriffe der linearen Algebra*, Vandenhoeck & Ruprecht in Göttingen 1977.

[16] Helmut Herold, *C Kompakt Referenz*, Addison Wesley Longman Verlag GmbH, 1999.

[17] Till Jeske, *C++*, Addison - Wesley, München 2000.

[18] Bruno Haible, Richard Kreckel, *CLN - a class library for numbers*, http://www.ginac.de/CLN, GNU GPL 2002.

[19] Y. Liu, M.T. Hill, N. Calabretta, H. de Waardt, G.D. Khoe, H.J.S Dorren, *Three-state all-optical memory based on coupled ring laser*, IEEE Photonics Technology Letters Vol. 15, No. 10, October 2003.

[20] Adriano Barenco, *Quantum physics and computers*, Contemporary Physics Vol. 37 No. 5, pp357-389, 1996.

[21] Ralph C. Merkle, *Two types of mechanical reversible logic*, Nanotechnology Volume 4, 1983.

Appendix B

Affidavit

Herewith I testify to have done this thesis strictly on my own under the supervision of Dr. Prellberg. I did not use other literature than cited in the bibliography and wrote the software for numerical analysis on my own in C++. This thesis is written in latex on a venerable debian-linux system featured with gnuplot, octave, octave-epstk, gcc, cln arbitrary precision numbers library and LaTeX2ϵ.

My thanks go to Mr. Prellberg for supporting my daring ambitions in theoretical physics.

Clausthal-Zellerfeld August 7, 2004